Modelling the wide-band laboratory response of rock samples to fluid and pressure changes.

Mark Chapman

PhD Thesis

University of Edinburgh 2001

The following thesis has been composed by me and, except where otherwise stated, constitutes my own work.

Signed:

0.1 Acknowledgements

A number of people have helped me with this thesis. In Edinburgh, in addition to my supervisors, Sergei Zatsepin and Stuart Crampin, I have had fruitful discussions with Peter Leary, Enru Liu and Anton Ziolkowski.

I am grateful to Jeremy Sothcott of Reading University for allowing me to view his data in advance of its publication and for permission to reproduce it in this thesis. His prompt responses to my queries were particularly appreciated.

I had the pleasure to spend a month visiting CSIRO Petroleum in Australia during my research and returned with many new insights into the problem. I particularly thank Kevin Dodds, Tony Siggins and Tony Endres for making my time there both enjoyable and productive.

0.2 Abstract

The Biot-Gassmann theory of poroelasticity forms the basis of most investigations of wave propagation in fluid saturated rock. In recent years the need to incorporate the concept of squirt flow into the theoretical framework has been recognised. Microstructural models which contain squirt flow give inconsistent predictions which contradict rigorous results from poroelastic theory.

I derive a microstructural poroelastic model which incorporates the squirt flow mechanism. The model is consistent in its limiting forms with the standard results of poroelasticity and effective medium theory. An important feature of the model is that it is relatively independent of assumptions about the aspect ratio spectrum.

I describe how the various parameters which occur in my model may be derived or estimated from experimental data, and proceed to a preliminary calibration of the model using published resonant bar data. Although I show that the data can be fit satisfactorily, significant ambiguity remains in the interpretation of the results.

A number of ultrasonic tests of P- and S- velocity, in rock similar to the resonant bar, as a function of both effective stress and pore fluid type show results which are at variance with the predictions of published poroelastic theories. I demonstrate that the anomaly can be explained with reference to physical effects predicted by my model. Moreover, the requirement to explain the ultrasonic results places constraints upon the modelling of the resonant bar data, removing much of the ambiguity from the analysis. I present a calibration which gives a consistent qualitative explanation of both the resonant bar and ultrasonic data.

The calibrated model makes a number of predictions concerning the effect of changing pore fluid viscosity, sample permeability and frequency. In principle experiments could be carried out to test these predictions.

0.3 Notations and Conventions.

I will adopt certain conventions in this thesis. Summation over repeated indices is to be understood except where the contrary is explicitly stated. I will take $\psi \in [0, \pi]$ and $\theta \in [0, 2\pi]$ to be Euler angles and, given a function $g(\psi, \theta)$, will understand "the integral of g over $d\Omega$" to refer to the expression:

$$\frac{1}{4\pi} \int_0^{2\pi} \int_0^{\pi} g(\psi, \theta) \sin\psi d\psi d\theta$$

I will also adopt the convention:

$$\dot{f} = \frac{\partial f}{\partial t};$$

for time variables t, and in a one dimensional problem will write:

$$f' = \frac{\partial f}{\partial x};$$

for a spatial variable, x.

The principal notations of the thesis are summarised on the following page.

Symbol	Unit	Meaning	Page Introduced
α	(-)	Tortuosity	20
γ	(-)	Coefficient	70
γ'	(-)	Coefficient	70
ϵ	(-)	Crack density	52
ϵ_{ij}	(-)	Strain tensor	36
η	Pa s	Fluid viscosity	18
ι	(-)	Crack fraction	72
κ_{dry}	Pa	Dry Bulk modulus	15
κ_f	Pa	Fluid Bulk modulus	22
κ_{hiP}	Pa	Limiting modulus	22
κ_m	Pa	Mineral Bulk modulus	15
κ_{sat}	Pa	Saturated Bulk modulus	15
κ_{uf}	Pa	Unrelaxed modulus	22
λ_{eff}	Pa	Effective modulus	45
μ	Pa	Reference Shear modulus	28
μ_{dry}	Pa	Dry Shear modulus	15
μ_{eff}	Pa	Effective modulus	45
μ_{sat}	Pa	Saturated Shear modulus	15
μ_{uf}	Pa	Unrelaxed modulus	22
ρ	kgm^{-3}	Saturated density	74
ρ_0	kgm^{-3}	Unstressed Fluid density	41
ρ_f	kgm^{-3}	Fluid density	18
σ_{ij}	Pa	stress tensor	17
σ_c	Pa	Coefficient	42
ς	m	Grain size	65
τ	s	Time scale	70
ϕ	(-)	Porosity	15
ϕ_c	(-)	Crack porosity	66
ϕ_p	(-)	Spherical porosity	66
ϕ_{soft}	(-)	Soft porosity	22
ω	s^{-1}	Angular frequency	55
a_i	m	i'th axis of ellipsoid	27
c_f	Pa^{-1}	Fluid compressibility	41

Symbol	Unit	Meaning	Page Introduced
c_v	M^3	Crack volume	43
C_{ijkl}	Pa	Reference elastic tensor	36
C^I_{ijkl}	Pa	Elastic tensor of inclusion	36
d_i	(-)	Coefficient	77
E_ijkl	Pa	Matrix elastic tensor	50
f_c	Hz	Biot frequency	19
G_{ij}	$(\text{Pa m})^{-1}$	Green's Function	28
I_{ijkl}	(-)	Identity tensor	38
k	m^2	Permeability	18
K_c	(-)	Coefficient	43
K_p	(-)	Coefficient	41
m_c	kgm^{-3}	Crack mass	43
m_j	kgm^{-3}	j'th Crack mass	67
m_p	kgm^{-3}	Pore mass	41
M	Pa	P-wave modulus	50
$\mathcal{M}$	Pa	Coefficient	77
N_c	(-)	Crack number	66
N_p	(-)	Pore number	66
p^*	Pa	Pore pressure	67
p_j	Pa	Crack pressure	67
p_v	m^3	Pore volume	40
r	(-)	Aspect ratio	34
S_{ijkl}	(-)	Eshelby Tensor	30
T_{ijkl}	(-)	Wu Tensor	38
T^s	(-)	Coefficient	38
U	Nm	Potential energy	46
$u(x)$	m	Displacement	28
v	(-)	Poisson's ratio	28
Z	$s^{\frac{1}{2}}$	Transition parameter	25

Table of Contents

Chapter 1

Introduction

It is widely accepted that subjecting rock to non-catastrophic increases in effective stress modifies its microstructure, usually by the closure of grain boundary micro-cracks, and that this significantly changes the elastic properties of the rock. The mathematical description of this process is based on the work of Eshelby (1957) who computed the response to applied stress of an ellipsoidal elastic inhomogeneity embedded in an infinite elastic matrix. A significant literature, known as effective medium theory (Watt et al., 1975), exists on the problem of using these results to calculate velocity as a function of micro-structure. Nur (1971) applied this formalism to predict the anisotropy induced by the imposition of differential stress on dry rock samples, and Zatsepin and Crampin (1997) extended the analysis to saturated rock.

Micro-cracks are also commonly suggested as a source of velocity dispersion and attenuation in rocks, since they are easily compressed by an elastic wave and so may give rise to "squirt flow" (Mavko and Nur, 1975). Despite this most work on dispersion takes place within the framework of poroelastic theory (Biot, 1956a, 1956b), which does not model micro-cracks explicitly. The development of poroelasticity by homogenisation theory (De Vries, 1989; Pride et al., 1992; Thimus et al., 1998) similarly fails to address this problem.

The evidence in support of Biot's theory is generally strong, with the confirmation of the existence of the celebrated "slow P-wave" (Plona, 1980) being a particular triumph for the theory. Nevertheless the theory tends to underes-

timate the magnitude of velocity dispersion and attenuation commonly observed in crustal rocks (Winkler, 1985; Han, 1987; Wang and Nur, 1990). In response to this a combined Biot-Squirt (BISQ) model has been developed (Dvorkin and Nur, 1993; Dvorkin et al., 1995) in which the "Biot" and "Squirt" mechanisms take place simultaneously, resulting in more realistic dispersive behaviour. In this approach fluid is exchanged between hypothetical "soft" and "hard" porosities; microcracks are not explicitly analysed on the basis of Eshelby's theory.

It seems reasonable to expect that effective medium theory could be applied directly to study this problem. Unfortunately most results available in the literature assume that the cracks and other inclusions are isolated from each other with respect to fluid flow, and this immediately rules out poroelastic and squirt flow effects.

A number of attempts have been made to study velocity dispersion and attenuation by incorporating various forms of fluid flow into effective medium theory (O'Connell and Budiansky, 1977; Johnstone et al., 1980; Hudson et al., 1996; Pointer et al., 2000). None of these can be considered to be definitive. No model has so far been able to reproduce the existence of the slow P-wave and so permit a comparison with Biot's theory.

A further advantage which the poroelastic models have is that they are expressed in terms of macroscopic parameters and so have great practical applicability. All parameters necessary to calculate velocity and attenuation at any frequency on the basis of the original Biot model can, assuming some geometric approximations (Berryman, 1980), be obtained directly from laboratory measurements. The method of Dvorkin et al. (1995) requires the fitting of one parameter which cannot be measured explicitly.

The situation with the dispersive effective medium models is far less advantageous. These models approximate cracks by thin ellipsoids with equal major axes, so the aspect ratio of the cracks enters the models. For a wide class of the non-dispersive effective medium models, all information about the aspect ratio distribution is encoded into a single parameter, the crack density, which can in principle be explicitly measured, at least for low porosity rocks (Murphy, 1985).

The dispersive models predict, however, that the shape of the dispersion curve depends on the distribution of the aspect ratios, which can hardly be estimated, let alone measured. The fact that grain boundary micro-cracks in real rocks are not ellipsoidal and so strictly speaking have no aspect ratio suggests that models which have aspect ratio distributions playing such a vital role are unlikely to be robust.

Nevertheless, the scope of effective medium theory to make definitive statements about the dispersion problem was demonstrated by Endres and Knight (1997). Without attempting to calculate attenuation or the shape of the velocity dispersion curve, Endres and Knight rigorously calculated the magnitude of velocity dispersion between zero frequency and a limiting high frequency for a range of geometrical models on the basis of Eshelby's theory. Of particular interest was their computation for the case of a medium containing a range of thin cracks and spherical pores, since it corresponds, at least qualitatively, to the situation studied by the dispersive effective medium models as well as the Dvorkin et al. (1995) approach. Endres and Knight predict that the magnitude of velocity dispersion depends not only on the absolute values of the porosities for cracks and spherical pores, but also on the relative porosities. This implies that the behaviour of cracks and pores cannot be independently modelled, the interaction between them is important. I show that Endres and Knight (1997) predict behaviour which contradicts the predictions of the Dvorkin et al. (1995) approach and those of the dispersive effective medium models.

In this thesis I derive a new poroelastic model from the basis of Eshelby theory. There are two main components to the theory. The first is to set up a model to describe the flow of fluid at the micro-scale. I consider pore space to consist of a combination of thin randomly oriented cracks and spherical pores distributed at random on the vertices of a lattice configuration. I then calculate the pressures which an elastic wave induces in each element, and allow for fluid flow between adjacent elements due to pressure gradients according to a flow law.

The second component to the theory is to develop a method for allowing velocities and attenuations to be calculated in media in which such complicated fluid

dynamics are taking place. I have chosen to use Eshelby's interaction energy approximation as the basis for my calculations, which means that strictly speaking the work is only valid for dilute concentrations of cracks and pores. In the classical approach, the porous medium is replaced by an equivalent homogeneous medium whose elastic tensor is used to compute velocities. I demonstrate that with fluid flowing according to my first model, the elastic tensor of the equivalent medium can be written in terms of the induced pore pressure in the spherical pores. This means that the general wave equation for the system becomes an equation coupling the propagating stress wave to the induced pore pressure. A similar equation arises from an analysis of the fluid dynamics model, and the two equations may be solved simultaneously. I find that the model predicts both a fast and a slow P-wave, in accordance with Biot's theory, but that the magnitude of the predicted dispersion is much higher. The behaviour of my model is entirely consistent with the analysis of Endres and Knight (1997).

Although certain parameters cannot be explicitly measured, I give methods for estimating them from specific observations. The model is free from the restriction of having to know the aspect ratio spectrum. In its most compact form, the only non-measurable parameter to be specified is a characteristic frequency. For rocks of high porosity, crack density is difficult to measure exactly and has to be fit somewhat arbitrarily.

The results of Zatsepin and Crampin (1997) concerning the relationship between crack density and effective stress can be incorporated directly into the model. This allows me to study the stress sensitivity of dispersion.

Sothcott et al. (2000) have carried out experiments on a range of sandstone cores. In particular they have developed a resonant bar technique which considerably extends the range of frequencies and effective stresses which can be studied. I calibrate the new model against these results, being guided both by the resonant bar data and ultrasonic measurements for different fluid saturants. I also repeat the analysis within the framework of the Dvorkin et al. (1995) model. The new model and the Dvorkin et al. model give broadly similar results and appear to complement each other.

I begin my thesis with a review of poro-elastic theory, beginning with the classical Gassmann (1951) formulae and moving to Biot's (1956a, b) theory. Various extensions and clarifications to the model are considered, culminating in the BISQ model of Dvorkin et al. (1995). I also discuss experimental evidence in favour of the various models.

Chapter three begins with a derivation of the mathematical results from Eshelby's theory which I will require later in the thesis. Eshelby's Interaction energy approximation is discussed, together with a range of more sophisticated methods of calculating the elastic tensor.

Chapter four constitutes a critical evaluation of the previous attempts to place fluid flow into Eshelby's framework. I criticise the models both theoretically and with respect to their practicality. I show that there are substantial contradictions between the various approaches , setting the scene for the developments in chapter four.

In Chapter five, I then move to the mathematical derivation of my new model, pointing out the various assumptions on which it depends. I show that the model is consistent with Gassmann's formulae at zero frequency and with Biot theory's prediction of the slow P-wave.

In Chapter six I show how to implement the theory in practice, discussing various problems which are likely to emerge. As an example, I calibrate the model against the new experimental data of Sothcott et al. (2000)

Chapter seven constitutes a discussion of the behaviour of the model, and I conclude with an overall assessment of the work.

Chapter 2

Review of poroelasticity.

Summary: I introduce the classical Biot-Gassmann theory of poroelasticity. The main qualitative prediction, that of a second compressional wave, has been verified experimentally, but in other respects the theory contradicts experimental observations. These contradictions can be explained with the introduction of the concept of "squirt flow". I review the attempts of a range of authors to incorporate squirt flow into the standard poroelastic model.

2.1 Classical poroelasticity

Poroelasticity is the study of the deformation of porous, permeable materials saturated with a fluid. The media under consideration consist of two interacting phases, implying a richer mathematical structure than is present in conventional elasticity. Poroelasticity has been applied to many different materials, from sponges to bones, but naturally in this thesis my attention will be focussed on rocks.

The most basic result in poroelasticity is due to Gassmann (1951). Gassmann considers that rock can be described in terms of three distinct components. The first is the mineral which makes up the rock. This is assumed to be a continuous, in other words non-porous, linearly elastic solid which has its own elastic tensor. The second component is the dry frame of the rock, consisting of the mineral

interspersed with a connected network of pores. This may be considered to be a homogeneous material on a scale larger than the individual pores, and this homogeneous material may be assigned its own elastic tensor. The fluid, itself a linearly elastic material, constitutes the third component.

Gassmann's analysis relies on a number of assumptions. It is only intended to apply to rocks for which the mineral and frame are elastically isotropic. An extension to the anisotropic case has been given by Brown and Korringa (1975). The theorem also assumes perfect pressure communication. This has two aspects; it assumes firstly that the porosity of the rock is completely connected and secondly that the fluid has enough time to flow to remove any pressure gradients, meaning that the pressure in the fluid is always the same at all points in the rock. One would expect this condition to be satisfied either in a static loading experiment or for the propagation of a very low frequency wave. A further assumption is that the rock forms a closed system, so that no net fluid flow is possible out of or into large regions of the sample. This means that Gassmann's equation would apply to jacketed, or undrained, experiments rather than those in which the fluid is free to move out of or into the rock sample. A final assumption is that no chemical interaction takes place between the fluid and the rock.

Under these assumptions, Gassmann finds expressions for the bulk and shear moduli, κ_{sat} and μ_{sat} respectively, of the saturated rock in terms of the mineral bulk modulus, κ_m, the dry frame moduli κ_{dry} and μ_{dry}, the fluid bulk modulus κ_f and the porosity ϕ:

$$\kappa_{sat} = \kappa_{dry} + \frac{(1 - \frac{\kappa_{dry}}{\kappa_m})^2}{\frac{\phi}{\kappa_f} + \frac{1-\phi}{\kappa_m} - \frac{\kappa_{dry}}{\kappa_m^2}}; \tag{2.1}$$

$$\mu_{sat} = \mu_{dry}. \tag{2.2}$$

Wang and Nur (1992) present evidence in favour of Gassmann's theorem for a wide range of different rock types. It is noticeable that Gassmann's equation appears to work well at high values of effective stress, where microcracks are closed, but substantially underestimates velocity for low values of effective stress.

The main practical use of Gassmann's Theorem lies not in predicting saturated velocity from dry velocity, but rather in predicting the effect of changing one fluid type for another , the fluid substitution problem. Writing the standard Gassmann equation for two different fluid types simultaneously allows the dry frame moduli to be eliminated, leaving a relationship between the bulk moduli of the two saturated solids.

A word must also be said about the meaning of the "dry frame moduli". In practice the assumption that the fluid does not interact chemically with the mineral making up the frame could be incorrect. Cadoret (1993) has shown that there is a substantial difference between the stiffness of a completely dry rock and that of a "moist" rock containing an extremely small amount of water. This distinction cannot be explained by arguments about the elasticity of the rock sample alone, and must be attributed to a chemical effect softening the frame of the rock (Tutuncu and Sharma, 1992, Murphy et al., 1984). Possible mechanisms for this effect include swelling of clays, changes in the internal surface energy of the rock and dissolution of mineral. Gassmann's Theorem will generally work better when the dry moduli used in the calculations are replaced with the "moist" moduli (Cadoret, 1993; Murphy et al., 1991). This creates difficulties for the fluid substitution problem since it is possible that the "moist" moduli may not be the same for different pore fluids.

Gassmann's equation is a static theory, in that frequency is not involved as a parameter. Biot (1956a, 1956b) derived the first theory of dynamic poroelasticity.

Biot's theory describes the dynamic interaction of the solid and fluid phases. To this end he defines separately the elastic fields in both the fluid and solid. In the solid the displacement vector is denoted by u, the stress tensor by σ and the strain tensor by ϵ. In the fluid the displacement is referred to as w and the hydrostatic stress tensor is $p\delta_{ij}$.

The theory relies on two fundamental assumptions. The first is that the constitutive relation of the composite can be written as:

$$\sigma_{ij} = \lambda_0 \epsilon_{kk} \delta_{ij} + 2\mu_0 \epsilon_{ij} - \beta p \delta_{ij}; \tag{2.3}$$

$$\xi = \frac{1}{M} p - \beta \epsilon_{kk}; \tag{2.4}$$

where $\xi = \nabla.w$ and λ_0, μ_0, β and M are constants. The second fundamental assumption is that the kinetic energy of the composite, T, may be written as:

$$2T = \rho_{11} \dot{u}_i \dot{u}_i + \rho_{12} \dot{u}_i \dot{w}_i + \rho_{22} \dot{w}_i \dot{w}_i. \tag{2.5}$$

In the absence of dissipation, Lagrange's equations now give:

$$\frac{\partial}{\partial t}(\frac{\partial T}{\partial \dot{u}_i}) = f_i; \tag{2.6}$$

$$\frac{\partial}{\partial t}(\frac{\partial T}{\partial \dot{w}_i}) = F_i; \tag{2.7}$$

where f_i is the component of force acting on the solid in the i-direction and F_i that acting on the fluid. Given that:

$$f_i = \sigma_{ik,k}; \tag{2.8}$$

$$F_i = p_{,i}; \tag{2.9}$$

we have a consistent set of equations in u and w. Taking the divergence of (2.8) and (2.9) leads to a coupled set of equations in ϵ_{kk} and ξ. Seeking solutions of the form:

$$\epsilon_{kk} = A_0 \exp i(yx - \omega t); \tag{2.10}$$

$$\xi = A_1 \exp i(yx - \omega t); \tag{2.11}$$

we find a quadratic dispersion equation implying the existence of two compressional wave speeds, in contradiction to the case of conventional elasticity. This has the interpretation that one wave, the fast wave analogous to the P-wave in conventional elasticity, has the displacements of the solid and fluid in phase with one another, while the other, slower, wave has the displacements out of phase. Taking the curl of (2.8) and (2.9) leads to a single velocity for the shear wave.

If the frequency of the wave is sufficiently low that the motion of the fluid can be considered to be of Poiseuille type, in other words low Reynolds number steady state flow, a dissipation function, D, may be defined as:

$$D = \frac{\eta\phi}{2k}(u_i - w_i)(u_i - w_i); \tag{2.12}$$

η being the fluid viscosity; ϕ the porosity; and k the permeability. The terms $\frac{\partial D}{\partial u_i}$ and $\frac{\partial D}{\partial \dot{w}_i}$ must then be added to the left hand sides of equations (2.6) and (2.7) respectively.

For higher frequencies the assumption of Poiseuille flow is incorrect. Biot (1956b) systematically analyses the breakdown of Poiseuille flow in the framework of the Navier-Stokes equation for oscillatory fluid motion between parallel plates and inside circular tubes. His conclusion is that the viscosity, η in D must be replaced by $\eta F(\vartheta)$, where:

$$F(\vartheta) = \frac{1}{4}\frac{\vartheta T(\vartheta)}{1 + 2iT(\vartheta)/\vartheta}; \tag{2.13}$$

$$T(\vartheta) = \frac{e^{3\pi i/4} J_1(\vartheta e^{\frac{-\pi i}{4}})}{J_0(\vartheta e^{\frac{-\pi i}{4}})}; \tag{2.14}$$

$$\vartheta = (\frac{\omega a^2 \rho_f}{\eta})^{\frac{1}{2}}; \tag{2.15}$$

where a is a pore size parameter; ρ_f is the fluid density; and J_n is the Bessel function of order n.

For very low frequencies, $F(\vartheta) \approx 1$ and we return to the Poiseuille model. It is helpful to consider the frequency dependence in Biot's model in terms of the characteristic frequency, or Biot frequency:

$$f_c = \frac{\phi\eta}{2\pi\rho_f k}. \tag{2.16}$$

For frequencies, $f \ll f_c$ inertial effects are not important. Indeed velocities calculated from Biot's theory will agree with the Gassmann formulae provided $f < 0.1 f_c$, (White, 1983). For frequencies f $\gg f_c$ inertial effects become important, and the velocity of the slow wave becomes appreciable. The model predicts that velocity increases with frequency, and decreases with increasing viscosity. Approximate expressions for the high frequency limiting velocities have been given by Geertsma and Smit (1961).

The Biot frequency f_c, has been calculated for a range of rocks and has been found to be variable, but high. Bourbie et al. (1987) quote f_c values in the range of 30 kHz to 1 GHz for water saturated samples. One would expect therefore that field observations would generally be best described by the low frequency limit. Geertsma and Smit (1961) have nevertheless shown that even at low frequencies the generation of a slow wave at interfaces has an important effect on reflection coefficients.

At first sight the Biot model appears to contain a great many free parameters. This is misleading, all parameters occurring in the model can be directly measured or estimated from measurements. In particular the coupling constants ρ_{11}, ρ_{12} and ρ_{22} may be given by:

$$\rho_{11} = (1-\phi)\rho_m - (1-\alpha)\phi\rho_f; \tag{2.17}$$

$$\rho_{12} = (1-\alpha)\phi\rho_f; \tag{2.18}$$

$$\rho_{22} = \alpha\phi\rho_f. \tag{2.19}$$

In these equations the subscript m refers to the mineral making up the rock. The parameter α is the tortuosity. When fluid moves through a rock it generally does not travel in a straight line. The tortuosity gives a measure of the average ratio of path length to displacement. It cannot strictly be measured, but Berryman (1980) suggested that the approximation:

$$\alpha = \frac{1}{2}(\frac{1}{\phi} + 1); \tag{2.20}$$

which arises from a strict study of packed spheres of equal radii, could be employed. With this assumption, and if we are prepared to take a parameter of the order of the average grain size for the pore-size parameter, Biot's theory allows saturated velocities at any frequency to be calculated directly from the dry rock velocities.

The main qualitative prediction of the Biot model was verified by Plona (1980). Plona observed the slow wave in laboratory tests on synthetic rock made out of glass beads. This was considered to be outstanding evidence in support of the validity of Biot's theory. It was not until Kelder and Smeulders (1997) observed the slow wave in Nivelsteiner sandstone that Plona's experiment was successfully repeated on a real rock sample.

Biot's theory predicts that the dispersion of the fast P-wave is small, typically less than 1% (Wang and Nur, 1992). The predicted S-wave dispersion is slightly higher, taking values up to about 4 %. The attenuations predicted by Biot's theory are small.

Abundant evidence exists that the velocities and attenuations predicted by Biot's theory are too low in comparison with laboratory measurements (Winkler, 1985, 1986; Han, 1987; Mochizuki, 1982; Wang and Nur 1990). This suggests that it underestimates the magnitude of frequency dispersion between field and laboratory frequencies.

A further disagreement between theory and evidence concerns the role of fluid viscosity. It is commonly observed that velocity increases with increasing viscosity (Nur, 1980; Jones and Nur, 1983; Jones, 1986). This is in direct contradiction to Biot's prediction of decreasing velocity with increasing viscosity.

These two concerns led to the acceptance of poroelastic models which incorporate the concept of "local" or "squirt" flow.

2.2 Poroelastic models incorporating squirt flow

In Biot's theory, fluid motion results from viscous and inertial coupling between the rock and fluid phases. This can be thought of as the fluid being "dragged along" with the motion of the solid. The only pressure gradients in the fluid point in the direction of propagation of the wave.

In reality this is unlikely to be the case. Fluid resides in a network of interconnected cracks and pores of different geometries and orientations. Seismic waves will compress these cracks and pores to different degrees, leading to pressure gradients in directions not equal to the axis of wave propagation and fluid may well flow down these gradients. Such flow is termed "squirt flow". The concept of squirt flow was suggested by Biot (1962), but it was not until the 1990's that attempts were made to incorporate it into poroelastic theory.

Mavko and Jizba (1991) derived results analogous to Gassmann's equations to take account of the possibility of squirt flow. They argue that at very high frequencies Gassmann's assumption of perfect pressure equalisation fails and that substantial pressure gradients are likely to persist, increasing the elastic moduli.

Mavko and Jizba find a way of estimating the likely magnitude of velocity dispersion, or in other words the degree to which Gassmann's equations underestimate laboratory measurements of velocity. Their method is based on two observations. Firstly they note that in general Gassmann's equations appear to work best for rock under high effective stress. They also observe that velocities in rock increase with increasing effective stress, probably due to the closure of microcracks. This

allows them to argue that microcracks are the cause of the velocity dispersion, and suggests a method for estimating the scale of the velocity dispersion.

When the dry bulk modulus is entered into Gassmann's equation, account is taken of the fact that when the rock is subjected to a confining stress fluid will flow from the compliant microcracks to the less compliant pores, and this will lead to significant deformation of the cracks. At high frequency this process will not have time to take place and this will stiffen the rock. To accurately predict the high frequency modulus it is necessary to supply a different dry frame modulus which will remove the effect of the microcracks. Mavko and Jizba suggest that one should extrapolate to find the limiting dry frame bulk modulus for high effective stress κ_{hiP} and use this in Gassmann's theorem. Of course this would be expected to give an overestimate of the saturated bulk modulus since even if they do not communicate with the pore space the cracks will be deformed by more than the mineral. As a correction Mavko and Jizba suggest replacing some of the mineral with fluid according to the following rule:

$$\frac{1}{\kappa_{uf}} = \frac{1}{\kappa_{hiP}} + \phi_{soft}\left(\frac{1}{\kappa_f} - \frac{1}{\kappa_m}\right); \tag{2.21}$$

where κ_{uf} is the "unrelaxed frame" bulk modulus which is to be entered into Gassmann or Biot's equations; κ_m is the mineral bulk modulus; and ϕ_{soft} is the fractional volume of the microcracks, which Mavko and Jizba suggest is usually small enough to ignore.

The calculation of the shear modulus is similar, the only difference being that not all cracks are compressed by the propagation of a shear wave leading to a smaller correction for dispersion. Mavko and Jizba find the formula for the unrelaxed frame shear modulus as:

$$\frac{1}{\mu_{uf}} = \frac{1}{\mu_{dry}} + \frac{4}{15}\left(\frac{1}{\kappa_{uf}} - \frac{1}{\kappa_{dry}}\right). \tag{2.22}$$

Mavko and Jizba (1991) apply their theory to a number of laboratory tests and obtain reasonable results.

Dvorkin and Nur (1993) presented a dynamic poroelastic model (BISQ) which incorporates both squirt and Biot flow. The method is limited to rocks which are partially saturated and under high effective stress so that microcracks are closed. In this sense the model is not an extension of Biot's theory since that theory was valid only for fully saturated rocks.

The basis of Dvorkin and Nur's approach lies in their description of the fluid dynamics in terms of a representative cylinder. Fluid flow from a point is considered to be axisymmetric around the axis of wave propagation, leading to the equation for the conservation of fluid mass:

$$\frac{\partial(\rho_f \phi)}{\partial t} + \frac{\partial[\rho_f (q - \phi u_t)]}{\partial x} + \frac{\partial(\rho_f \tilde{q})}{\partial r} + \frac{\rho_f \tilde{q}}{r} = 0; \tag{2.23}$$

where q is the filtration velocity in the direction of wave propagation and $\tilde{q}$ is that transverse to the wave. This is converted into an equation for the fluid pressure, and solved as a function of r subject to the condition that the pressure vanishes on the surface of the cylinder r=R, where R is the characteristic squirt-flow length. The assumption is then made that the pressure at any point may be replaced by the average pressure in a representative cylinder centred at that point, and then this pressure is entered into the standard Biot theory.

The BISQ model predicts much higher magnitudes of dispersion than does the standard Biot model. A further important feature is that the characteristic frequency of the squirt flow mechanism is proportional to permeability divided by viscosity, rather than viscosity divided by permeability as in the Biot frequency. This explains why velocities are observed to increase with fluid viscosity.

Dvorkin and Nur do not give any formulae for shear wave velocities on the basis of their model. It should also be noted that the low frequency limiting velocity of the BISQ model is lower than that given by Gassmann's theorem. This is because of the boundary condition that the pressure should vanish on the surface of the representative cylinder, as opposed to the case of equal non-zero pressure at every point in Gassmann's analysis. Dvorkin and Nur point out that their model does

not contradict Gassmann's theorem since it is only valid for partial saturations whereas Gassmann's equations refer to fully saturated rock.

The case of fully saturated rocks was dealt with by Dvorkin et al. (1995). Strictly speaking this is a viscoelastic rather than a poroelastic model; no Biot flow is envisaged and the model does not predict the existence of a slow P-wave. The concept of the model is to extend the Mavko and Jizba (1991) analysis in order to be able to calculate velocity at any frequency between the Gassmann low frequency limit and the Mavko-Jizba high frequency limit.

Dvorkin et al. (1995) divide the pore space of the rock into two components; "soft" porosity which closes as effective stress is increased and "stiff" porosity which does not. When a seismic wave propagates, they expect fluid to be transferred from the compliant soft porosity to the stiffer porosity. Their calculation of the velocities then depends on solving a succession of sub-problems. The first is to calculate the bulk modulus of what they refer to as the "modified solid". The modified solid refers to the mineral interspersed with the saturated soft porosity.

Dvorkin et al. (1995) assert that the modified solid may be modelled by means of a representative cylinder with radius R, where R is again the characteristic squirt flow length. The fluid flow is taken to be axisymmetric, with no flow in the direction of the wave. The boundary condition on the surface of the cylinder is chosen to be such that the pressure is equal to the uniform pressure which would obtain in the fluid under the conditions of Gassmann's theorem. Under the assumption that the pressure in the modified solid is equal to the volumetric average of the pressure in the representative cylinder, this allows the calculation of a frequency dependent bulk modulus for the modified solid from the dry frame, mineral and limiting high pressure moduli.

It is now necessary to define the modified frame. This is the modified solid interspersed with the dry stiff pores which were removed in the consideration of the modified solid. The bulk modulus of the modified frame may be found in terms of the bulk modulus of the modified solid, the limiting high pressure bulk modulus of the rock and the mineral bulk modulus.

The full, complex valued, frequency dependent bulk modulus for the saturated rock is then found by an application of Gassmann's theorem in which the role of the dry frame modulus is played by the bulk modulus of the modified frame and the mineral bulk modulus is replaced by that of the modified solid. A similar method holds for the calculation of the shear modulus.

An appealing feature of Dvorkin et al.'s (1995) model is that the characteristic squirt flow length, the rock permeability and the viscosity are collected together into only one parameter, Z. This Z parameter controls the frequency at which the transition from low to high frequency behaviour takes place. This has important implications for the fluid substitution problem; when one fluid is replaced by another a different value of Z has to be used according to the formula:

$$Z_1 = \sqrt{\frac{\eta_1}{\eta_2}} Z_2. \tag{2.24}$$

Higher values of the fluid viscosity move the transition point to lower frequencies, meaning that the model is consistent with observations of velocity increasing with fluid viscosity. Z is the only free parameter in the model. There is no a priori method for estimating it, one must choose it to fit the data as well as is possible.

Since the elastic moduli in Dvorkin et al.'s (1995) model are complex, one can calculate the frequency dependent Quality factors for both P- and S- wave propagation. This is an example of the Kramers-Kronig relations in a causal, linearly viscoelastic media (Bourbie et al., 1987). If one knows the velocity dispersion for all frequencies then it is possible to calculate the Quality factor for all frequencies.

2.3 Conclusion

The Biot-Gassmann theory of poroelasticity represents an elegant and robust description of wave propagation in fluid-saturated porous media. It contains no free parameters, every constant on which the solution depends can be measured independently, making its predictions definite.

The observation of the slow compressional wave implies that Biot's theory cannot be dismissed. Nevertheless there appear to be systematic errors in the theory; it underestimates velocity dispersion and its behaviour with respect to fluid viscosity is incorrect.

The concept of squirt flow is a simple attempt to address the failings of Biot's theory. Despite the attempts of a number of authors there is at present no model which consistently extends Biot's analysis to include squirt flow; the BISQ model is only valid for partially saturated rock while Dvorkin et al.'s (1995) model contains no Biot flow or slow wave. Whatever success these models achieve, substantial scope exists for a theory which can successfully combine Biot's analysis with squirt flow.

Chapter 3

Review of effective medium theory.

Summary: I derive the fundamental results of Eshelby (1957) concerning the deformation of an ellipsoidal inclusion embedded in an infinite linearly elastic matrix. For the case of fluid filled inclusions these results may be extended so that the dependence on the fluid bulk modulus is replaced by dependence on an independently determined pore fluid pressure. I show that the results for the deformation of a single inclusion are fundamental to a range of techniques for the calculation of velocities in media with a distribution of inclusions. Some assumptions about the distribution of the inclusions are necessary in these approaches. I give derivations of two simple methods which assume that the concentration of inclusions is dilute. Other more complicated methods replace the dilute concentration assumption with different geometric assumptions.

3.1 The plug problem

Consider a uniform, homogeneous linearly elastic material containing a hole H. Let H be the ellipsoid:

$$\frac{x_1^2}{a_1^2} + \frac{x_2^2}{a_2^2} + \frac{x_3^2}{a_3^2} \leq 1; \tag{3.1}$$

for some suitable choice of coordinates.

Consider further a plug P, made of the same material as the matrix, which can be deformed into the same shape and size as H by the imposition of a uniform traction $-\sigma_n^T$ across the surface of P.

Place the stressed plug in the hole, and allow the imposed stress to relax by applying a uniform traction σ_n^T to the surface of the hole. The plug will attempt to return to its unstressed state, but in general will be unable to do so as it is constrained by the rest of the matrix. We refer to the calculation of this constrained displacement as the plug problem.

The constrained displacement due to the insertion of the plug is given by;

$$u_i^c(x) = \int_S G_{ij}\sigma_{jk}n_k dS; \tag{3.2}$$

where:

$$G_{ij} = \frac{1}{16\pi\mu(1-v)}[\frac{3-4v}{|x-x'|}\delta_{ij} + \frac{(x_i-x_i')(x_j-x_j')}{|x-x'|^3}]; \tag{3.3}$$

according to Love(1927). μ is the matrix shear modulus; v is the matrix Poisson's ratio; S is the surface of H; and n is the unit normal to S.

Applying the divergence Theorem to (3.2) and noting that $\sigma_{jk,k} = 0$ in a static problem, we have:

$$u_i^c(x) = \sigma_{jk}^T \int_V G_{ij,k} dV. \tag{3.4}$$

I show in Appendix B that this may be written as:

$$u_i^c(x) = \frac{\epsilon_{jk}^T}{8\pi(1-v)} \int_V \frac{g_{ijk}(l)}{r_0^2} dx'; \tag{3.5}$$

where:

$$l = \frac{x-x'}{|x-x'|}; \tag{3.6}$$

$$r_0 = |x - x'|; \tag{3.7}$$

$$g_{ijk} = (1 - 2v)(\delta_{ij}l_k + \delta_{ik}l_j - \delta_{jk}l_i) + 3l_il_jl_k; \tag{3.8}$$

and ϵ^T = is the strain tensor corresponding to the stress σ^T.

Moving to polar coordinates, with origin at x, we have:

$$u_i^c(x) = \frac{\epsilon_{jk}^T}{8\pi(1-v)} \int_0^{2\pi} \int_0^{\pi} \int_0^{r(\psi,\theta)} \frac{g_{ijk}}{r_0^2} |J| dr_0 d\psi d\theta; \tag{3.9}$$

where in these coordinates:

$$l = (\sin\psi\cos\theta, \sin\psi\sin\theta, \cos\psi). \tag{3.10}$$

For this transformation, $|J| = r_0^2 \sin\psi$, so:

$$u_i^c(x) = \frac{\epsilon_{jk}^T}{8\pi(1-v)} \int_0^{2\pi} \int_0^{\pi} \int_0^{r(\psi,\theta)} g_{ijk} \sin\psi dr_0 d\psi d\theta. \tag{3.11}$$

As is shown in Appendix C, this equation may be written:

$$u_i^c(x) = \frac{x_m \epsilon_{jk}^T}{8\pi(1-v)} \int_0^{2\pi} \int_0^{\pi} \frac{\lambda_m g_{ijk}}{g} \sin\psi d\psi d\theta; \tag{3.12}$$

where:

$$\lambda_i = \frac{l_i}{a_i^2}; \tag{3.13}$$

$$g = \frac{l_1^2}{a_1^2} + \frac{l_2^2}{a_2^2} + \frac{l_3^2}{a_3^2}. \tag{3.14}$$

Clearly:

$$u^c_{i,j} = \frac{\epsilon^T_{kl}}{8\pi(1-v)} \int_0^{2\pi} \int_0^{\pi} \frac{\lambda_j g_{ikl}}{g} \sin\psi d\psi d\theta; \tag{3.15}$$

and so:

$$\epsilon^c_{ij} = \frac{\epsilon^T_{kl}}{16\pi(1-v)} \int_0^{2\pi} \int_0^{\pi} \frac{\lambda_i g_{jkl} + \lambda_j g_{ikl}}{g} \sin\psi d\psi d\theta. \tag{3.16}$$

This is the celebrated result that the strain inside an ellipsoidal inclusion is uniform.

Equation (3.16) my be written symbolically as:

$$\epsilon^c_{ij} = S_{ijkl}\epsilon^T_{kl}. \tag{3.17}$$

Eshelby (1957) gives expressions for S_{ijkl} for the general case, $a_1 < a_2 < a_3$, but in this thesis I will only require the results for a sphere ($a_1 = a_2 = a_3$) and the oblate spheroid ($a_1 = a_2 > a_3$).

The terms of the tensor S are given by:

$$S_{ijkl} = \frac{1}{16\pi(1-v)} \int_0^{2\pi} \int_0^{\pi} \frac{\lambda_i g_{jkl} + \lambda_j g_{ikl}}{g} \sin\psi d\psi d\theta. \tag{3.18}$$

It is apparent that S must satisfy the symmetries:

$$S_{ijkl} = S_{ijlk} = S_{jikl} = S_{jilk}; \tag{3.19}$$

which implies that S can be written in standard matrix form (Christensen, 1980) with the convention:

$$\begin{array}{lll} 1 \leftrightarrow (11) & 2 \leftrightarrow (22) & 3 \leftrightarrow (33) \\ 4 \leftrightarrow (23) & 5 \leftrightarrow (13) & 6 \leftrightarrow (12). \end{array} \tag{3.20}$$

Now by Appendix D the only non-zero entries in S may be:

$$\begin{array}{cccccc} S_{11} & S_{12} & S_{13} & S_{21} & S_{22} & S_{23} \\ S_{31} & S_{32} & S_{33} & S_{44} & S_{55} & S_{66}. \end{array} \tag{3.21}$$

From equation (3.18) we have the formulae:

$$S_{iijj} = Qa_j^2 I_{ij} - RI_i \qquad (i \neq j); \tag{3.22}$$

$$S_{ijij} = Q\frac{1}{2}(a_i^2 + a_j^2)I_{ij} + R\frac{1}{2}(I_i + I_j); \tag{3.23}$$

where the summation convention has been suspended and:

$$Q = \frac{3}{8\pi(1-v)}; \tag{3.24}$$

$$R = \frac{1-2v}{8\pi(1-v)}; \tag{3.25}$$

$$I_{ij} = \int_0^{2\pi}\int_0^{\pi} \frac{l_i^2 l_j^2}{a_i^2 a_j^2 g}\sin\psi d\psi d\theta; \tag{3.26}$$

$$I_i = \int_0^{2\pi}\int_0^{\pi} \frac{l_i^2}{a_i^2 g}\sin\psi d\psi d\theta. \tag{3.27}$$

I show in Appendix E that (3.26) and (3.27) may be written as:

$$I_i = 2\pi a_1 a_2 a_3 a_i^2 \int_0^{\infty} \frac{du}{(a_i^2+u)\Delta}; \tag{3.28}$$

$$I_{ij} = \begin{cases} 2\pi a_1 a_2 a_3 a_i^2 a_j^2 \int_0^{\infty} \dfrac{du}{(a_i^2+u)(a_j^2+u)\Delta} & (i=j) \\ \dfrac{2}{3}\pi a_1 a_2 a_3 a_i^2 a_j^2 \int_0^{\infty} \dfrac{du}{(a_i^2+u)(a_j^2+u)\Delta} & (i\neq j); \end{cases} \tag{3.29}$$

where:

$$\Delta = (a_1^2 + u)^{\frac{1}{2}}(a_2^2 + u)^{\frac{1}{2}}(a_3^2 + u)^{\frac{1}{2}}. \tag{3.30}$$

For the cases of a sphere and an oblate spheroid, the integrals in (3.28) and (3.29)may be evaluated explicitly and then the terms in the tensor S calculated from (3.22) and (3.23).

Starting with the sphere, $a_1 = a_2 = a_3 = a$ and so:

$$I_1 = 2\pi a^3 \int_0^\infty \frac{du}{(a^2 + u)^{\frac{5}{2}}} = \frac{4}{3}\pi; \tag{3.31}$$

and by symmetry $I_1 = I_2 = I_3$.

Also:

$$I_{11} = 2\pi a^3 \int_0^\infty \frac{du}{(a^2 + u)^{\frac{7}{2}}} = \frac{4\pi}{5a^2}; \tag{3.32}$$

so that similarly:

$$I_{12} = \frac{4\pi}{5a^2}; \tag{3.33}$$

and in general:

$$I_{ij} = \frac{4\pi}{5a^2} \begin{bmatrix} 1 & \frac{1}{3} & \frac{1}{3} \\ \frac{1}{3} & 1 & \frac{1}{3} \\ \frac{1}{3} & \frac{1}{3} & 1 \end{bmatrix}. \tag{3.34}$$

From equations (3.22) and (3.23) we now have:

$$S_{1111} = \frac{1}{15}\frac{7 - 5v}{1 - v}; \tag{3.35}$$

$$S_{1122} = \frac{1}{15}\frac{5v-1}{1-v}; \tag{3.36}$$

$$S_{1212} = \frac{1}{15}\frac{4-5v}{1-v}. \tag{3.37}$$

The remaining terms of S follow by symmetry, and so the full tensor is given in standard matrix form by:

$$S_{ij}^{sphere} = \frac{1}{15(1-v)}\begin{bmatrix} 7-5v & 5v-1 & 5v-1 & 0 & 0 & 0 \\ 5v-1 & 7-5v & 5v-1 & 0 & 0 & 0 \\ 5v-1 & 5v-1 & 7-5v & 0 & 0 & 0 \\ 0 & 0 & 0 & 2(4-5v) & 0 & 0 \\ 0 & 0 & 0 & 0 & 2(4-5v) & 0 \\ 0 & 0 & 0 & 0 & 0 & 2(4-5v) \end{bmatrix}. \tag{3.38}$$

We now consider the oblate spheroid. Although formulae for the general case $a_1 = a_2 > a_3$ are available in Eshelby (1957), in this thesis attention will be focused on the case of spheroids of small aspect ratio, $a_3/a_1 \ll 1$. As the aspect ratio tends to zero, the spheroid will approximate a plane crack.

From equation (3.28), we have:

$$I_1 = 2\pi a_1^2 a_3 \int_0^\infty \frac{du}{(a_1^2+u)(a_3^2+u)^{\frac{1}{2}}}; \tag{3.39}$$

and making the substitutions;

$$u = a_1^2 \tan^2\psi; \tag{3.40}$$

$$w = (1-r^2)^{\frac{1}{2}}\cos\psi; \tag{3.41}$$

where we define the aspect ratio, r, by;

$$r = \frac{a_3}{a_1}; \tag{3.42}$$

we find:

$$\begin{aligned} I_1 &= \frac{4\pi}{1-r^2}\int_0^{(1-r^2)^{\frac{1}{2}}} \frac{w^2 dw}{(r^2+w^2)^{\frac{1}{2}}} \\ &= \frac{2\pi r}{(1-r^2)^{\frac{3}{2}}}[\cos^{-1} r - r(1-r^2)^{\frac{1}{2}}]. \end{aligned} \tag{3.43}$$

Now we make the assumption that $r \ll 1$ and so:

$$I_1 = \pi^2 r + O(r^2). \tag{3.44}$$

Noting now that:

$$I_1 + I_2 + I_3 = \frac{1}{4\pi}\int_0^{\pi}\int_0^{2\pi} \frac{l_i^2 a_i^{-2}}{g} d\Omega = 4\pi; \tag{3.45}$$

and:

$$I_1 = I_2; \tag{3.46}$$

we have:

$$I_3 = 4\pi - 2\pi^2 r. \tag{3.47}$$

I show in Appendix F that;

$$I_{i1} + I_{i2} + I_{i3} = \frac{4\pi}{3a_i^2} \qquad 1 \leq i \leq 3; \tag{3.48}$$

$$a_1^2 I_{i1} + a_2^2 I_{i2} + a_3^2 I_{i3} = I_i \qquad 1 \leq i \leq 3. \tag{3.49}$$

Since the subscripts 1 and 2 are interchangeable we deduce that I_{ij} is given by:

$$I_{ij} = \begin{bmatrix} \frac{3\pi^2 r}{4a_1^2} & \frac{\pi^2 r}{4a_1^2} & \frac{4\pi}{3a_1^2} - \frac{\pi^2 r}{a_1^2} \\ \frac{\pi^2 r}{4a_1^2} & \frac{3\pi^2 r}{4a_1^2} & \frac{4\pi}{3a_1^2} - \frac{\pi^2 r}{a_1^2} \\ \frac{4\pi}{3a_1^2} - \frac{\pi^2 r}{a_1^2} & \frac{4\pi}{3a_1^2} - \frac{\pi^2 r}{a_1^2} & \frac{4\pi}{3a_3^2} - \frac{2\pi^2 r}{a_1^2} \end{bmatrix} + O(r^2). \tag{3.50}$$

Straightforward calculation using equations (3.22) and (3.23) gives the expression for S:

$$S_{ij}^{crack} = Y + O(r^2); \tag{3.51}$$

where Y is the tensor:

$$\begin{bmatrix} \frac{13-8v}{32(1-v)}\pi r & \frac{8v-1}{32(1-v)}\pi r & \frac{2v-1}{8(1-v)}\pi r & 0 & 0 & 0 \\ \frac{8v-1}{32(1-v)}\pi r & \frac{13-8v}{32(1-v)}\pi r & \frac{2v-1}{8(1-v)}\pi r & 0 & 0 & 0 \\ \frac{v}{1-v} - \frac{1+4v}{8(1-v)}\pi r & \frac{v}{1-v} - \frac{1+4v}{8(1-v)}\pi r & 1 - \frac{1-2v}{4(1-v)}\pi r & 0 & 0 & 0 \\ 0 & 0 & 0 & 1 - \frac{2-v}{1-v}\frac{\pi}{2}r & 0 & 0 \\ 0 & 0 & 0 & 0 & 1 - \frac{2-v}{1-v}\frac{\pi}{2}r & 0 \\ 0 & 0 & 0 & 0 & 0 & \frac{7-8v}{16(1-v)}\pi r \end{bmatrix}. \tag{3.52}$$

This completes the solution of the plug problem.

3.2 The ellipsoidal inclusion

In this section we solve the problem of the response of an inclusion embedded in a different material to the imposition of an external stress field. The method used is to find a plug problem which produces an identical stress and strain in the inclusion and then use the results of the previous section. To this end we define two problems.

Problem 1

We place an ellipsoidal inclusion with elastic tensor C^I inside a matrix with elastic tensor C, and impose a stress field σ^∞ at infinity. The strain inside the inclusion may be written as:

$$\epsilon^{inc} = \epsilon^\infty + \epsilon^p; \tag{3.53}$$

for some ϵ^p where $\epsilon^\infty = C^{-1}\sigma^\infty$. The stress in the inclusion will then be given by:

$$\sigma^{inc} = C^I(\epsilon^\infty + \epsilon^p). \tag{3.54}$$

Our task is to find ϵ^p.

Problem 2

We consider a plug problem with eigenstrain ϵ^T and superpose a stress field σ^∞ at infinity. The stress in the plug will then be given by:

$$\sigma^{inc} = \sigma^\infty + \sigma^c - \sigma^T. \tag{3.55}$$

If we define the original shape of the hole to correspond to zero strain, the strain of the hole is:

$$\epsilon^{inc} = \epsilon^\infty + \epsilon^c. \tag{3.56}$$

For a given eigenstrain ϵ^T we may solve for ϵ^c through the relation:

$$\epsilon^c = S\epsilon^\infty; \tag{3.57}$$

and therefore solve Problem 2.

Now the solutions to Problems 1 and 2 will be identical precisely if the stresses and strains in the inclusions are identical. We therefore seek an eigenstrain which will ensure that this condition is satisfied and carry the solution of Problem 2 over to Problem 1.

Equality of strain immediately gives:

$$\epsilon^p = \epsilon^c; \tag{3.58}$$

and so the condition for equality of stress becomes:

$$C^I(\epsilon^\infty + \epsilon^c) = \sigma^\infty + \sigma^c - \sigma^T. \tag{3.59}$$

The required eigenstrain is given by solving (3.59):

$$\epsilon^T = [(C - C^I)S - C]^{-1}(C^I - C)\epsilon^\infty. \tag{3.60}$$

The strain in the inclusion of Problem 1 is then:

$$\epsilon^{inc} = \epsilon^\infty + S[(C - C^I)S - C]^{-1}(C^I - C)\epsilon^\infty. \tag{3.61}$$

After rearrangement, this may be written as:

$$\epsilon^{inc} = T\epsilon^\infty; \tag{3.62}$$

where

$$T = [I + SC^{-1}(C^I - C)]^{-1}. \tag{3.63}$$

This solves Problem 1.

The tensor T will be referred to as the "Wu T tensor" since it was first given in explicit form in the paper Wu (1966). For the case of a crack filled with a viscous fluid we can take the fluid shear modulus to be $i\omega\eta$ (Walsh, 1969) where ω is the wave frequency. Equations (3.52) and (3.63) then allow us to define the quantity T^s as,

$$T^s = 2T_{1313} = \frac{\frac{\mu}{\mu - i\omega\eta}}{\frac{i\omega\eta}{\mu - i\omega\eta} + \frac{2-v}{1-v}\frac{\pi}{2}r} \tag{3.64}$$

3.3 The inclusion at constant pressure

It is frequently of interest to study the deformation of an inclusion containing fluid which will be kept at constant pressure by some unspecified pumping or draining process. Under these circumstances the use of the Wu T tensor is inappropriate, since the deformation depends on the pressure inside the inclusion and not the bulk modulus of the fluid.

To solve this problem we proceed in the same way as in the previous section, the only difference being that the stress in the inclusion, σ^{inc} is replaced by the constant hydrostatic pressure $p\delta$.

Equating stress in the two problems once again:

$$p\delta = \sigma^{\infty} + \sigma^c - \sigma^T; \tag{3.65}$$

which may be expressed as:

$$\epsilon^T = (I - S)^{-1}C^{-1}(\sigma^{\infty} - p\delta). \tag{3.66}$$

The strain in the inclusion is therefore:

$$\epsilon^{inc} = \epsilon^{\infty} + S(I - S)^{-1}C^{-1}(\sigma^{\infty} - p\delta); \tag{3.67}$$

which we rewrite as:

$$\epsilon^{inc} = (I - S)^{-1}C^{-1}[\sigma^{\infty} - CSC^{-1}p\delta]. \tag{3.68}$$

Zatsepin & Crampin (1997) introduce the notation:

$$P_r = SC^{-1}; \tag{3.69}$$

and refer to P_r as the singular part of the second derivative of the Green's function. With this convention we have:

$$\epsilon^{inc} = (I - P_rC)^{-1}C^{-1}(\sigma^{\infty} - CP_rp\delta); \tag{3.70}$$

in agreement with the formula presented by Zatsepin & Crampin (1997).

It will be necessary later to have an explicit form of equation (3.68) for the cases of a sphere and spheroid of small aspect ratio. Beginning with the sphere:

$$(I - S) = \frac{1}{15(1-v)} \begin{bmatrix} 8-10v & 1-5v & 1-5v & 0 & 0 & 0 \\ 1-5v & 8-10v & 1-5v & 0 & 0 & 0 \\ 1-5v & 1-5v & 8-10v & 0 & 0 & 0 \\ 0 & 0 & 0 & 7-5v & 0 & 0 \\ 0 & 0 & 0 & 0 & 7-5v & 0 \\ 0 & 0 & 0 & 0 & 0 & 7-5v \end{bmatrix}; \tag{3.71}$$

and so $(I - S)^{-1}$ will be given by the expression:

$$\frac{3(1-v)}{2(1-2v)(7-5v)}\begin{bmatrix} 9-15v & 5v-1 & 5v-1 & 0 & 0 & 0 \\ 5v-1 & 9-15v & 5v-1 & 0 & 0 & 0 \\ 5v-1 & 5v-1 & 9-15v & 0 & 0 & 0 \\ 0 & 0 & 0 & 10(1-2v) & 0 & 0 \\ 0 & 0 & 0 & 0 & 10(1-2v) & 0 \\ 0 & 0 & 0 & 0 & 0 & 10(1-2v) \end{bmatrix}. \tag{3.72}$$

Convolving this result with the elastic compliance tensor we find that $(I-S)^{-1}C^{-1}$ may be written as:

$$(I-S)^{-1}C^{-1} = \frac{3(1-v)}{4\mu(7-5v)(1-2v)}X; \tag{3.73}$$

where X is the tensor:

$$\begin{bmatrix} \frac{(1-2v)(9+5v)}{1+v} & \frac{(2v-1)(1+5v)}{1+v} & \frac{(2v-1)(1+5v)}{1+v} & 0 & 0 & 0 \\ \frac{(2v-1)(1+5v)}{1+v} & \frac{(1-2v)(9+5v)}{1+v} & \frac{(2v-1)(1+5v)}{1+v} & 0 & 0 & 0 \\ \frac{(2v-1)(1+5v)}{1+v} & \frac{(2v-1)(1+5v)}{1+v} & \frac{(1-2v)(9+5v)}{1+v} & 0 & 0 & 0 \\ 0 & 0 & 0 & 10(1-2v) & 0 & 0 \\ 0 & 0 & 0 & 0 & 10(1-2v) & 0 \\ 0 & 0 & 0 & 0 & 0 & 10(1-2v) \end{bmatrix}. \tag{3.74}$$

If p_v is the volume of the sphere and p_v^0 is the unstressed volume we have:

$$p_v = p_v^0(1-\epsilon_{ii}^{inc}); \tag{3.75}$$

and if the fluid is kept at zero pressure we then have:

$$p_v = p_v^0(1-\frac{3}{4\mu}\frac{1-v}{1+v}\sigma_{ii}). \tag{3.76}$$

Otherwise we note that:

$$CSC^{-1}\delta = \frac{1}{3}\frac{1+v}{1-v}(1,1,1,0,0,0); \tag{3.77}$$

so that in general:

$$p_v = p_v^0(1 - \frac{3}{4\mu}\frac{1-v}{1+v}\sigma_{ii} + \frac{3}{4\mu}p). \tag{3.78}$$

If we introduce the relationship between density and pressure in the fluid:

$$\rho_f = \frac{\rho_0}{1 - pc_f}; \tag{3.79}$$

where ρ_0 is the unstressed fluid density and c_f the fluid compressibility, then for small pressure and stress variations the mass in each pore may be written as:

$$m_p = \rho_f p_v = \rho_0 p_v^0[1 - \frac{3}{4\mu}\frac{1-v}{1+v}\sigma_{ii} + (\frac{3}{4\mu} + c_f)p]; \tag{3.80}$$

so that if:

$$K_p = \frac{4\mu c_f}{3}; \tag{3.81}$$

$$m_p^0 = \rho_0 p_v^0; \tag{3.82}$$

we may write this as:

$$m_p = m_p^0 + \frac{3m_p^0}{4\mu}[(1 + K_p)p - \frac{1-v}{1+v}\sigma_{ii}]. \tag{3.83}$$

We now perform the same calculation for cracks. For this case:

$$(I - S) = X_1 + O(r^2); \tag{3.84}$$

where the tensor X_1 is given by:

$$\begin{bmatrix} 1-\frac{13-8v}{32(1-v)}\pi r & \frac{1-8v}{32(1-v)}\pi r & \frac{1-2v}{8(1-v)}\pi r & 0 & 0 & 0 \\ \frac{1-8v}{32(1-v)}\pi r & 1-\frac{13-8v}{32(1-v)}\pi r & \frac{1-2v}{8(1-v)}\pi r & 0 & 0 & 0 \\ \frac{-v}{1-v}+\frac{1+4v}{8(1-v)}\pi r & \frac{-v}{1-v}+\frac{1+4v}{8(1-v)}\pi r & \frac{1-2v}{4(1-v)}\pi r & 0 & 0 & 0 \\ 0 & 0 & 0 & \frac{2-v}{1-v}\frac{\pi}{2}r & 0 & 0 \\ 0 & 0 & 0 & 0 & \frac{2-v}{1-v}\frac{\pi}{2}r & 0 \\ 0 & 0 & 0 & 0 & 0 & 1-\frac{7-8v}{16(1-v)}\pi r \end{bmatrix}. \tag{3.85}$$

From this we deduce that:

$$(I-S)^{-1} = \frac{4}{\pi r}\begin{bmatrix} 0 & 0 & 0 & 0 & 0 & 0 \\ 0 & 0 & 0 & 0 & 0 & 0 \\ \frac{v(1-v)}{1-2v} & \frac{v(1-v)}{1-2v} & \frac{(1-v)^2}{1-2v} & 0 & 0 & 0 \\ 0 & 0 & 0 & \frac{2(1-v)}{2-v} & 0 & 0 \\ 0 & 0 & 0 & 0 & \frac{2(1-v)}{2-v} & 0 \\ 0 & 0 & 0 & 0 & 0 & 0 \end{bmatrix} + O(1); \tag{3.86}$$

and so:

$$(I-S)^{-1}C^{-1} = \frac{2(1-v)}{\pi\mu r}\begin{bmatrix} 0 & 0 & 0 & 0 & 0 & 0 \\ 0 & 0 & 0 & 0 & 0 & 0 \\ 0 & 0 & 1 & 0 & 0 & 0 \\ 0 & 0 & 0 & \frac{2}{2-v} & 0 & 0 \\ 0 & 0 & 0 & 0 & \frac{2}{2-v} & 0 \\ 0 & 0 & 0 & 0 & 0 & 0 \end{bmatrix} + O(1). \tag{3.87}$$

If we now introduce the notation (Zatsepin & Crampin 1997):

$$\sigma_c = \frac{\pi\mu r}{2(1-v)}; \tag{3.88}$$

then the volume of a crack with fluid at zero pressure is given by:

$$c_v = c_v^0(1 - \frac{\sigma_{33}}{\sigma_c}). \tag{3.89}$$

Noting that:

$$CSC^{-1}\delta = (\frac{v}{1-v}, \frac{v}{1-v}, 1, 0, 0, 0); \tag{3.90}$$

we see that in general:

$$c_v = c_v^0(1 - \frac{\sigma_{33}}{\sigma_c} + \frac{p}{\sigma_c}). \tag{3.91}$$

If we write

$$K_c = \sigma_c c_f; \tag{3.92}$$

$$m_c^0 = \rho_o c_v^0; \tag{3.93}$$

then the fluid mass in a crack is given by:

$$m_c = m_c^0 + \frac{m_c^0}{\sigma_c}[(1 + K_c)p - \sigma_{33}]. \tag{3.94}$$

3.4 Calculation of the effective elastic tensor.

General methods exist (Voigt, 1928; Reuss, 1929; Hashin and Shtrikman, 1963) for placing upper and lower bounds on the effective elastic moduli of composite materials in terms of the relative volume concentrations and elastic moduli of the various constituents. These bounds reflect uncertainty in the geometry of the configuration. When it is assumed that the composite material consists of a linearly elastic frame interspersed with ellipsoidal inclusions, the results just derived can be utilised to provide more accurate calculations for the effective elastic tensor. If one specifies the positions of all the inclusions the effective tensor can in principle be calculated exactly, but the computational difficulty of the procedure and the fact that in practice one will not know the relative positions of the inclusions has led to the adoption of more simplified methods. Eshelby (1957) gave two methods for computing the elastic tensor; the volumetric averaging procedure and the interaction energy approach.

The volumetric averaging procedure begins with the definition of the average stress and strain fields in the composite. We assume that there exists a length scale, l say, which is large compared to the size of the individual cracks and pores but which is still small compared to the wavelength of the seismic wave under consideration. We now consider a representative cube with volume $V = l^3$, and define the average stress and strain in the cube to be:

$$< \sigma_{ij} >= \frac{1}{V} \int_V \sigma_{ij}(x) dx; \tag{3.95}$$

$$< \epsilon_{ij} >= \frac{1}{V} \int_V \epsilon_{ij}(x) dx. \tag{3.96}$$

The effective elastic tensor is now defined as the linear transformation between $< \epsilon_{ij} >$ and $< \sigma_{ij} >$:

$$< \sigma_{ij} >= C_{ijkl} < \epsilon_{kl} >; \tag{3.97}$$

and the velocities in the composite material may be calculated from the effective tensor in the usual way.

In general the stress and strain fields $\sigma_{ij}(x)$ and $\epsilon_{ij}(x)$ will be extremely complicated functions of position and the explicit computation of the integrals (3.95) and (3.96) is out of the question. For an isotropic medium equation (3.97) may be rearranged as:

$$\begin{aligned} \lambda_{eff} < \epsilon_{kk} > \delta_{ij} + 2\mu_{eff} < \epsilon_{ij} > \; &= \; \lambda_m < \epsilon_{kk} > +2\mu < \epsilon_{ij} > \\ &+ \sum_i \frac{1}{V_i} \int_{V_i} (\sigma_{ij}^{inc} - \lambda_m \delta_{ij} \epsilon_{kk}^{inc} + 2\mu \epsilon_{ij}^{inc}); \end{aligned} \tag{3.98}$$

where λ_m and μ are the standard elastic constants for the matrix, λ_{eff} and μ_{eff} are those of the effective medium and the inclusions are indexed by i.

We now make the dilute concentration assumption to simplify the computation. Specifically we assume that the spatially varying strain field in the matrix can be replaced by a constant strain field, and that each inclusion behaves exactly as if it were the only inclusion embedded in a homogeneous matrix subjected to the application of the constant strain field at infinity. It must be emphasised that this is a drastic assumption, and one that cannot be realized physically.

The stress and strain in each inclusion can now be computed from the Wu T tensor:

$$\epsilon_{ij}^{inc} = T_{ijkl}^{(i)} < \epsilon_{kl} >; \tag{3.99}$$

$$\sigma_{ij}^{inc} = C_{ijkl}^{(i)} \epsilon_{kl}^{inc}. \tag{3.100}$$

One can then find λ_{eff} and μ_{eff} by letting $< \epsilon_{ij} >$ have first $< \epsilon_{12} >= 1$ and all other components equal to zero and then $< \epsilon_{11} >= 1$ with all other components zero.

It is equally possible to repeat the above argument for the compliances, C^{-1}_{ijkl}, assuming a constant stress field in the solid. This is a different assumption and naturally gives a slightly different answer.

An alternative method for the calculation of the effective elastic tensor comes through Eshelby's interaction energy approach. This is essentially an elegant mathematical trick to overcome the problem of the spatial variability of the elastic field in the matrix. It assumes once again that there is only a small concentration of inclusions, but it has at least the advantage of being exact for the case of a single inclusion in an infinite matrix. The following derivation follows Christensen (1980).

We consider two otherwise identical volumes of matrix, one of which contains an ellipsoidal inclusion the other of which does not. Both volumes are loaded with identical surface tractions. The elastic energy in the volume without the inclusion, problem (a), is given by:

$$U_0 = \frac{1}{2}\int_V \sigma^0_{ij}\epsilon^0_{ij}dx; \tag{3.101}$$

where σ^0 and ϵ^0 are the stress and strain fields in the solid. We will denote the energy in the volume with the inclusion, problem (b), as:

$$U = \frac{1}{2}\int_V \sigma_{ij}\epsilon_{ij}dx. \tag{3.102}$$

By definition we have:

$$U = U_0 + \frac{1}{2}\int_v (\sigma_{ij}\epsilon_{ij} - \sigma^0_{ij}\epsilon^0_{ij})dx. \tag{3.103}$$

An application of the divergence theorem leads to:

$$U = U_0 + \frac{1}{2}\int_S \sigma^0_i(u_i - u^0_i)dS; \tag{3.104}$$

where S is the surface of the volume, σ_i^0 is the i'th component of traction applied to the surface of the volume, which is identical for both problems, and u_i^0 is the i'th component of displacement in problem (a) and u_i that in problem (b).

We now consider a further problem, problem (c). This is identical to problem (a) with the addition of a set of body forces over the region that the inclusion would have occupied designed to ensure that the stress and strain fields outside the area of the inclusion are identical to those in problem (b).

We denote the stress field in problem (c) by $\hat{\sigma} = \sigma^0 + \sigma'$ and similarly for the strain field. The elastic energy in problem (c), $\hat{U}$ is given by:

$$\begin{aligned} \hat{U} &= \frac{1}{2}\int_V \hat{\sigma_{ij}}\hat{\epsilon_{ij}}dx \\ &= \frac{1}{2}\int_V (\sigma_{ij}^0 + \sigma_{ij}')(\epsilon_{ij}^0 + \epsilon_{ij}')dx. \end{aligned} \tag{3.105}$$

If we define furthermore:

$$U_{int} = \frac{1}{2}\int_V (\sigma_{ij}^0\epsilon_{ij}' + \sigma_{ij}'\epsilon_{ij}^0)dx; \tag{3.106}$$

then we find, rearranging and applying the divergence theorem once again:

$$\begin{aligned} U_{int} &= \int_V \sigma_{ij}^0\epsilon_{ij}'dx \\ &= \int_S \sigma_i^0(u_i - u_i^0)dS. \end{aligned} \tag{3.107}$$

Equation 3.104 now gives:

$$U = U_0 + \frac{1}{2}U_{int}. \tag{3.108}$$

This expression for U_{int} may be manipulated into a convenient form. We now define Σ to be any closed surface within the volume which contains the inclusion.

V is therefore divided into two regions, V_1 and V_2 lying inside and outside Σ. We may therefore write:

$$\begin{aligned} U_{int} &= \int_{V_1} \sigma^0_{ij}\epsilon'_{ij}dx + \int_{V_2} \sigma^0_{ij}\epsilon'_{ij}dx \\ &= \int_{V_1} \sigma^0_{ij}\epsilon'_{ij}dx + \int_{V_2} \sigma'_{ij}\epsilon^0_{ij}dx. \end{aligned} \tag{3.109}$$

An application of the divergence theorem now gives:

$$U_{int} = \int_S \sigma'_i u^0_i dS - \int_\Sigma \sigma'_{ij} u^0_i d\Sigma + \int_\Sigma \sigma^0_i u'_i d\Sigma. \tag{3.110}$$

Provided that the surface of the volume is far away from the inclusion, we may take $\sigma'_i = 0$ on S. This gives:

$$U_{int} = \int_\Sigma (\sigma^0_i u'_i - \sigma'_i u^0_i) d\Sigma. \tag{3.111}$$

Since problems (b) and (c) are identical outside the inclusion we have, after some rearrangement:

$$U_{int} = \int_\Sigma (\sigma^0_i u_i - \sigma_i u^0_i) d\Sigma. \tag{3.112}$$

The surface Σ may be chosen to be the surface of the inclusion, in which case we have, employing the divergence theorem once again:

$$\begin{aligned} U &= U_0 + \frac{1}{2}\int_{S_{inc}} (\sigma^0_i u_i - \sigma_i u^0_i) dS_{inc} \\ &= U_0 + \frac{1}{2}\int_{V_{inc}} (\sigma^0_{ij}\epsilon_{ij} - \sigma_{ij}\epsilon^0_{ij}) dx. \end{aligned} \tag{3.113}$$

This formula generalises for the case of multiple inclusions:

$$U = U_0 + \frac{1}{2}\sum_i \int_{V_i} (\sigma^0_{ij}\epsilon_{ij} - \sigma_{ij}\epsilon^0_{ij}) dx. \tag{3.114}$$

An identical argument under the assumption of constant displacement, rather than traction, on the surface of the representative volume leads to the formula:

$$U = U_0 - \frac{1}{2}\sum_i \int_{V_i} (\sigma^0_{ij}\epsilon_{ij} - \sigma_{ij}\epsilon^0_{ij})dx. \tag{3.115}$$

We now define the effective elastic constants through the concept of energy equivalence. Consider once again the representative cube consisting of the matrix material interspersed with the inclusions. Under the application of specified surface displacements u^0, equation (3.115) permits the calculation of the elastic energy in the representative cube. The equivalent homogeneous medium, whose elastic tensor will be the effective elastic tensor of the composite, is defined to be the homogeneous material which will contain the same elastic energy as the composite when subjected to identical surface tractions. Since the equivalent medium is homogeneous, the elastic fields will be identical at all points in the cube and the elastic energy U_{EQ} is given by:

$$U_{EQ} = \frac{V}{2} C_{ijkl}\epsilon^0_{ij}\epsilon^0_{kl}; \tag{3.116}$$

where C_{ijkl} is the effective elastic tensor.

The effective tensor can now be calculated exactly provided we know the state of stress and strain inside each inclusion. For this we once again make the dilute concentration assumption, treating each inclusion as if it were embedded in an infinite homogeneous matrix subjected to a stress field σ^0 at infinity.

To find the effective shear modulus we take:

$$\epsilon^0 = \begin{bmatrix} 0 & 0 & s \\ 0 & 0 & 0 \\ s & 0 & 0 \end{bmatrix}. \tag{3.117}$$

for some s. Equating energy in the two problems now gives, noting that stress and strain are constant within each inclusion:

$$\frac{V}{2}C_{ijkl}\epsilon^0_{ij}\epsilon^0_{kl} = \frac{V}{2}E_{ijkl}\epsilon^0_{ij}\epsilon^0_{kl} - \frac{1}{2}\sum_t V_t(\sigma^0_{ij}\epsilon_{ij} - \sigma_{ij}\epsilon^0_{ij}); \tag{3.118}$$

where C is the effective elastic tensor and E is the elastic tensor of the matrix material. This may be simplified to:

$$\mu_{eff} = \mu - \frac{1}{4s^2}\sum_t \phi_t(\sigma^0_{ij}\epsilon_{ij} - \sigma_{ij}\epsilon^0_{ij}); \tag{3.119}$$

where ϕ_t is the fractional volume of the t'th inclusion. Since $\sigma^0_{ij} = E_{ijkl}\epsilon^0_{kl}$ the effective shear modulus follows directly when we calculate the stress and strain in each inclusion from the Wu T tensor.

If we take:

$$\epsilon^0 = \begin{bmatrix} s & 0 & 0 \\ 0 & 0 & 0 \\ 0 & 0 & 0 \end{bmatrix}; \tag{3.120}$$

an expression for the effective P-wave modulus follows as:

$$M_{eff} = M - \frac{1}{s^2}\sum_t \phi_t(\sigma^0_{ij}\epsilon_{ij} - \sigma_{ij}\epsilon^0_{ij}); \tag{3.121}$$

where $M = \lambda + 2\mu$.

A substantial amount of effort has been devoted to attempts to overcome the necessity of invoking the dilute concentration assumption (Watt et al., 1975). This is worthwhile since the dilute concentration assumption is almost certainly incorrect for high porosity rocks. However I note once again that the effective elastic constants depend on the precise details of the geometric distributions of the inclusions, and none of these methods require this distribution as an input. It therefore follows that in all cases the dilute concentration assumption has been replaced with a different assumption, and this new assumption is generally no more correct than the dilute assumption. I now briefly review some of the main methods.

The self-consistent scheme (Hill, 1965; Wu, 1966; Budiansky & O'Connell, 1976; Korringa et al., 1979) proposes a simple alternative to the dilute assumption. Instead of assuming that each inclusion is embedded in an infinite volume of matrix material it is assumed that the inclusions are embedded in an infinite volume of the composite material. Specifically when we invoke the Wu T tensor for the calculation of the elastic field in each inclusion we replace C with C_{eff} and S with S_{eff}, where the Poisson ratio of the composite is used in the calculation of S_{eff}, in equation (3.63), so that:

$$T = [I + S_{eff}C_{eff}^{-1}(C^I - C_{eff})]^{-1}. \tag{3.122}$$

When this adjustment is made to either the volumetric averaging procedure or the interaction energy approach we naturally find coupled equations for the effective moduli which usually have to be solved numerically. It must be noted that the mathematical derivation of both these procedures relied on the fact that the inclusion was embedded in the matrix material and the derivations are therefore no longer strictly valid. Christensen (1980) dismissed the self-consistent scheme as physically unreasonable.

The concept of the differential medium theory (Norris, 1985) comes once again from equations (3.98) and (3.118), both of which are of the form:

$$C_{ijkl}^{eff} = C_{ijkl}^{m} + \sum_t P(t); \tag{3.123}$$

where P(t) depends on the deformation of each inclusion. In the differential effective medium theory one begins with the matrix material and instead of immediately forming the sum of P over all inclusions one adds the inclusions one at a time, with the effective tensor calculated after the first step taking the place of the matrix tensor when the second inclusion is added, and so on. Since the inclusions are small compared to the representative volume the process can be formulated as a differential equation. One finds coupled differential equations of the effective shear and bulk moduli which may be solved numerically. The final values of the effective moduli depend on the order in which the inclusions are added.

Hudson (1980, 1981) uses scattering theory to find the elastic moduli of materials permeated with thin ellipsoidal penny shaped cracks. His results are valid to second order in the number density of cracks, ϵ, where:

$$\epsilon = \frac{Na^3}{V}; \tag{3.124}$$

a being the crack radius and N the number of cracks in a volume V. Hudson (1991) suggests that the model is accurate for crack densities up to 0.1. Hudson gives results for cracks with a variety of interior conditions; dry, containing fluid and filled with a weak material. Kuster and Toksoz (1974) give results from scattering theory for inclusions of arbitrary aspect ratio, but their results are only valid for dilute conditions and isotropic distributions of inclusions.

The strength of Hudson's work lies in the possibility it affords to construct crack distributions which will account for a given seismic anisotropy. However, the lack of porosity in the model means that it would be inadvisable to use it to carry out fluid substitution for a porous rock. Frequency does not appear as a parameter in the theory, but if one were to require elastic moduli under the assumption of perfect pressure equalisation it would be possible to calculate the results for dry cracks from Hudson's model and enter these into the Brown and Korringa (1975) formulae (Mavko et al., 1998).

3.5 Conclusions

Eshelby (1957) gives rigorous results for the elastic field of an ellipsoidal inclusion subjected to a constant stress and strain at infinity, and a straightforward extension of his analysis gives dependence on pore fluid pressure when this is determined independently by some unspecified physical process.

I consider all the techniques for calculating velocities from Eshelby's results to be only rough approximations. All the methods rely on physical assumptions which are most unlikely to apply to real rocks. It is impossible to say definitely

which method will give the best results. In my later work I will use the interaction energy approach in view of its computational simplicity, and the fact that the assumption on which it is based, that of a dilute concentration of inclusions, can be easily stated and understood.

All the velocity models considered relied on the assumption that fluid did not leave individual cracks and pores as the seismic wave propagated. This is of course in contradiction to the assumption of the Biot-Gassmann poroelastic theory. The advantage of the Eshelby based velocity models over poroelastic theory is that they allow velocities to be interpreted in terms of the rock microstructure, which is ignored in the Biot-Gassmann theory.

Chapter 4

Dispersive effective medium theories.

Summary: I survey a number of methods for placing fluid flow into Eshelby based effective medium theory. A number of contradictions exist between the various approaches. All the models show viscoelastic behaviour, they are not consistent with Biot's prediction of a slow compressional wave. Results of Endres and Knight (1997), while limited in their scope, provide a mathematically rigorous foundation for analysing the differences between the various models and a basis for further progress.

4.1 The model of O'Connell and Budiansky, 1977

O'Connell and Budiansky (1977) made the first systematic attempt to incorporate fluid motion into an Eshelby based effective medium theory. They analysed wave propagation in an elastic solid permeated with fluid saturated cracks of small aspect ratio, giving frequency dependent expressions for the bulk and shear moduli.

When the rock is subjected to hydrostatic stress, the pressure in each crack will be identical and there is no reason for fluid flow to take place. This leads to frequency independent behaviour. In the limit:

$$\frac{\kappa_m r}{\kappa_f} \ll 1; \tag{4.1}$$

when cracks are isolated with respect to fluid flow, the cracks have a very small effect on the compressibility of the rock. This leads O'Connell and Budiansky to conclude that:

$$\kappa_{sat} = \kappa_m; \tag{4.2}$$

independently of frequency.

The situation with the shear modulus is different. A pure shear applied to the rock sample will induce a different pressure in each crack according to its orientation. Inter-crack pressure gradients may then be expected to exist, and this will give rise to squirt flow. O'Connell and Budiansky model the dilatation, θ, in a crack as:

$$\frac{d\theta}{dt} = \frac{d\tilde{\sigma}}{dt} + \frac{4r^3a^3\tilde{\sigma}}{\eta}; \tag{4.3}$$

where $\tilde{\sigma}$ is the normal stress acting on the crack, η is the viscosity of the fluid and a is the crack radius. The term in $\frac{d\tilde{\sigma}}{dt}$ gives the standard elastic deformation while that in $\tilde{\sigma}$ gives the effect of fluid flow. I note that this equation can hardly be true in general, since if it were fluid would flow out of cracks in response to hydrostatic stress, in contradiction of the earlier assumption.

With this arrangement a self-consistent scheme is applied, and they obtain a frequency dependent shear modulus. The precise nature of the frequency dependence is given by the critical squirt flow frequency, ω_1:

$$\omega_1 = \frac{\kappa_m r^3}{\eta}. \tag{4.4}$$

This parameter controls the frequency at which the transition from low to high frequency regimes occurs. When a range of different aspect ratios are present one has a corresponding range of characteristic frequencies. O'Connell and Budiansky argue that the effects of these characteristic frequencies should be added together

linearly and independently. In this way the shape of the dispersion curve depends directly on the shape of the aspect ratio spectrum.

O'Connell and Budiansky find also that their model predicts the existence of a "viscous relaxation" effect above a certain frequency at which the shear stresses in fluid in individual cracks cease to relax. This effect has previously been studied by Walsh (1969). The critical frequency associated with this effect is:

$$\omega_2 = \frac{\mu r}{\eta}; \tag{4.5}$$

where clearly $\omega_2 \gg \omega_1$. O'Connell and Budiansky conclude that ω_2 is generally too high for the Walsh effect to be of practical interest.

Since a wide range of crack aspect ratios may be expected to be present in any particular rock sample, one would expect on the basis of this model that dispersion would be spread over a very wide frequency range. In particular, one would not expect to see the sharp peaks in attenuation which were observed by Nur and Simmons (1969) and Gordon (1974). O'Connell and Budiansky accept that it is hard to explain these observations in the framework of their model. The anomaly has been confirmed and discussed by Jones (1986) and Sams et al. (1997).

I find the results relating to distributions of aspect ratios rather unconvincing. The assumption which leads directly to these results is equation (4.3). I have already pointed out that this equation appears not to hold when the applied stress is hydrostatic, which is unsatisfactory. It is clear also that this assumption would lead to a violation of mass conservation if the crack distribution were anisotropic, as I now show.

Consider a rock under shear which contained only two cracks. Let the first be oriented so that the normal stress acting on it was zero, and let the second be oriented so that it felt non-zero compression. Equation (4.3) applied to the first crack states that no flow takes place into or out of this crack, but when applied to the second crack it states that flow takes place out of this crack. Both of these statements cannot be correct. It follows that equation (4.3) does not

adequately describe the flow of fluid between cracks and should therefore be treated with caution. I argue that the consideration of the effect of distributed aspect ratios should be analysed in the framework of a model which does not share this shortcoming.

The model takes no account of the effect of equant pores in the rock, which would lead to flow between cracks and pores under compression. O'Connell and Budiansky's analysis leads only to viscoelastic behaviour, there is no prediction of a slow compressional wave.

Johnston et al. (1979) give results similar to O'Connell and Budiansky's but in their model the driving mechanism is flow between thin cracks and spherical pores. Velocities and attenuations are calculated from the Kuster and Toksoz (1974) model, where the fluid bulk modulus is assigned a frequency dependent imaginary part. They find that the characteristic frequency for their mechanism is proportional to the square of the crack aspect ratio, but they do not consider the case where a range of aspect ratios are present. Their model predicts that when no pores are present there is no dispersion in either the bulk or shear modulus.

4.2 The model of Hudson et al., 1996

The paper Hudson et al. (1996) represents an attempt to incorporate a detailed fluid dynamical description into the Hudson model (Hudson 1980, 1981). Despite the detailed nature of the mathematical description, some anomalies remain in the predictions of the model.

The basis of the method of Hudson et al. (1996) lies in the distinction between the pore scale of the individual inclusions and some larger scale over which the rock is considered to be homogeneous. On this larger scale Hudson et al. (1996) write the standard equation for conservation of fluid mass, [4]:

$$\frac{d}{dt}(\int_V \rho_f \phi dV) = -\int_S \rho_f w.ndS; \tag{4.6}$$

where n is the unit normal to the surface and w is the volume flux. The square braces refer to the equation numbers used in Hudson et al. (1996). The divergence theorem is then applied, yielding, [5]:

$$\frac{\partial}{\partial t}(\rho_f \phi) = -\nabla.(\rho_f w). \tag{4.7}$$

The volume flux w is assumed to follow D'Arcy's law, [6]:

$$w = -\frac{k}{\eta}\nabla p; \tag{4.8}$$

where p is the average pressure; k the permeability; and η the viscosity so that they have, [7]:

$$\frac{\partial}{\partial t}(\rho_f \phi) = \nabla.(\rho_f \frac{k}{\eta}\nabla p). \tag{4.9}$$

There must be an implicit assumption of a relationship between porosity and permeability in this equation. Otherwise the application of D'Arcy's law in this way would mean that the volume flux through a macroscopic surface element would be independent of the microstructural porosity of the rock. In effect if one doubled the porosity of the rock the flow out of a macroscopic volume element for any given pressure gradient would be unchanged.

On the microscale, the response of the porosity associated with any given crack shape to stress and pressure variations is given by, [11]:

$$\phi = \phi^0 + \phi^1(\sigma + p^{inc}I) - \frac{\phi^0 p^{inc}}{\kappa_m}; \tag{4.10}$$

where ϕ^0 is the unstressed porosity, ϕ^1 a 3×3 matrix and p^inc is the pressure in the inclusion. Variations in fluid density with pressure are accounted for with the equation, [8]:

$$\frac{\rho_0}{\rho^{inc}} - 1 = -\frac{p^{inc}}{\kappa_f}; \tag{4.11}$$

where ρ_0 is the unstressed fluid density.

If we consider firstly the case where inclusions of only one shape and orientation are present, the pressure in each inclusion in the macroscopic volume element will be identical. In this case, and working to first order throughout, equation (4.9) is made to read, [13]:

$$\phi^1 \frac{\partial \sigma}{\partial t} + \frac{\partial p}{\partial t}(\phi^1_{kk} + \frac{\phi^0}{\kappa_f} - \frac{\phi^0}{\kappa_m}) = \frac{k}{\eta}\nabla^2 p. \tag{4.12}$$

This equation gives the relationship between pore pressure and the stress field of the propagating wave when the fluid is permitted to move in response to the pressure gradients induced by the propagation of the wave. Two considerable complications ensue when more than one type of inclusion is permitted. Firstly each family of inclusions within the same volume element will be at a different pressure. Secondly flow will take place within the volume element between inclusions of different shapes and orientations as well as flow into and out of the volume element itself.

Since the pressure is different in each inclusion, Hudson et al. introduce the notation p^n for the pressure in the nth family of inclusions. Additionally however, he also introduces an overall or local average pressure p_f. With this arrangement they model the fluid motion with the equations, [19], [18], [28]:

$$\frac{\partial}{\partial t}(\rho_f \phi_n) = -\frac{\phi^0_n \rho_0}{\kappa_f \tau}(p^n - p_f); \tag{4.13}$$

$$m_f = \sum_n \phi_n \rho^n_f; \tag{4.14}$$

$$\frac{\partial m_f}{\partial t} = \nabla.(\rho_f \frac{k}{\eta}\nabla p_f); \tag{4.15}$$

τ being a time-scale parameter, where it is assumed that, [17]:

$$\phi_n = \phi_n^0 + \phi_n^1(\sigma + p^n I) - \frac{\phi_n^0 p^n}{\kappa_m}. \tag{4.16}$$

At first sight this is a very appealing arrangement. Fluid flows between cracks in the same volume element due to pressure gradients resulting from different geometries and orientations, and out of the volume element due to the gradient of the average pressure field. Nevertheless I consider that this system of equations is problematic.

The problem stems from the definition of the average pressure p_f. If p_f were a simple arithmetic average over p^n, then equations (4.13) and (4.14) together would immediately give the result for cracks of only one shape:

$$\frac{\partial m_f}{\partial t} = -\frac{\phi^0 \rho_0}{\kappa_f \tau} \sum_n (p^n - p_f) = 0; \tag{4.17}$$

in direct contradiction of equation (4.15).

It is clear then that p_f cannot be the mean pressure in the volume element. Of course if the volume element were considered to be sealed then (4.13) and (4.14) would be correct provided that p_f was the equilibrium pressure defined by Zatsepin & Crampin (1997). This suggests that the correct interpretation of the model is for p_f to be a fictitious equilibrium pressure based on the fluid mass in the element at any particular time. However fluid should flow out of the element in response to the spatial gradient in the physical pressure rather than the spatial gradient of a fictitious pressure, so there appears to be no justification for the presence of p_f in equation (4.15).

These concerns can be made more specific with an example. I will now show that in the special case of two identical sets of cracks the more general method of Hudson et al. (1996) gives results which contradict their earlier results.

I consider that there are two families of cracks which I shall denote ϕ_1 and ϕ_2. I next assume that these sets of cracks are identical, so that the physical problem is exactly the same as that which led to equation (4.12), and notationally the same if I write:

$$\phi = \phi_1 + \phi_2; \tag{4.18}$$

etc. Clearly I must have $p^1 = p^2 = p$. If however $p_f = p$ then (4.13) and (4.14) would immediately give $\dot{m}_f = 0$, in contradiction to (4.15) and indeed(4.9). In fact:

$$p_f = p + \frac{\phi_1^0 \rho_0}{\kappa_f \tau} \frac{\partial}{\partial t}(\rho_f \phi_1); \tag{4.19}$$

so that (4.15) becomes:

$$\phi^1 \frac{\partial \sigma}{\partial t} + \frac{\partial p}{\partial t}(\phi^1_{kk} + \frac{\phi^0}{\kappa_f} - \frac{\phi^0}{\kappa_m}) = \frac{k}{\eta} \nabla^2 [p + \frac{\tau \kappa_f}{\phi^0 \rho_0} \{\phi^1 \frac{\partial \sigma}{\partial t} + \frac{\partial p}{\partial t}(\phi^1_{kk} + \frac{\phi^0}{\kappa_f} - \frac{\phi^0}{\kappa_m})\}]. \tag{4.20}$$

This equation is not the same as (4.12), even though the physical problems are identical and all the variables have exactly the same meaning.

In the model just described pore space is considered to consist entirely of microcracks. This rules out the mechanism examined by Mavko and Jizba (1991) where fluid flows from compliant cracks to stiffer, more rounded, pores. To address this issue Hudson et al. (1996) formulate an "equant porosity" model, for rocks containing cracks and much smaller pores.

The driving mechanism of the model is pressure diffusion from the crack into the smaller pores. No attempt is made to model explicitly the behaviour of the pores and there is no account taken of mass balance between the cracks and pores. The only difference between the equant porosity model and the standard Hudson (1981) model is in the crack opening parameter U_{33}, which gives the response of a crack to normal stress. The result is:

$$U_{33} = \frac{4}{3} \frac{\lambda + 2\mu}{\lambda + \mu} (1 + K)^{-1}; \tag{4.21}$$

where:

$$K = \frac{\kappa_f}{\pi\mu r}\frac{\lambda+2\mu}{\lambda+\mu}[1+3(1-i)J/2c]^{-1}; \tag{4.22}$$

$$J^2 = \frac{\phi_m \kappa_f k}{2\omega\eta}; \tag{4.23}$$

k being the permeability and ϕ_m the porosity associated with the small pores. Note that the expression given for J^2 in Hudson et al. (1996) was in error. This has been corrected in a subsequent paper (Hudson et al., 1999).

When the frequency, ω, is equal to zero the result reduces to exactly that given for dry cracks by Hudson (1981). This means that at zero frequency the saturated rock behaves exactly as if it were dry, in contradiction to Gassmann's theorem. Nevertheless I consider that the model could be extremely useful for the study of rock under partial saturation.

4.3 The model of Endres and Knight, 1997

Endres and Knight (1997), in a substantial generalisation of the paper Budiansky and O'Connell (1980), gave rigorous results for calculating the magnitude of dispersion produced by the squirt flow effect for a range of pore space geometries. Their high frequency elastic moduli are the standard effective medium theory results which assume that no fluid exchange takes place. For the low frequency moduli they assume perfect fluid pressure communication, allowing the magnitude of dispersion to be calculated by a comparison of low and high frequency moduli. They show that their low frequency results are compatible with Gassmann's theorem.

While the formulae which Endres and Knight present are valid for distributions of inclusions with any aspect ratio between zero and one, their analysis of the simple case of a collection of spherical pores and cracks of small aspect ratios shows behaviour which is more complicated than that of any of the models studied so far. This shows clearly the limitations of these models.

In the case where no spherical pores are present, Endres and Knight show that there is no dispersion in bulk. This is because a hydrostatic stress induces the same pressure in each crack with the result that no fluid flow takes place. There is dispersion in the shear modulus, however, since a shear stress will in general induce different pressures in cracks of different orientations, giving scope for fluid flow. This situation cannot occur in the Mavko and Jizba (1991) model or the Dvorkin et al. (1995) model since in these formulations the dispersion in the shear modulus is simply proportional to that in the bulk modulus. The Johnstone et al. (1979) model similarly fails to take account of this possibility.

O'Connell and Budiansky (1977) argue that there is no dispersion in the bulk modulus. In the case where there are both cracks and pores present, Endres and Knight show that in fact there can be substantial dispersion in the bulk modulus because hydrostatic stress induces a higher pressure in the cracks than in the pores, leading to relieving fluid flow.

When there are no cracks present at all there is no dispersion in either bulk or shear, so one could say loosely that it is the cracks which are responsible for the dispersion. Endres and Knight show that the nature of this dispersion is controlled strongly by the accompanying porosity. It follows that a theory which models the behaviour of cracks independently of porosity is likely to be inadequate.

4.4 Conclusions

I have surveyed a range of techniques for incorporating fluid flow into effective medium theory. Substantial disagreement exists between the various approaches over virtually every aspect of the problem. O'Connell and Budiansky (1977) analyse the case in which cracks alone are present and find substantial dispersion in the shear modulus with no dispersion in the bulk modulus, contradicting Johnston et al. (1979) who argue that there is no dispersion whatsoever in the absence of pores and indeed the poroelastic formulation of Mavko and Jizba (1991) who assert that the shear dispersion is always proportional to the bulk dispersion. Hudson et al.

(1996) propose a model for the interactions between cracks and pores but their formulation contradicts Gassmann's theorem. Their model for distributions of cracks cannot handle the existence of pores, and relies on rather unclear averaging procedures.

Endres and Knight (1997) clarify the issue substantially. They give mathematically rigorous results for the magnitude of dispersion as a function of the geometry of the pore space. Their results are not valid for intermediate frequencies between the high and low frequency limits and they cannot calculate attenuation, but they have great value in acting as a constraint on more ambitious models which depend on understanding the interactions between cracks and pores. It remains an open problem to devise a scheme for placing fluid flow into Eshelby theory in such a way as to retain the logic of Endres and Knight (1997) and consistency with the Biot-Gassmann theory of poroelasticity.

A key issue concerns the prediction of O'Connell and Budiansky (1977) that the shape of the dispersion curve is dependent on the shape of the aspect ratio spectrum. The BISQ model (Dvorkin and Nur, 1993) and the Dvorkin et al., (1995) model predict behaviour which is not dependent on the aspect ratio spectrum, largely because they assume dependence on a poorly defined characteristic squirt flow length. Since O'Connell and Budiansky's modelling of the fluid flow processes is rather crude, their prediction concerning the importance of the aspect ratio spectrum should be viewed with caution. The predictive power of their theory is greatly reduced by the need to make an almost arbitrary assumption about the distribution of aspect ratios. Cracks in rock are not perfectly ellipsoidal and so strictly speaking cannot be assigned an aspect ratio. It could be argued that an approach which has such a poorly defined parameter playing a key role will not provide a robust framework in which to analyse the problem of dispersion.

Chapter 5

Derivation of the model.

Summary: I derive a poroelastic model from Eshelby theory. The model is consistent both with Gassmann's theorem and with Biot's prediction of a slow compressional wave. Under mild assumptions the only dependence on crack distributions comes through the single crack density parameter, in contrast to earlier models where the aspect ratio spectrum played a crucial role.

5.1 Fluid dynamics formulation.

In the previous chapter I surveyed attempts by a range of authors to model the effect of fluid flow in the framework of Eshelby theory. No model was fully satisfactory in its description of the fluid dynamics, and no model could reproduce the main results of Biot theory.

To begin my modelling, I consider rock to consist of a linearly elastic solid permeated with 2 kinds of voids; uniformly sized and shaped ellipsoidal cracks of small aspect ratio and uniformly sized spherical pores. The first original feature of the model is that all fluid flow has to take place between one element of pore space and another. This means that for elements a and b I will write independently of shapes and orientations:

$$\partial_t m_a = \frac{\rho_0 k \varsigma}{\eta}(p_b - p_a); \tag{5.1}$$

where m_a is the mass in element a; ρ_0 is the fluid density; k is permeability; ς is the grain size; and p_a is the fluid pressure in element a. I will require this equation to hold equally well if subscripts a and b are interchanged, ensuring the conservation of pore fluid mass.

The purpose of the model is to describe the propagation of plane waves, so I may fix a direction which will be taken to be the direction of the wave. If the pressure distribution in the elements were random, we would expect that the flow resolved in the direction of the wave would be one half of the flow resolved perpendicular to the direction of the wave. This suggests setting up a lattice configuration where each element of pore space at any coordinate x on the axis of wave propagation is considered to be connected to some multiple of 6 other elements, one with coordinate $x - \varsigma$, another with coordinate $x + \varsigma$, and 4 with coordinate x.

At each vertex I wish to randomly place an element of pore space, but must first describe the various orientations which the cracks may take up. Each possible crack orientation may be represented by a point on the surface of the unit sphere. I now partition the surface of the unit sphere into N_c equal elements of area. I will now let:

$$\varpi = \frac{(\phi_c/c_v)}{(\phi_p/p_v)}; \tag{5.2}$$

where ϕ_c is the fraction of the total volume occupied by cracks and c_v is the volume of an individual crack and similarly for pores. I then define:

$$N_p = \frac{N_c}{\varpi}; \tag{5.3}$$

and:

$$N = N_c + N_p. \tag{5.4}$$

Now define a collection of elements C consisting of N_c cracks, each with a different orientation corresponding to one of the elements of the partition, together

with N_p pores. At each vertex of the lattice I will place an element of pore space drawn at random from C.

The expected pressure in the element at any given vertex is now:

$$E[p(x)] = \frac{1}{N}\sum_{j=1}^{N_c} E[p_j(x)] + \frac{N_p}{N}E[p^*(x)]; \tag{5.5}$$

where p_j represents the pressure in a crack of orientation j and p^* is the pressure in the pores.

Assuming that the flow law (5.1) holds between all adjacent vertices of the lattice and that these flows may be added linearly, I write:

$$E[\partial_t m_i(x)] = \frac{4\rho_0 k\varsigma}{\eta}(E[p(x)]-E[p_i(x)])+\frac{\rho_0 k\varsigma}{\eta}(E[p(x+\varsigma)]+E[p(x-\varsigma)]-2E[p_i(x)]). \tag{5.6}$$

Observing no distinction between values and their expectations, the full system may be written in a convenient matrix form:

$$\begin{bmatrix} \dot{m}_1 \\ \vdots \\ \dot{m}_{N_c} \\ \vdots \\ \dot{m}_N \end{bmatrix} = \frac{4\rho_0 k\varsigma}{\eta N}\begin{bmatrix} (1-N) & 1 & 1 & & 1 \\ 1 & (1-N) & 1 & \cdots & 1 \\ 1 & 1 & (1-N) & & 1 \\ & \vdots & & \ddots & \vdots \\ 1 & 1 & 1 & \cdots & (1-N) \end{bmatrix}\begin{bmatrix} p_1 \\ p_2 \\ p_3 \\ \vdots \\ p^* \end{bmatrix}$$
$$+\frac{\rho_0 k\varsigma}{\eta N}\begin{bmatrix} 1 & 1 & 1 & & 1 \\ 1 & 1 & 1 & \cdots & 1 \\ 1 & 1 & 1 & & 1 \\ & \vdots & & \ddots & \vdots \\ 1 & 1 & 1 & \cdots & 1 \end{bmatrix}\begin{bmatrix} p_1(x-\varsigma)+p_1(x+\varsigma) \\ p_2(x-\varsigma)+p_2(x+\varsigma) \\ p_3(x-\varsigma)+p_3(x+\varsigma) \\ \vdots \\ p^*(x-\varsigma)+p^*(x+\varsigma) \end{bmatrix} - \frac{2\rho_0 k\varsigma}{\eta}\begin{bmatrix} p_1 \\ p_2 \\ p_3 \\ \vdots \\ p^* \end{bmatrix}. \tag{5.7}$$

As with all effective medium theories, it is necessary to assume that the wavelength is larger than the grain size. This means that I can write:

$$p_i(x-\varsigma)+p_i(x+\varsigma)=2p_i(x)+\varsigma^2 p_i''(x); \tag{5.8}$$

whereupon if:

$$\bar{p}=\frac{1}{N}\sum_{i=1}^{N}p_i; \tag{5.9}$$

the system transforms to:

$$\begin{bmatrix}\dot{m}_1\\ \dot{m}_2\\ \dot{m}_3\\ \vdots\\ \dot{m}_N\end{bmatrix} = \frac{6\rho_0 k\varsigma}{\eta N}\begin{bmatrix}(1-N) & 1 & 1 & & 1\\ 1 & (1-N) & 1 & \cdots & 1\\ 1 & 1 & (1-N) & & 1\\ & \vdots & & \ddots & \vdots\\ 1 & 1 & 1 & \cdots & (1-N)\end{bmatrix}\begin{bmatrix}p_1\\ p_2\\ p_3\\ \vdots\\ p^*\end{bmatrix} + \frac{\rho_0 k\varsigma^3}{\eta}\begin{bmatrix}\bar{p''}\\ \bar{p''}\\ \bar{p''}\\ \vdots\\ \bar{p''}\end{bmatrix}. \tag{5.10}$$

If I now let:

$$A=\begin{bmatrix}1 & 1 & 1 & & 1\\ 1 & -1 & 0 & \cdots & 0\\ 1 & 0 & -1 & & 0\\ & \vdots & & \ddots & \vdots\\ 1 & 0 & 0 & \cdots & -1\end{bmatrix}; \tag{5.11}$$

then:

$$A\begin{bmatrix}\dot{m}_1\\ \dot{m}_2\\ \dot{m}_3\\ \vdots\\ \dot{m}_N\end{bmatrix} = \frac{6\rho_0 k\varsigma}{\eta}\begin{bmatrix}0 & 0 & 0 & & 0\\ 0 & -1 & 0 & \cdots & 0\\ 0 & 0 & -1 & & 0\\ & \vdots & & \ddots & \vdots\\ 0 & 0 & 0 & \cdots & -1\end{bmatrix} A\begin{bmatrix}p_1\\ p_2\\ p_3\\ \vdots\\ p^*\end{bmatrix}$$
$$+\frac{\rho_0 k\varsigma^3}{\eta} A\begin{bmatrix}\bar{p''}\\ \bar{p''}\\ \bar{p''}\\ \vdots\\ \bar{p''}\end{bmatrix}. \tag{5.12}$$

Now if I write:

$$\bar{m} = \frac{1}{N}\sum_{i=1}^{N} m_i; \tag{5.13}$$

then the first row reads:

$$\dot{\bar{m}} = \frac{\rho_0 k\varsigma^3}{\eta}\bar{p''}; \tag{5.14}$$

and subsequent rows:

$$\dot{m}_1 - \dot{m}_i = \frac{6\rho_0 k\varsigma}{\eta}(p_i - p_1), \qquad 2 \le i \le N. \tag{5.15}$$

Now the choice of subscript 1 is clearly arbitrary, so in general:

$$\dot{m}_i - \dot{m}_j = \frac{6\rho_0 k\varsigma}{\eta}(p_j - p_i), \qquad 1 \le i, j \le N. \tag{5.16}$$

Fixing $j > N_c$ and summing from $i = 1, \cdots, N_c$ I find:

$$< \dot{m} >_c - \dot{m}^* = \frac{6\rho_0 k\varsigma}{\eta}(p^* - < p >_c); \tag{5.17}$$

where:

$$< p >_c = \frac{1}{N_c} \sum_{i=1}^{N_c} p_i; \tag{5.18}$$

$$< m >_c = \frac{1}{N_c} \sum_{i=1}^{N_c} m_i; \tag{5.19}$$

and since the conditions in each pore are identical I have introduced the notation m^* for the mass in each pore. Equation (5.17) describes the exchange of fluid between the cracks and pores.

Now evidently from equations (3.94) and (3.83)

$$< \dot{m} >_c = \frac{c_v \rho_0}{\sigma_c} [(1 + K_c) < \dot{p} >_c - \frac{\dot{\sigma}}{3}]; \tag{5.20}$$

$$\dot{m}^* = \frac{3 p_v \rho_0}{4\mu} [(1 + K_p)\dot{p}^* - \frac{1 - v}{1 + v} \dot{\sigma}]; \tag{5.21}$$

provided that the partition of the unit sphere is taken to be sufficiently refined that $\frac{1}{N_c} \sum_{i=1}^{N_c} \sigma_i = \sigma/3$, where σ_i is the normal stress acting on the i'th crack and σ is the trace of the applied stress tensor. Then with the definitions:

$$\gamma = \frac{3 p_v \sigma_c (1 + K_p)}{4 c_v \mu (1 + K_c)}; \tag{5.22}$$

$$\gamma' = \gamma \frac{1 - v}{1 + v} \frac{1}{1 + K_p}; \tag{5.23}$$

$$\frac{1}{\tau} = \frac{6 k \varsigma \sigma_c}{\eta c_v (1 + K_c)}; \tag{5.24}$$

equation (5.17) may be written as:

$$< \dot{p} >_c - \gamma \dot{p}^* + [\gamma' - \frac{1}{3(1 + K_c)}] \dot{\sigma} = \frac{1}{\tau} (p^* - < p >_c). \tag{5.25}$$

This expression may be integrated, giving:

$$\begin{aligned} < p >_c &= \gamma p^* + [\frac{1}{3(1+K_c)} - \gamma']\sigma \\ &\quad -\frac{1}{\tau}\int_0^t [(\gamma - 1)p^*(s) + (\frac{1}{3(1+K_c)} - \gamma')\sigma(s)]e^{\frac{s-t}{\tau}} ds. \end{aligned} \tag{5.26}$$

Arguing directly from (5.16) with the same logic gives the expression:

$$\begin{aligned} p_i &= \frac{\sigma_i}{1+K_c} + \gamma p^* - \gamma'\sigma \\ &\quad -\frac{1}{\tau}\int_0^t [\frac{\sigma_i(s)}{1+K_c} + (\gamma - 1)p^* - \gamma'\sigma(s)]e^{\frac{s-t}{\tau}} ds. \end{aligned} \tag{5.27}$$

These expressions are appealing since in the limit $\tau \to 0$:

$$\frac{1}{\tau}e^{\frac{s-t}{\tau}} \to \delta(s-t); \tag{5.28}$$

where $\delta(s-t)$ is the Dirac delta function, and so:

$$p_i \to p^*. \tag{5.29}$$

This means that in the limit of immediate pressure relaxation pressure in each crack is identical and the same as that in the pores, in accordance with Gassmann's theory.

So far I have described how the pressure in each element of pore space may be given in terms of the 2 fields, p^* and σ. It is clear that p^* and σ must themselves be coupled. From equations (5.9) and (5.13):

$$\bar{p} = \iota < p >_c + (1-\iota)p^*; \tag{5.30}$$

$$\bar{m} = \iota < m >_c + (1-\iota)m^*; \tag{5.31}$$

where:

$$\iota = \frac{N_c}{N}. \tag{5.32}$$

Noting also:

$$\begin{aligned} < \dot{p} >_c &= \gamma \dot{p^*} + \frac{(1-\gamma)}{\tau} p^* + [\frac{1}{3(1+K_c)} - \gamma'](\dot{\sigma} - \frac{1}{\tau}\sigma) \\ &+ \frac{1}{\tau^2}\int_0^t [(\gamma - 1)p^*(s) + [\frac{1}{3(1+K_c)} - \gamma']\sigma(s)]e^{\frac{s-t}{\tau}} ds; \end{aligned} \tag{5.33}$$

$$\begin{aligned} < p >_c'' &= \gamma p^{*''} + (\frac{1}{3(1+K_c)} - \gamma')\sigma'' \\ &- \frac{1}{\tau}\int_0^t [(\gamma - 1)p^{*''}(s) + (\frac{1}{3(1+K_c)} - \gamma')\sigma''(s)]e^{\frac{s-t}{\tau}} ds; \end{aligned} \tag{5.34}$$

I can write equation (5.14) as:

$$\begin{aligned} &\frac{\iota}{\tau}(1-\gamma)p^* + \gamma \dot{p^*} - \frac{\iota}{\tau}(\frac{1}{3(1+K_c)} - \gamma')\sigma - \gamma'\dot{\sigma} \\ &+ \frac{\iota}{\tau^2}\int_0^t [(\gamma - 1)p^*(s) + (\frac{1}{3(1+K_c)} - \gamma')\sigma(s)]e^{\frac{s-t}{\tau}} ds \\ &= \frac{\varsigma^2}{6\tau}(\iota\gamma + (1-\iota))p^{*''} + \frac{\varsigma^2\iota}{6\tau}(\frac{1}{3(1+K_c)} - \gamma')\sigma'' \\ &- \frac{\varsigma^2\iota}{6\tau^2}\int_0^t [(\gamma - 1)p^{*''}(s) + (\frac{1}{3(1+K_c)} - \gamma')\sigma''(s)]e^{\frac{s-t}{\tau}} ds. \end{aligned} \tag{5.35}$$

This may be reduced to the differential equation:

$$\begin{aligned} &\gamma \ddot{p^*} + \frac{1}{\tau}(\iota + (1-\iota)\gamma)\dot{p^*} - \frac{\varsigma^2}{6\tau}(1 - \iota(1-\gamma))\dot{p}^{*''} - \frac{\varsigma^2}{6\tau^2}p^{*''} \\ &= \gamma'\ddot{\sigma} + \frac{1}{\tau}[\frac{\iota}{3(1+K_c)} + (1-\iota)\gamma']\dot{\sigma} + \frac{\varsigma^2\iota}{6\tau}(\frac{1}{3(1+K_c)} - \gamma')\dot{\sigma}''. \end{aligned} \tag{5.36}$$

This equation gives the required coupling between the fields p^* and σ. Taking the Fourier Transform of equation (5.36) gives the expression:

$$[-(\omega\tau)^2\gamma + i(\omega\tau)(\iota + \gamma(1-\iota)) + \frac{i}{6}(\varsigma y)^2(\omega\tau)(1-\iota(1-\gamma)) + \frac{1}{6}(\varsigma y)^2]\tilde{p} = \quad (5.37)$$
$$[-(\omega\tau)^2\gamma' + i(\omega\tau)[\frac{\iota}{3(1+K_c)} + (1-\iota)\gamma'] - \frac{i}{6}(\varsigma y)^2(\omega\tau)(\frac{\iota}{3(1+K_c)} - \iota\gamma')]\tilde{\sigma};$$

where y is the wavenumber and $\tilde{p}$ and $\tilde{\sigma}$ are the Fourier transforms of p^* and σ respectively.

5.2 The P-wave dispersion equation.

To find the dispersion equation for the propagation of P-waves it is necessary to derive a second equation between p^* and σ. This second equation arises out of a generalisation of Eshelby's approach to finding the effective elastic constants of a solid permeated with inclusions. Eshelby's interaction energy formula for the effective P-wave modulus is (3.121):

$$M_{eff} = M - \frac{1}{s^2}\sum_t \phi_t(\sigma_{ij}^w \epsilon_{ij}^{inc} - \sigma_{ij}^{inc}\epsilon_{ij}^w); \quad (5.38)$$

where the superscript 'w' refers to the field of the travelling wave, superscript 'inc' refers to the field in the inclusion and $s = \epsilon_{11}^w$. In the classical approach to the problem ϵ^{inc} would be calculated using the Wu T tensor:

$$\epsilon^{inc} = T\epsilon^w; \quad (5.39)$$

and then σ^{inc} would follow from:

$$\sigma^{inc} = C^{inc}\epsilon^{inc}. \quad (5.40)$$

These values would be inserted directly into (5.38) to give an effective P-wave modulus as a function of the inclusions' geometry and elastic constants.

In our case, however, the state of stress and strain in the fluid saturated inclusion depend on the details of the fluid dynamics. Under the assumption of a zero fluid shear modulus, ϵ^{inc} and σ^{inc} could be calculated from equation (5.27) and equation (3.68), reproduced below:

$$\epsilon^{inc} = (I - S)^{-1}C^{-1}(\sigma^{w} - CSC^{-1}p\delta). \tag{5.41}$$

To achieve consistency with the approach of Walsh (1969) I will calculate the off-diagonal terms of σ^{inc} and ϵ^{inc} using the Wu T tensor under the assumption that the fluid shear modulus is $i\omega\eta$. The result of this calculation was given in (3.64). In this way, our effective elastic tensor will depend on both σ and p^*, and the general wave equation:

$$\rho\ddot{u}_i = \sigma_{ij,j}; \tag{5.42}$$

where ρ is the density of the composite, will give nothing more than an equation coupling σ and p^*. This will be the second equation which I need for the derivation of the dispersion relationship.

To carry out this process explicitly, we first need to ensure that the tensors in equation (5.38) are referred to the same axes. In classical elasticity the stress and strain tensors associated with the propagation of a P-wave are given by:

$$\sigma^{w} = \frac{\sigma(t)}{3\kappa_m}\begin{bmatrix} \lambda_m + 2\mu & 0 & 0 \\ 0 & \lambda_m & 0 \\ 0 & 0 & \lambda_m \end{bmatrix}; \tag{5.43}$$

$$\epsilon^{w} = \frac{\sigma(t)}{3\kappa_m}\begin{bmatrix} 1 & 0 & 0 \\ 0 & 0 & 0 \\ 0 & 0 & 0 \end{bmatrix}; \tag{5.44}$$

where λ_m and μ are the matrix lame constants. I now rotate these tensors into the frame of a crack whose normal (x_1, say) has Euler angles (ψ, θ), and find that the relevant terms are:

$$\sigma^{wloc} = \frac{\sigma(t)}{3\kappa_m} \begin{bmatrix} \lambda_m + 2\mu\cos^2\psi & 0 & -2\mu\sin\psi\cos\psi \\ 0 & \lambda_m & 0 \\ -2\mu\sin\psi\cos\psi & 0 & \lambda_m + 2\mu\sin^2\psi \end{bmatrix}; \tag{5.45}$$

$$\epsilon^{wloc} = \frac{\sigma(t)}{3\kappa_m} \begin{bmatrix} \cos^2\psi & 0 & -\sin\psi\cos\psi \\ 0 & 0 & 0 \\ -\sin\psi\cos\psi & 0 & \sin^2\psi \end{bmatrix}; \tag{5.46}$$

where the notation "loc" is introduced to signify that the tensor has been rotated into the local frame of the crack.

The tensors ϵ^{inc} and σ^{inc} are given by (3.64), (3.68), (3.87), (3.90):

$$\epsilon^{inc} = \begin{bmatrix} \frac{\sigma_{11}^{wloc} - p(\psi,\theta)}{\sigma_c} & T^s\epsilon_{12}^{wloc} & T^s\epsilon_{13}^{wloc} \\ T^s\epsilon_{21}^{wloc} & 0 & 0 \\ T^s\epsilon_{31}^{wloc} & 0 & 0 \end{bmatrix}; \tag{5.47}$$

$$\sigma^{inc} = \begin{bmatrix} p(\psi,\theta) & 2i\omega\eta T^s\epsilon_{12}^{wloc} & 2i\omega\eta T^s\epsilon_{13}^{wloc} \\ 2i\omega\eta T^s\epsilon_{21}^{wloc} & p(\psi,\theta) & 0 \\ 2i\omega\eta T^s\epsilon_{31}^{wloc} & 0 & p(\psi,\theta) \end{bmatrix}; \tag{5.48}$$

where as in (3.64):

$$T^s = \frac{\frac{\mu}{(\mu - i\omega\eta)}}{\frac{i\omega\eta}{\mu - i\omega\eta} + \frac{2-v}{1-v}\frac{\pi}{2}r}. \tag{5.49}$$

Equations (5.27) and (5.45) give the expression:

$$\begin{aligned} p(\psi,\theta) \;=\; & \frac{\sigma(t)}{3\kappa_m}\frac{\lambda_m + 2\mu\cos^2\psi}{1+K_c} + \gamma p^* - \gamma'\sigma(t) \\ & -\frac{1}{\tau}\int_0^t \frac{\sigma(s)}{3\kappa_m}\frac{\lambda_m + 2\mu\cos^2\psi}{1+K_c} + (\gamma-1)p^*(s) - \gamma'\sigma(s)]e^{\frac{s-t}{\tau}}ds; \end{aligned} \tag{5.50}$$

so that:

$$\begin{aligned}\epsilon_{ij}^{inc}\sigma_{ij}^{w} &= \frac{\sigma(t)}{3\kappa_m}\{\frac{K_c(\lambda_m+2\mu\cos^2\psi)^2}{3\kappa_m\sigma_c(1+K_c)}\sigma(t)-\frac{\gamma(\lambda_m+2\mu\cos^2\psi)}{\sigma_c}p^*(t) \\ &+\frac{\gamma'(\lambda_m+2\mu\cos^2\psi)}{\sigma_c}\sigma(t)+\frac{1}{\tau}\int_0^t[\frac{(\lambda_m+2\mu\cos^2\psi)^2}{3\kappa_m\sigma_c(1+K_c)}\sigma(s) \\ &+\frac{(\gamma-1)(\lambda_m+2\mu\cos^2\psi)}{\sigma_c}p^*(s)-\frac{\gamma'(\lambda_m+2\mu\cos^2\psi)}{\sigma_c}\sigma(s)]e^{\frac{s-t}{\tau}}ds \\ &+4\mu T^s\sin^2\psi\cos^2\psi\frac{\sigma(t)}{3\kappa_m}\}.\end{aligned} \tag{5.51}$$

I now integrate this expression over $d\Omega$ to obtain:

$$\begin{aligned}\epsilon_{ij}^{inc}\sigma_{ij}^{wloc} &= \frac{\sigma(t)}{3\kappa_m}\{[\frac{K_cL_2}{3\kappa_m\sigma_c(1+K_c)}+\frac{\gamma'L_1}{\sigma_c}+\frac{8}{45}\frac{\mu}{\kappa_m}T^s]\sigma(t) \\ &-\frac{\gamma L_1}{\sigma_c}p^*(t)+\frac{1}{\tau}\int_0^t[(\frac{L_2}{3\kappa_m\sigma_c(1+K_c)}-\frac{\gamma'L_1}{\sigma_c})\sigma(s) \\ &+\frac{(\gamma-1)L_1}{\sigma_c}p^*(s)]e^{\frac{s-t}{\tau}}ds\}.\end{aligned} \tag{5.52}$$

where I have introduced the notation:

$$L_1=\lambda_m+\mu; \tag{5.53}$$

$$L_2=\lambda_m^2+2\lambda_m\mu+\frac{3}{2}\mu^2; \tag{5.54}$$

By similar means it may be shown that:

$$\begin{aligned}\sigma_{ij}^{inc}\epsilon_{ij}^{wloc} &= \frac{\sigma(t)}{3\kappa_m}\{(\frac{L_1}{3\kappa_m(1+K_c)}-\gamma'-\frac{8}{15}i\omega\eta T^s\frac{1}{\kappa_m})\sigma(t) \\ &+\gamma p^*(t)-\frac{1}{\tau}\int_0^t[(\frac{L_1}{3\kappa_m(1+K_c)}-\gamma')\sigma(s) \\ &+(\gamma-1)p^*(s)]e^{\frac{s-t}{\tau}}ds\};\end{aligned} \tag{5.55}$$

so I may write:

$$\sum^{cracks} \phi_i(\epsilon^{inc}\sigma^w - \epsilon^w\sigma^{inc}) = \frac{\phi_c\sigma(t)}{3\kappa_m}\{d_1\sigma(t)+d_2p^*(t)+\frac{1}{\tau}\int_0^t[d_3\sigma(s)+d_4p^*(s)]e^{\frac{s-t}{\tau}}ds\}; \tag{5.56}$$

where:

$$\mathcal{M} = \frac{\mu}{\frac{i\omega\eta}{\mu-i\omega\eta}+\frac{2-v}{1-v}\frac{\pi}{2}r}; \tag{5.57}$$

$$d_1 = \frac{K_cL_2}{3\kappa_m\sigma_c(1+K_c)} + \frac{\gamma'L_1}{\sigma_c} - \frac{L_1}{3\kappa_m(1+K_c)} + \gamma' + \frac{8}{45\kappa_m}\mathcal{M}; \tag{5.58}$$

$$d_2 = -\gamma(\frac{L_1}{\sigma_c}+1); \tag{5.59}$$

$$d_3 = \frac{L_2}{3\kappa_m\sigma_c(1+K_c)} - \frac{\gamma'L_1}{\sigma_c} + \frac{L_1}{3\kappa_m(1+K_c)} - \gamma'; \tag{5.60}$$

$$d_4 = (\gamma-1)(\frac{L_1}{\sigma_c}+1) \tag{5.61}$$

and ϕ_c is the porosity associated with the cracks.

I now perform the same calculations for pores. Applying equations (3.73) to (3.77) I find:

$$\epsilon_{11}^{inc} = \frac{3}{4\mu}\frac{1-v}{1+v}[\lambda_m + 2\mu\frac{9+5v}{7-5v}]\frac{\sigma(t)}{3\kappa_m} - \frac{p^*(t)}{4\mu}; \tag{5.62}$$

$$\epsilon_{22}^{inc} = \epsilon_{33}^{inc} = \frac{3}{4\mu}\frac{1-v}{1+v}[\lambda_m - 2\mu\frac{1+5v}{7-5v}]\frac{\sigma(t)}{3\kappa_m} - \frac{p^*(t)}{4\mu}. \tag{5.63}$$

Equations (5.43) and (5.44) now give:

$$\epsilon_{ij}^{inc}\sigma_{ij}^{w} = \frac{\sigma(t)}{3\kappa_m}\{\frac{3}{4\mu}\frac{1-v}{1+v}[(\lambda_m+2\mu\frac{9+5v}{7-5v})(\lambda_m+2\mu) \\ +2\lambda_m(\lambda_m-2\mu\frac{1+5v}{7-5v})]\frac{\sigma(t)}{3\kappa_m}-\frac{3\kappa_m}{4\mu}p^*\}; \tag{5.64}$$

$$\sigma_{ij}^{inc}\epsilon_{ij}^{w} = \frac{\sigma(t)}{3\kappa_m}p^*(t); \tag{5.65}$$

so that I may write:

$$\sum^{pores}\phi_i(\epsilon^{inc}\sigma^w-\sigma^{inc}\epsilon^w) = \phi_p\frac{\sigma(t)}{3\kappa_m}[d_5\sigma(t)-d_6p^*]; \tag{5.66}$$

where:

$$d_5 = \frac{1}{4\kappa_m\mu}\frac{1-v}{1+v}[(\lambda_m+2\mu\frac{9+5v}{7-5v})(\lambda_m+2\mu)+2\lambda_m(\lambda_m-2\mu\frac{1+5v}{7-5v})]; \tag{5.67}$$

$$d_6 = \frac{3}{4}\frac{\kappa_m}{\mu}+1; \tag{5.68}$$

and ϕ_p is the porosity associated with the spherical pores.

Equation (5.38) now gives:

$$M_{eff}\sigma(x,t) = M\sigma(x,t)-3\phi_c\kappa_m[d_1\sigma(x,t)+d_2p^*(x,t) \\ +\frac{1}{\tau}\int_0^t(d_3\sigma(x,s)+d_4p^*(x,s))e^{\frac{s-t}{\tau}}ds] \\ -3\phi_p\kappa_m[d_5\sigma(x,t)-d_6p^*(x,t)]. \tag{5.69}$$

By analogy with the analysis of Biot(1956a), I will seek solutions of the form:

$$p^* = F_1\exp i(yx-\omega t); \tag{5.70}$$

$$\sigma = F_2 \exp i(yx - \omega t). \tag{5.71}$$

If I now multiply equation (5.69) by $\exp(-iyx)$ I see that M_{eff} must be independent of x. This means that I can differentiate (5.38) to arrive at:

$$\begin{aligned} M_{eff}\sigma'' &= M\sigma'' - 3\phi_c\kappa_m[d_1\sigma'' + d_2 p^{*''} \\ &\quad + \frac{1}{\tau}\int_0^t (d_3\sigma''(s) + d_4 p^{*''}(s))e^{\frac{s-t}{\tau}} ds \\ &\quad - 3\phi_p\kappa_m[d_5\sigma'' - d_6 p^{*''}]. \end{aligned} \tag{5.72}$$

If I take the Fourier transform of this equation I get:

$$\begin{aligned} F(M_{eff}\sigma'') &= -y^2 M\tilde{\sigma} + y^2 3\phi_c\kappa_m[d_1\tilde{\sigma} + d_2\tilde{p} \\ &\quad + \frac{1}{1 + i\omega\tau}(d_3\tilde{\sigma} + d_4\tilde{p})] + y^2 3\phi_p\kappa_m[d_5\tilde{\sigma} - d_6\tilde{p}]. \end{aligned} \tag{5.73}$$

However, the equation of motion is given by:

$$\rho\ddot{\sigma} = M_{eff}\sigma''; \tag{5.74}$$

so taking the Fourier transform I find:

$$\begin{aligned} -\rho\omega^2\tilde{\sigma} &= -y^2 M\tilde{\sigma} + y^2 3\phi_c\kappa_m[d_1\tilde{\sigma} + d_2\tilde{p} \\ &\quad + \frac{1}{1 + i\omega\tau}(d_3\tilde{\sigma} + d_4\tilde{p})] + y^2\phi_p 3\kappa_m[d_5\tilde{\sigma} - d_6\tilde{p}]; \end{aligned} \tag{5.75}$$

which may be rewritten as:

$$\begin{aligned} &\{(y^2 M - \rho\omega^2) - \phi_c y^2 3\kappa_m[d_1 + \frac{d_3}{1 + i\omega\tau}] - \phi_p y^2 d_5\}\tilde{\sigma} \\ &\quad -\{y^2\phi_c\kappa_m[d_2 + \frac{d_4}{1 + i\omega\tau}] - y^2 3\kappa_m\phi_p d_6\}\tilde{p} = 0. \end{aligned} \tag{5.76}$$

If I write (5.76) as:

$$[A_1 + A_2 y^2]\tilde{\sigma} + [A_3 + A_4 y^2]\tilde{p} = 0; \tag{5.77}$$

and (5.37) as:

$$[B_1 + B_2 y^2]\tilde{\sigma} + [B_3 + B_4 y^2]\tilde{p} = 0; \tag{5.78}$$

then the dispersion equation of the system is given by:

$$\begin{vmatrix} A_1 + A_2 y^2 & A_3 + A_4 y^2 \\ B_1 + B_2 y^2 & B_3 + B_4 y^2 \end{vmatrix} = 0. \tag{5.79}$$

Note that this equation is quadratic in y^2, so the model predicts the existence of 2 compressional waves, in agreement with Biot's theory of poroelasticity. Frequency dependent P-wave velocities can be calculated directly from equation (5.79).

5.3 The S-wave dispersion equation.

The situation with shear waves is less complicated. Equation (3.119) gives:

$$\mu_{eff} = \mu - \frac{\mu^2}{[\sigma(t)]^2} \sum \phi_i (\sigma^w \epsilon^{inc} - \sigma^{inc} \epsilon^w); \tag{5.80}$$

where stress tensor associated with the propagation of a shear wave is given by;

$$\sigma^w = \begin{bmatrix} 0 & 0 & \sigma(t) \\ 0 & 0 & 0 \\ \sigma(t) & 0 & 0 \end{bmatrix}. \tag{5.81}$$

When this tensor is rotated into the frame of a crack whose normal has Euler angles (ψ, θ) we find:

$$\sigma^{wloc} = \sigma(t) \begin{bmatrix} 2\sin\psi\cos\psi\cos\theta & \cos\psi\sin\theta & \cos\theta(\cos^2\psi - \sin^2\psi) \\ \cos\psi\sin\theta & 0 & -\sin\psi\sin\theta \\ \cos\theta(\cos^2\psi - \sin^2\psi) & -\sin\psi\sin\theta & -2\sin\psi\cos\psi\cos\theta \end{bmatrix}. \tag{5.82}$$

The strains are given by:

$$\epsilon^w = \frac{1}{2\mu}\sigma^w; \tag{5.83}$$

$$\epsilon^{wloc} = \frac{1}{2\mu}\sigma^{wloc}; \tag{5.84}$$

The stress and strain in a crack of orientation (ψ, θ) are:

$$\sigma^{inc} = \begin{bmatrix} p(\psi,\theta) & 2i\omega\eta T^s\epsilon_{12}^{wloc} & 2i\omega\eta T^s\epsilon_{13}^{wloc} \\ 2i\omega\eta T^s\epsilon_{21}^{wloc} & p(\psi,\theta) & 0 \\ 2i\omega\eta T^s\epsilon_{31}^{wloc} & 0 & p(\psi,\theta) \end{bmatrix}; \tag{5.85}$$

$$\epsilon^{inc} = \begin{bmatrix} \frac{\sigma_{11}^{wloc} - p(\psi,\theta)}{\sigma_c} & T^s\epsilon_{12}^{wloc} & T^s\epsilon_{13}^{wloc} \\ T^s\epsilon_{21}^{wloc} & 0 & 0 \\ T^s\epsilon_{31}^{wloc} & 0 & 0 \end{bmatrix}; \tag{5.86}$$

where equation (5.27) gives now:

$$p(\psi,\theta) = \frac{2\sin\psi\cos\psi\cos\theta\sigma(t)}{1+K_c} - \frac{1}{\tau}\int_0^t \frac{2\sin\psi\cos\psi\cos\theta\sigma(s)}{1+K_c} e^{\frac{s-t}{\tau}} ds. \tag{5.87}$$

For cracks, then, I find:

$$\begin{aligned} \sigma_{ij}^w\epsilon_{ij}^{inc} - \sigma_{ij}^{inc}\epsilon_{ij}^w \;=\; & 4\sin^2\psi\cos^2\psi\cos^2\theta\frac{\sigma(t)}{\sigma_c}[\frac{K_c}{1+K_c}\sigma(t) \\ & + \frac{1}{\tau}\int_0^t \frac{\sigma(s)}{1+K_c} e^{\frac{s-t}{\tau}} ds + \{\frac{\sigma(t)}{\mu}\}^2[\cos^2\psi\sin^2\theta \\ & + \cos^2\theta(\cos^2\psi - \sin^2\psi)^2]\mathcal{M}. \end{aligned} \tag{5.88}$$

Integrating over $d\Omega$ gives:

$$\sum_{cracks} \phi_t(\sigma_{ij}^{wloc}\epsilon_{ij}^{inc} - \epsilon_{ij}^{wloc}\sigma_{ij}^{inc}) = \frac{4}{15}\frac{\sigma(t)}{\sigma_c}[\frac{K_c}{1+K_c}\sigma(t) + \frac{1}{\tau}\int_0^t \frac{\sigma(s)}{1+K_c}e^{\frac{s-t}{\tau}}ds] + \frac{2}{5}\{\frac{\sigma(t)}{\mu}\}^2\mathcal{M}. \tag{5.89}$$

For pores from (3.73) and (3.74):

$$\epsilon^{inc} = \frac{15}{2\mu}\frac{1-v}{7-5v}\sigma(t)\begin{bmatrix} 0 & 0 & 1 \\ 0 & 0 & 0 \\ 1 & 0 & 0 \end{bmatrix}; \tag{5.90}$$

where I have neglected terms of order $\frac{i\omega\eta}{\mu}$ and therefore:

$$\sigma^{inc} = 0; \tag{5.91}$$

and so:

$$\sum^{pores} \phi_i(\sigma_{ij}^{w}\epsilon_{ij}^{inc} - \sigma_{ij}^{inc}\epsilon_{ij}^{w}) = \phi_p\frac{15}{\mu}\frac{1-v}{7-5v}[\sigma(t)]^2. \tag{5.92}$$

Substituting these results into equation (5.80) I find:

$$\mu_{eff}\sigma = \mu\sigma - \frac{4}{15}\phi_c\frac{1}{1+K_c}\frac{1}{\sigma_c}[K_c\sigma + \frac{1}{\tau}\int_0^t \sigma(s)e^{\frac{s-t}{\tau}}ds] - \frac{2}{5}\phi_c\mathcal{M}\sigma - 15\phi_p\frac{1-v}{7-5v}\mu\sigma. \tag{5.93}$$

Noting once again that μ_{eff} is independent of x, I may differentiate twice with respect to x to obtain:

$$\mu_{eff}\sigma'' = \mu\sigma'' - \frac{4}{15}\phi_c\frac{1}{1+K_c}\frac{1}{\sigma_c}[K_c\sigma'' + \frac{1}{\tau}\int_0^t \sigma''(s)e^{\frac{s-t}{\tau}}ds] - \frac{2}{5}\phi_c\mathcal{M}\sigma'' - 15\phi_p\frac{1-v}{7-5v}\mu\sigma''. \tag{5.94}$$

The equation of motion is:

$$\rho\ddot{\sigma} = \mu_{eff}\sigma''; \tag{5.95}$$

so taking the Fourier transform and dividing by $\tilde{\sigma}$ I obtain the dispersion equation:

$$\begin{aligned}\rho\omega^2 &= y^2(\mu - \frac{4}{15}\phi_c\frac{1}{1+K_c}\frac{1}{\sigma_c}[K_c + \frac{1}{1+i\omega\tau}] \\ &\quad -\phi_c\frac{2}{5}\mathcal{M} - 15\phi_p\mu\frac{1-v}{7-5v}).\end{aligned} \tag{5.96}$$

Equation (5.96) permits the explicit computation of frequency dependent S-wave velocities.

5.4 Recovery of Gassmann's theorem

Thomsen (1985) notes that the conditions on which Gassmann's theorem is based are very general, and he argues convincingly that any theory which makes stronger assumptions than Gassmann, such as the model just derived, should nevertheless reproduce Gassmann's theorem when its conditions are satisfied. Endres and Knight (1997) prove the Gassmann consistency of Eshelby's interaction energy method when pore pressure equalisation is allowed for, but show that neither the self consistent scheme nor the differential effective medium approximation give Gassmann consistent result. I now show that my model is Gassmann consistent in the zero frequency limit.

The case of the shear modulus is straightforward. Considering the Fourier transform of equation (5.93) and dividing by $\tilde{\sigma}$ I find:

$$\begin{aligned}\mu_{eff} &= \mu - \frac{4}{15}\phi_c\frac{1}{1+K_c}\frac{1}{\sigma_c}[K_c + \frac{1}{1+i\omega\tau}] \\ &\quad -\frac{2}{5}\phi_c\mathcal{M} - 15\phi_p\mu\frac{1-v}{7-5v}.\end{aligned} \tag{5.97}$$

I note that the fluid properties appear in three variables, τ, K_c and $\mathcal{M}$. In the expression $\mathcal{M}$, the fluid viscosity appears multiplied by frequency, ω. This means that when $\omega = 0$, $\mathcal{M}$ will be independent of viscosity and fluid type. Similarly, τ is multiplied by ω and so this dependence on fluid properties disappears in the zero frequency limit. When the term in τ disappears, however, the terms in $(1 + K_c)$ cancel out, and the whole expression is therefore independent of fluid type. Explicitly, when $\omega = 0$ I have:

$$\mu_{eff} = \mu - \frac{4}{15}\frac{\phi_c}{\sigma_c} - \frac{2}{5}\phi_c\frac{(2-2v)\mu}{(2-v)\pi r} - 15\phi_p\mu\frac{1-v}{7-5v}; \tag{5.98}$$

and it is clear that there is no dependence on fluid properties in this equation. This verifies Gassmann's theorem for the shear modulus.

I will now derive the dry frame bulk modulus. I consider rock subjected to a constant stress field:

$$\sigma^w = \sigma \begin{bmatrix} 1 & 0 & 0 \\ 0 & 1 & 0 \\ 0 & 0 & 1 \end{bmatrix}. \tag{5.99}$$

The expression for the effective bulk modulus is then, from equation(3.116):

$$\kappa_{eff} = \kappa_m - \frac{\kappa_m^2}{\sigma^2}\sum_t \phi_t(\sigma_{ij}^w\epsilon_{ij}^{inc} - \sigma_{ij}^{inc}\epsilon_{ij}^w). \tag{5.100}$$

For dry conditions we naturally have:

$$\sigma^{inc} = 0; \tag{5.101}$$

and so,

$$\kappa_{dry} = \kappa_m - \kappa_m^2(\frac{9}{4\mu}\frac{1-v}{1+v}\phi_p + \frac{\phi_c}{\sigma_c}). \tag{5.102}$$

For the saturated case, I firstly assume that at zero frequency the wave length is sufficiently long that I do not have to consider spatial variations in the stress field. Indeed, Gassmann's theorem also relies on this assumption. This means that I may ignore spatial derivatives and equation (5.10) becomes:

$$\begin{bmatrix} \dot{m}_1 \\ \dot{m}_2 \\ \dot{m}_3 \\ \vdots \\ \dot{m}^* \end{bmatrix} = \frac{6\rho_0 k\varsigma}{\eta N} \begin{bmatrix} 1-N & 1 & 1 & & 1 \\ 1 & 1-N & 1 & \cdots & 1 \\ 1 & 1 & 1-N & & 1 \\ & \vdots & & \ddots & \vdots \\ 1 & 1 & 1 & \cdots & 1-N \end{bmatrix} \begin{bmatrix} p_1 \\ p_2 \\ p_3 \\ \vdots \\ p^* \end{bmatrix}. \tag{5.103}$$

In the static limit $\dot{m}_i = 0$ and since the square matrix in equation (5.103) has nullity 1 I have:

$$p_1 = p_2 = \cdots = p^*. \tag{5.104}$$

I denote this common pressure simply by p. Now equation (5.14) gives:

$$[\phi_p \frac{9}{4\mu}\frac{1-v}{1+v} + \frac{\phi_c}{\sigma_c}]\sigma = [\phi_p \frac{3}{4\mu}(1+K_p) + \frac{\phi_c}{\sigma_c}(1+K_c)]p; \tag{5.105}$$

or alternatively:

$$p = \frac{\phi_p \frac{9}{4\mu}\frac{1-v}{1+v} + \frac{\phi_c}{\sigma_c}}{\phi_p \frac{3}{4\mu} + \frac{\phi_c}{\sigma_c} + \frac{\phi}{\kappa_f}}\sigma; \tag{5.106}$$

where I have introduced the notation $\phi = \phi_c + \phi_p$. Equation (5.100) now gives:

$$\kappa_{sat} = \kappa_m - \kappa_m^2(\frac{9}{4\mu}\frac{1-v}{1+v}\phi_p + \frac{\phi_c}{\sigma_c}) + \frac{\kappa_m^2 p}{\sigma}(\frac{\phi_c}{\sigma_c} + \frac{3}{4\mu}\phi_p + \frac{\phi}{\kappa_m}); \tag{5.107}$$

which may be written with equations (5.102) and(5.106) as,

$$\kappa_{sat} = \kappa_{dry} + \frac{\kappa_m^2(\frac{\phi_c}{\sigma_c} + \frac{3}{4\mu}\phi_p + \frac{\phi}{\kappa_m})(\frac{9}{4\mu}\frac{1-v}{1+v}\phi_p + \frac{\phi_c}{\sigma_c})}{\frac{3}{4\mu}\phi_p + \frac{\phi_c}{\sigma_c} + \frac{\phi}{\kappa_f}}. \tag{5.108}$$

At this point a complication arises. In equation (3.91) I wrote:

$$c_v = c_v^0(1 - \frac{\sigma_{33}}{\sigma_c} + \frac{p}{\sigma_c}) + O(1). \tag{5.109}$$

In fact the exact expression is:

$$c_v = c_v^0(1 - \frac{\sigma_{33}}{\sigma_c} - \frac{\sigma_{ll}}{3\kappa_m} + \frac{p}{\sigma_c}); \tag{5.110}$$

where, following Zatsepin & Crampin (1997), I neglected the term in $\frac{1}{\kappa m}$ in favour of the terms in $\frac{1}{\sigma_c}$ which are $O(\frac{1}{r})$. To prove Gassmann's theorem explicitly I require to use the exact expression. I do not believe that it is worthwhile to complicate the derivation of the model by including a term which is negligible, so at this point I will just note that I may equally well write equation (5.108) to the same accuracy as:

$$\kappa_{sat} = \kappa_{dry} + \frac{\kappa_m^2(\frac{\phi_c}{\sigma_c} + \frac{3}{4\mu}\phi_p + \frac{\phi_p}{\kappa_m})(\frac{9}{4\mu}\frac{1-v}{1+v}\phi_p + \frac{\phi_c}{\sigma_c})}{\frac{3}{4\mu}\phi_p + \frac{\phi_c}{\sigma_c} - \frac{\phi_c}{\kappa_m} + \frac{\phi}{\kappa_f}}. \tag{5.111}$$

I now note that:

$$\frac{3}{4\mu}\phi_p = \frac{9}{4\mu}\frac{1-v}{1+v}\phi_p - \frac{\phi_p}{\kappa_m}; \tag{5.112}$$

and by equation (5.102):

$$\frac{9}{4\mu}\frac{1-v}{1+v}\phi_p + \frac{\phi_c}{\sigma_c} = \frac{1}{\kappa_m} - \frac{\kappa_{dry}}{\kappa_m^2}; \tag{5.113}$$

so that equation (5.111) may be written as:

$$\kappa_{sat} = \kappa_{dry} + \frac{(1 - \frac{\kappa_{dry}}{\kappa_m})^2}{\frac{1-\phi}{\kappa_m} + \frac{\phi}{\kappa_f} - \frac{\kappa_{dry}}{\kappa_m^2}}. \tag{5.114}$$

This is Gassmann's theorem.

5.5 Extension of the analysis to distributions of crack aspect ratios.

I noted previously that in the analysis of O'Connell and Budiansky (1977) there was associated with each crack a critical frequency proportional to the cube of the crack aspect ratio, and that the shape of the dispersion curve predicted by the model therefore depended on the distribution of crack aspect ratios. Unlike the O'Connell and Budiansky model, my analysis takes account of overall mass conservation, and this leads to a critical frequency which is almost independent of aspect ratio.

The time scale parameter τ is given by equation (5.24), reproduced here for convenience:

$$\tau = \frac{\eta c_v (1 + K_c)}{6k\varsigma\sigma_c}; \tag{5.115}$$

and since:

$$\sigma_c = \frac{\pi\mu r}{1 - v}; \tag{5.116}$$

and:

$$c_v = \frac{4}{3}\pi a^3 r; \tag{5.117}$$

the aspect ratio in these terms will cancel out between the top and bottom lines. This leaves the only aspect ratio dependence in the term K_c, which is given by:

$$K_c = \frac{\pi}{1 - v}\mu c_f r. \tag{5.118}$$

The term μc_f will generally be around 20 for water saturated rocks, (Thomsen, 1995), so if we take $r < 10^{-2}$, or to be sure $r < 10^{-3}$, then it follows that $K_c \approx 0$, and τ will be given by:

$$\tau = \frac{2\eta a^3(1-v)}{9k\varsigma\mu}; \tag{5.119}$$

where there is no dependence on aspect ratio whatsoever. This means that the pressure in a crack is independent of aspect ratio, and I can consider cracks with distributed aspect ratios without having to modify my calculations for the pressure in each crack as a function of its orientation.

There is of course dependence on the cube of the crack radius, and this may be thought to lead to a distribution of different τ values for cracks of different sizes. This may be correct, but I note that the cracks being of the same size was an important assumption underlying the derivation of the fluid dynamics model. In my analysis I assumed that each crack was connected to 6 other elements of pore space. If the cracks had been of different sizes then the larger cracks would have to be connected to more elements than would smaller cracks. It is not at all clear how this situation should be modelled, but I could plausibly scale the number of connections with the cube of the crack radius, in which case one would have a single τ value for each crack. I am happy with the assumption that the cracks are uniformly sized, Biot (1956 b) made a similar assumption and the assumption is implicit in the single characteristic squirt flow length in the BISQ approach. Cracks in rocks are not uniformly sized, although when plotted by volume, particle size distributions are often very peaked at a characteristic length near the maximum grain size (Mair et al., 2000). I think it is fair to say that the assumption of uniformly sized cracks is far weaker than the assumption of uniformly shaped cracks.

The only remaining dependence on the aspect ratio is in the parameters, $\mathcal{M}$ and d_1 to d_4. Terms d_1 to d_4 are $O(\frac{1}{r})$. When they enter the dispersion equation they are multiplied by ϕ_c, which may be given by:

$$\phi_c = \frac{4}{3}\pi\frac{Na^3r}{V} = \frac{4}{3}\pi\epsilon r; \tag{5.120}$$

where N is the number of cracks in a volume V and ϵ the crack density. This means that the products $\phi_c d_i$ may be written in the form:

$$\phi_c d_i = C\epsilon + C_1 O(r); \tag{5.121}$$

where C and C_1 are independent of aspect ratio. Naturally if the aspect ratio is small enough then I may ignore the $O(r)$ term and the aspect ratio dependence in the terms d_1 to d_4 disappears. This is essentially the logic behind the statement that the crack density is the appropriate parameter in which to express the effect of cracks on the elasticity of rock (Budiansky and O'Connell, 1976; Hudson, 1980, 1981), without having to make reference to the aspect ratio spectrum (Murphy, 1985).

The situation with the term $\mathcal{M}$ is more subtle. Considering the expression for $\mathcal{M}$:

$$\mathcal{M} = \frac{\mu}{\frac{i\omega\eta}{\mu - i\omega\eta} + \frac{2-\upsilon}{1-\upsilon}\frac{\pi}{2}r}; \tag{5.122}$$

we see that at low frequencies the term in the aspect ratio will dominate the term in viscosity and $\mathcal{M}$ will essentially be frequency independent. $\mathcal{M}$ will then be $O(\frac{1}{r})$, and the previous argument will apply once again, giving dependence on crack density rather than aspect ratio. When frequency increases to a point where $\frac{\omega\eta}{\mu}$ is greater than $\frac{1}{r}$, the term in the aspect ratio is dominated by the frequency dependent viscous term. This effect, leading to velocity dispersion and attenuation, has been studied by Walsh (1969). The frequency at which the effect becomes apparent is controlled by the aspect ratio, and this leads directly to a situation where the shape of the dispersion curve is determined by the aspect ratio spectrum. Nevertheless, for this effect to occur at frequencies less than 10 MHz the crack aspect ratio has to be extremely low.

I carried out extensive numerical experiments into the effect of changing the aspect ratio in my model whilst keeping the crack density the same. For values of the other parameters which will lead to reasonable results, there is almost complete independence of aspect ratio in the frequency range 0 - 1 MHz for aspect ratios between around 10^{-2} and 10^{-5}. For aspect ratios larger than 10^{-2} the $O(r)$ terms

can sometimes have an effect while for aspect ratios smaller than 10^{-5} the Walsh effect can be noticeable.

In view of this fact I will not refer to the aspect ratio in the remainder of this thesis, but will rather assume that all the aspect ratios are in this band where crack density alone is important. The input into the model will be the crack density. I will choose the aspect ratio arbitrarily to be 10^{-3} for all cracks, I could equally well choose 10^{-4}, say, with virtually identical results, and will then convert this to ϕ_c using equation (5.120).

5.6 Conclusions

The model which I have derived in this chapter may be considered to be a genuine poroelastic model in the sense that it is consistent both with Gassmann's theorem and with Biot's prediction of a slow compressional wave. No model previously derived from Eshelby's theory satisfies both of these constraints.

Since the model is derived from Eshelby there is naturally a dependence on the geometry of the inclusions. This comes through two parameters, the crack density ϵ and the "relative crack density" ι. It is important that there is no dependence on the aspect ratio spectrum; this makes the theory potentially of practical use, since one is not required to specify an arbitrary number of unknown parameters. It also means that stress-sensitivity can easily be incorporated into the model with only the specification of a relationship between crack density and effective stress.

I assumed that the Walsh effect does not play any role. For the Walsh effect to be important there would have to be cracks of extremely small aspect ratio, and this has been criticised as being physically implausible (Bourbie et al., 1987). As I pointed out in Chapter One, a broad body of evidence exists in favour of the concept of squirt flow affecting wave propagation in fluid saturated rocks. Such wide ranging evidence does not exist in favour of the Walsh effect, and it is this which leads me to discount it while retaining the local flow effects.

A number of limitations exist in the model. As ever, it is strictly valid only for low concentrations of cracks and pores. The flow law (5.1) is strictly valid only for Pouiselle flow. One might argue that I should replace the viscosity in (5.1) with Biot's complex viscosity, but I consider that such complexity is not justified at this stage.

The model also depends on the cracks and pores being uniformly sized. It is not immediately clear how the model should be extended for distributions of crack sizes, or whether in fact this would have any effect at all. I suggest that Occam's razor demands that I investigate the model in its current form, and only consider possible complications if it cannot explain specific observations.

Chapter 6

Calibration of the model.

Summary: In this chapter I describe how the various parameters which occur in my model may be derived or estimated from empirical measurements. I then proceed to a preliminary calibration of the model using Sothcott et al.'s (2000) resonant bar experimental data. Although I show that the data can be fit satisfactorily, significant ambiguity remains in the interpretation of the results. A number of ultrasonic tests of P and S velocity, in rock similar to the resonant bar, as a function of both effective stress and pore fluid species show results which are at variance with the predictions of published poroelastic theories. I demonstrate that the anomaly can be explained with reference to physical effects predicted by my model. Moreover, the requirement to explain the ultrasonic results places constraints upon the modelling of the resonant bar data, removing much of the ambiguity from the analysis. I present a calibration which gives a consistent qualitative explanation of both the resonant bar and ultrasonic data. I repeat my analysis within the framework of Dvorkin et al. (1995), and compare the predictions of the two models.

6.1 Estimation of parameters.

Perhaps the greatest impediment to the application of micro-structural velocity models to the analysis of laboratory data lies in the number of parameters which have to be specified. Many parameters which have a well defined meaning in the theoretical modelling, for example crack aspect ratio, cannot be directly measured by themselves and therefore become adjustable parameters, greatly reducing the predictive power of the theory. It is therefore imperative to apply the utmost effort to the reduction of the number of adjustable parameters.

Certain of the parameters in the theory can be measured by standard laboratory techniques. These are the porosity, permeability and density of the rock sample together with the fluid properties - fluid density, compressibility and viscosity. The grain size, while strictly speaking not being measurable, can be estimated with reasonable precision from SEM photographs.

The situation with the reference elastic tensor is more subtle. In principle one ought to use the elastic tensor of the mineral which makes up the rock. This can be measured directly, but two problems arise immediately. The first difficulty is for samples with complex mineralogy where the use of any one mineral elastic tensor would be inappropriate. A second problem affects rocks with high porosity. The modelling presented so far is limited to dilute concentrations of pores. If it were to be applied to a high porosity sandstone then the velocity predictions would be expected to be rather poor. If the purpose of the model were to describe the dependence of velocity on mineralogy and porosity, as was the case for example in Hornby et al. (1994), I would have to use methods such as the self consistent scheme (Hill, 1965) or the differential effective medium model (Norris, 1985) to attempt to account for the elastic interactions. My interest, however, lies in the variation of a given velocity with frequency, effective stress and pore fluid type, and so I am happy just to choose the two reference elastic parameters to give me a reasonable agreement with the velocities in the actual rock under consideration.

Without this assumption it would not be possible to apply the model to rocks of high porosity.

The parameter γ cannot be measured explicitly or calculated rigorously from parameters which can be measured. Nevertheless, to prevent it becoming a further adjustable parameter and to ensure as far as possible that reasonable values are taken I will propose an approximation which I will comply with in all the work in this thesis. We recall that from equation (5.22):

$$\gamma = \frac{3p_v\sigma_c(1+K_p)}{4c_v\mu(1+K_c)}. \tag{6.1}$$

Since crack aspect ratios will be small, $K_c = \sigma_c/\kappa_f \ll 1$, and I can take, in effect, $K_c = 0$. I now assume that cracks and pores can be thought of as being all of the one radius, a say, so that $p_v = \frac{4}{3}\pi a^3$ and $c_v = \frac{4}{3}\pi a^3 r$. The aspect ratio now cancels out, and I am left with:

$$\gamma = \frac{3\pi}{8(1-v)}(1+K_p). \tag{6.2}$$

An estimate of the Poisson's ratio can be made from P and S velocities of the rock, reducing the problem to the estimation of K_p. We recall from equation (3.81):

$$K_p = \frac{4}{3}\frac{\mu}{\kappa_f}. \tag{6.3}$$

Since μ is to be a fitted parameter I prefer not to use it for this estimation. Instead I will write:

$$K_p = \frac{4}{3}\frac{\rho_s}{\rho_f}(\frac{Vs}{Vf})^2; \tag{6.4}$$

where ρ_s and ρ_f are the densities of the saturated solid and fluid respectively; Vs is a representative shear velocity of the saturated solid; and Vf is the acoustic velocity in the fluid. I can now estimate γ, and an estimate for γ' follows immediately.

The hardest parameter to estimate by ad-hoc means is the time scale parameter τ. I have found that there is little prospect of estimating this parameter to an accuracy which is sufficient to model experimental data, so I will just take it to be a fitting parameter at the first stage. Later in this chapter I give an example of how constraints on τ can be given by a combination of experimental observations. The dependence of permeability on effective stress (King et al., 1994) suggests the possibility that τ will depend on effective stress. For simplicity I will ignore this possibility at the first stage.

Additionally the crack density has to be fit arbitrarily, with the complication that the crack density has to be a function of effective stress. Extensive experience of fitting crack densities in stress sensitive experiments (S. Zatsepin, pers, comm.) shows that crack density appears to behave according to the empirical law:

$$\epsilon = \epsilon_0 \exp(-c_{cr}\sigma_{eff}). \tag{6.5}$$

It remains to specify the two parameters ϵ_0 and c_{cr}, and these must be arbitrarily fit.

My final approximation concerns the relative crack density ι. We recall that ι was the probability that any element of pore space chosen at random would be a crack, defined in (5.32) as:

$$\iota = \frac{N_c}{N}. \tag{6.6}$$

Consider a section of rock with volume V. Making the assumption of a single crack and pore radius, a, once again I then have:

$$\phi_c = \frac{N_c \frac{4\pi}{3} a^3 r}{V}; \tag{6.7}$$

$$\phi_p = \frac{N_p \frac{4\pi}{3} a^3 r}{V}. \tag{6.8}$$

Recalling that $N = N_c + N_p$, we have:

$$\iota = \frac{\phi_c/r}{\phi_c/r + \phi_p}; \tag{6.9}$$

or in terms of the crack densities,

$$\iota = \frac{\frac{4}{3}\pi\epsilon}{\frac{4}{3}\pi\epsilon + \phi_p}. \tag{6.10}$$

As soon as the crack density parameters ϵ_0 and c_{cr} are specified I will therefore be able to calculate ι for any value of effective stress.

6.2 A preliminary calibration

I now proceed to a first attempt at calibrating the model against resonant bar data of Sothcott et al. (2000). The data in question are reproduced in Appendix A.

The density of the saturated resonant bar was measured as 2288 kgm^{-3}. The porosity of the bar itself was not measured, but that of an adjacent plug was found to be 22.7%, and I will use this value. I will take 2×10^{-4} m as a reasonable estimate of the average grain size.

The bar was saturated with brine, which had a density of 1097 kgm^{-3} and a bulk modulus of 2.9×10^9 Pa. The viscosity of the brine was not measured, but it will not be far from the value of water, so I will take it to be 1 cP.

I now carry out the procedure for the estimation of γ and γ' which I outlined in the previous section, beginning with the estimation of K_p. For my representative shear wave velocity I will simply take the average shear velocity over all effective stresses and all frequencies, which I find to be 2236 ms^{-1}. The acoustic velocity in brine is 1630 ms^{-1}, giving the estimate:

$$K_p = \frac{4}{3}\frac{\rho_s}{\rho_f}\frac{V_s^2}{V_f^2} = 5.21. \tag{6.11}$$

The average P-wave velocity of the sample is 3659 ms^{-1}, so an estimate of the Poisson's ratio follows from (Mavko et al., 1998):

$$v = \frac{1}{2}\frac{(\frac{V_p}{V_s})^2 - 2}{(\frac{V_p}{V_s})^2 - 1} = 0.2. \tag{6.12}$$

The value of γ is therefore:

$$\gamma = \frac{3\pi}{8}\frac{1}{1-v}(1 + K_p) = 9.15. \tag{6.13}$$

and γ' follows as:

$$\gamma' = \gamma\frac{1-v}{1+v}\frac{1}{1+K_p} = .97. \tag{6.14}$$

I must now choose the values for the reference elastic tensor. My choice is $\lambda_m = 5.5 \times 10^9$ Pa and $\mu = 2.45 \times 10^{10}$ Pa. Ideally I could have chosen the mineral elastic moduli for this purpose, but the failure of the model to account for the elastic interactions amongst the cracks and pores requires me to take smaller values in order to fit the data.

In Figures (6-1) and (6-2) I now reproduce the data, together with the velocity curves for the above parameters in the absence of cracks.

The theoretical curves may be thought of as representing the velocity at very high values of effective stress when all cracks are closed. It should be noted that in the absence of cracks there is almost no dispersion taking place. I will therefore have to introduce cracks into the model to explain the data.

I now have to choose the crucial parameters ϵ_0, c_{cr} and τ which will describe the dependence of velocity on effective stress and frequency. A number of different choices are possible, but at this stage I will choose ϵ_0=0.24, $c_{cr} = .07$ MPa^{-1} and $\tau = 2\times10^{-5}$s. The full list of parameters is summarised in Table (6-1)

This choice results in what appears to be a reasonable fit to the data, and I reproduce the modelling in Figures (6-3) and (6-4).

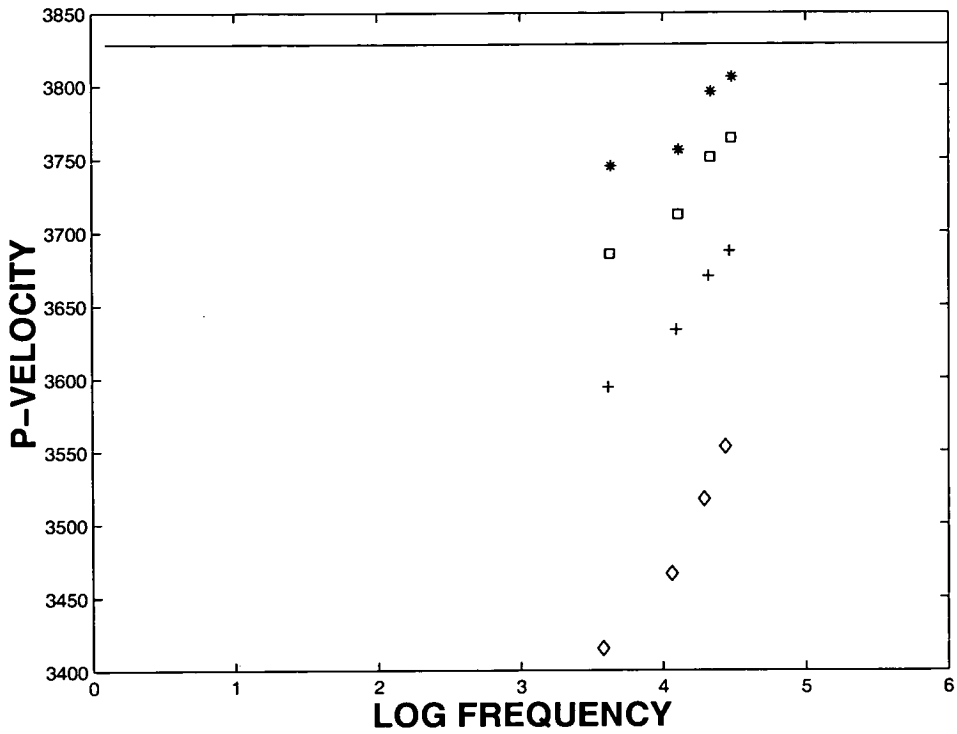

Figure 6–1: Theoretical dispersion curve in the absence of cracks (solid line) together with the resonant bar data points: $*$ - 40 MPa, $\square$ - 30 MPa, $+$ -20 MPa, $\diamond$ - 10 MPa.

Parameter	Unit	Value
λ_m	Pa	5.5×10^9
μ	Pa	2.45×10^{10}
ρ	kgm^{-3}	2288
ϕ_p	number	0.227
ϵ_0	number	0.24
c_{cr}	MPa^{-1}	0.07
τ	s	2×10^{-5}
γ	number	9.15
γ'	number	0.97
ς	m	2×10^{-4}

Table 6–1: The preliminary calibration of the model.

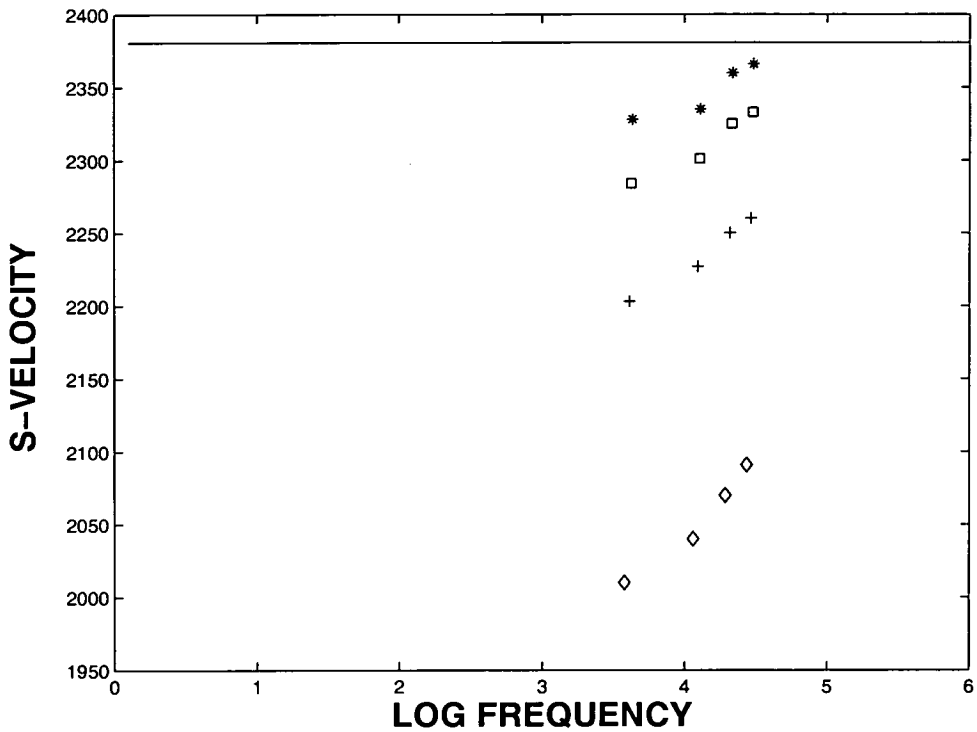

Figure 6–2: Theoretical dispersion curve in the absence of cracks (solid line) together with the resonant bar data points: $*$ - 40 MPa, $\square$ - 30 MPa, $+$ - 20 MPa, $\diamond$ - 10 MPa.

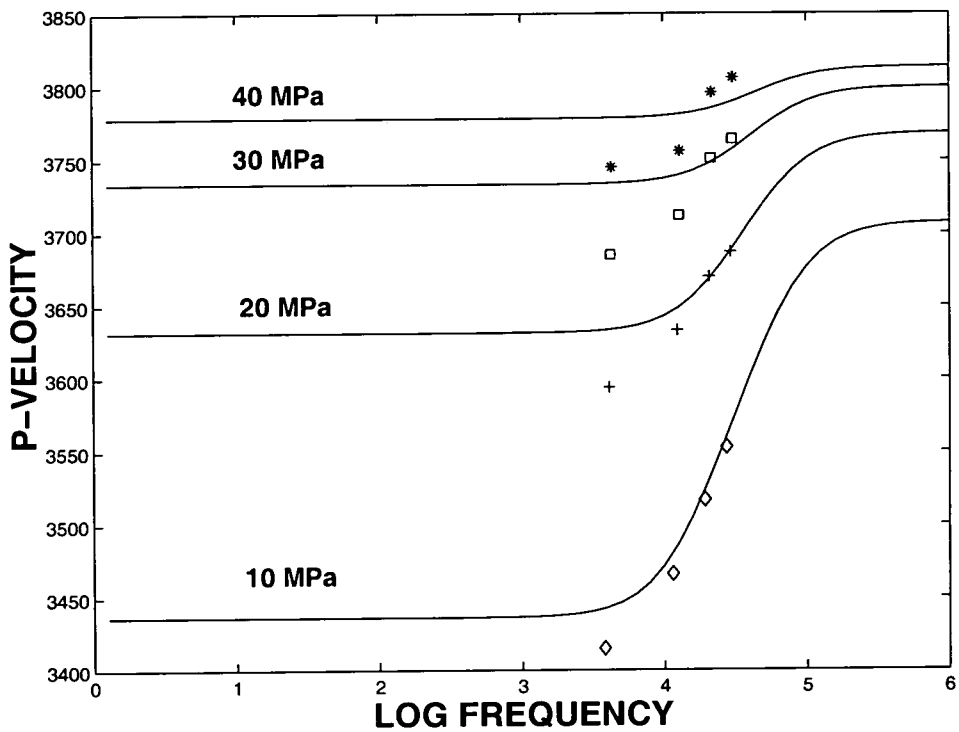

Figure 6–3: Theoretical dispersion curves for different effective stresses together with resonant bar measurements: $*$ - 40 MPa, $\square$ - 30 MPa, $+$ - 20 MPa, $\diamond$ - 10 MPa

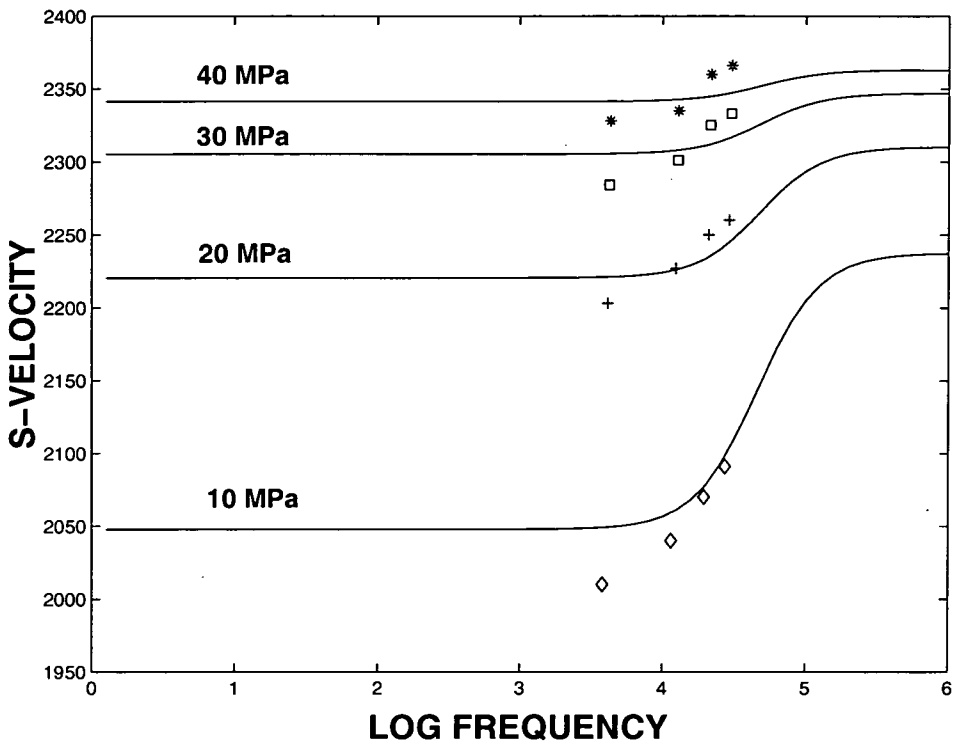

Figure 6–4: Theoretical dispersion curves for different effective stresses together with resonant bar measurements: $*$ - 40 MPa, $\square$ - 30 MPa, $+$ - 20 MPa, $\diamond$ - 10 MPa

One can see that the introduction of cracks leads not only to an overall drop in the velocity of both P- and S- waves at all frequencies, but also to an increase in the magnitude of the dispersion between low and high frequencies. The point at which transition between the low and high frequency regimes begins is controlled by the choice of the parameter τ.

Modelling the Quality factor, Q, is intrinsically problematic. In the preceding analysis I calculate, as a function of frequency, both the real and imaginary parts of the wavenumber, y. Under ideal conditions Q would be defined to be:

$$Q_{id} = \frac{\Re y}{\Im y}. \tag{6.15}$$

This analysis assumes that all attenuation is due to fluid motion, which implies in effect that Q would be infinite for dry rock. This is of course far from the case. In particular, inter-granular friction (Walsh, 1966) and thermo-elastic effects (Savage, 1966) are generally proposed as important mechanisms for attenuation in such rocks. The data for the dry resonant bar which I present in appendix A show Q values which are much higher than for the saturated case, which are relatively independent of frequency and which increase substantially with increasing effective stress. There is at present no quantitative theory which can satisfactorily model these effects.

Clearly I require to take account of inter-granular friction before I model the Quality factor. One possible solution would be to supply imaginary parts for the reference elastic tensor so as to be able to reproduce the dry Quality factor results. I believe that this approach is unsatisfactory. Saturating the rock will lubricate inter-granular contact points, and I expect that this will have a substantial effect on the magnitude of the induced attenuation.

The best that I can do is to introduce an arbitrary Q term $Q^0_{\sigma_{eff}}$ for each value of effective stress, and then calculate the final Q from:

$$\frac{1}{Q} = \frac{1}{Q^0_{\sigma_{eff}}} + \frac{1}{Q_{id}}. \tag{6.16}$$

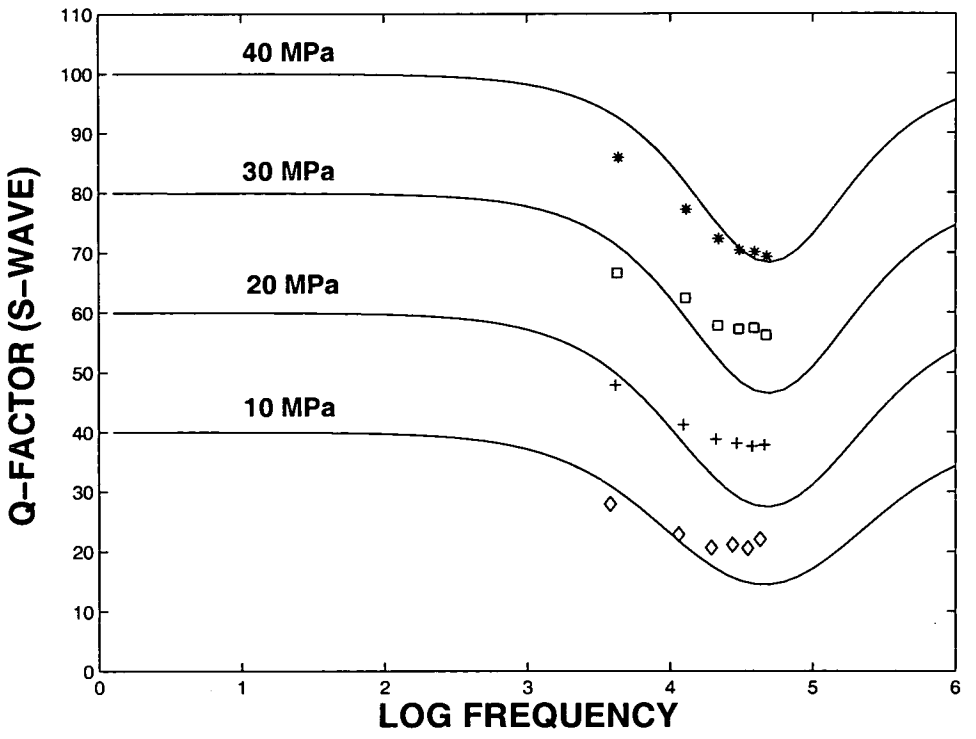

Figure 6–5: Theoretical modelling of Qs for different effective stresses together with resonant bar measurements: $*$ - 40 MPa, $\square$ - 30 MPa, $+$ - 20 MPa, $\diamond$ - 10 MPa.

The increase in the number of adjustable parameters greatly reduces the predictive power of the model. Nevertheless, if I take the values, $Q_{10}^0 = 40$, $Q_{20}^0 = 60$, $Q_{30}^0 = 80$, $Q_{40}^0 = 100$, the resulting modelling of Qs is given in Figure (6-5).

The data for the P-wave Quality factor appear to be rather noisy, and I therefore will not attempt to model them explicitly.

The modelling which I have presented would be likely to be considered the best possible fit to the data in the absence of other observations. Indeed, the agreement with the data is very encouraging. A number of questions remain however.

It would indeed be a coincidence if the characteristic frequency of the rock, $(1/\tau)$, happened to be exactly at the point where the resonant bar observations were taken. It is equally possible that the characteristic frequency could be below or above the measurement frequencies, the magnitude of the dispersion being

larger, and the data points could be at either the beginning or the end of the transition from low frequency to high frequency. Typically, absolute errors introduced by uncertainty over the slope of the dispersion curve will tend to increase with the magnitude of dispersion. Attempts to differentiate between these possibilities by means, for example, of least squares fitting will therefore always favour the interpretation presented, that of a low magnitude of dispersion, but this is not evidence that it is correct.

The modelling is also suspicious in that it predicts higher values of Qs at ultrasonic frequencies than experience leads one to suspect. It is imperative, therefore to consider further observations to provide additional constraints for the modelling.

One could attempt to estimate the scale of total dispersion from observing the ultrasonic velocities of adjacent plugs. However the variation in the velocities between individual plugs inhibits this approach. I argue that a more robust method arises from a most unexpected source - fluid substitution effects in ultrasonic tests.

6.3 Fluid substitution effects at ultrasonic frequencies.

In addition to his work on the resonant bar, Sothcott carried out ultrasonic measurements on adjacent plugs as a function of both effective stress and pore fluid species. Fluid substitution, the prediction of the effect on velocity of changing the saturating fluid, generally depends on being able to calculate the effect of the different fluid bulk moduli on the bulk modulus of the saturated rock. This requires knowledge of the elastic interactions between individual pores. My model neglects such interactions and is therefore not perfectly suited to the purpose. I will therefore begin the analysis by considering poroelastic theories for fluid substitution which do not share this limitation, and will only return to my model when these theories fail.

We recall that Gassmann's (1951) theory allows the prediction of saturated velocities from dry velocities, knowing only the properties of the fluid, porosity

$\sigma_{eff}(MPa)$	Vp	Vs
10	3537	2193
20	3999	2558
30	4146	2692
40	4201	2734

Table 6–2: Dry velocities of the ultrasonic plug.

of the rock and elastic constants of the mineral making up the rock. Gassmann's Theorem is strictly valid only for very low frequencies, in contrast to the high (700 kHz) frequencies which were used in the ultrasonic tests, but the ubiquity of the theory demands that I begin my analysis with it.

The first step in the application of Gassmann's Theorem is to calculate the dry frame moduli of the rock from the dry velocities. I present the dry velocities in Table (6-2)

The dry frame moduli, κ_{dry} and μ_{dry} are defined from:

$$V_s^{dry} = (\frac{\mu_{dry}}{\rho_{dry}})^{\frac{1}{2}}; \tag{6.17}$$

$$V_p^{dry} = (\frac{\kappa_{dry} + \frac{4}{3}\mu_{dry}}{\rho_{dry}})^{\frac{1}{2}}. \tag{6.18}$$

Given that the density of the dry rock was measured as 2044 kgm^{-3}, I calculate the dry frame moduli are as given in Table (6-3).

I now proceed to calculate the saturated moduli from these dry frame moduli according to Gassmann's Theorem:

$$\kappa_{sat} = \kappa_{dry} + \frac{(1 - \frac{\kappa_{dry}}{\kappa_m})^2}{\frac{\phi}{\kappa_f} + \frac{1-\phi}{\kappa_m} - \frac{\kappa_{dry}}{\kappa_m^2}}; \tag{6.19}$$

$$\mu_{sat} = \mu_{dry}. \tag{6.20}$$

σ_{eff} (MPa)	κ_{dry} (Pa)	μ_{dry} (Pa)
10	1.25×10^{10}	9.83×10^9
20	1.48×10^{10}	1.34×10^{10}
30	1.54×10^{10}	1.48×10^{10}
40	1.57×10^{10}	1.53×10^{10}

Table 6–3: Dry moduli for the ultrasonic plug.

In these equations, κ_m is the bulk modulus of the mineral making up the rock. I will take the value for Quartz, 3.8×10^{10} Pa for this purpose. κ_f is the bulk modulus of the fluid, which is 2.9×10^9 Pa for brine and 1.63×10^9 Pa for the oil which was used in the experiments. I will take, once again, 22.7% for the value of the porosity, ϕ.

The values of the saturated velocities then follow from:

$$V_p = (\frac{\kappa_{sat} + \frac{4}{3}\mu_{sat}}{\rho_{sat}})^{\frac{1}{2}}; \tag{6.21}$$

$$V_s = (\frac{\mu_{sat}}{\rho_{sat}})^{\frac{1}{2}}. \tag{6.22}$$

The density of the saturated rock was 2288 kgm^{-3} for brine saturation and 2227 kgm^{-3} for oil saturation.

The results for brine saturation are presented in Table (6-4) while those for oil saturation appear in Table (6-5).

For ease of comparison I now plot these predictions, together with the data, in Figures (6-6) and (6-7).

I consider that Gassmann's Theorem gives a poor fit to the data. Its predictions for P-wave velocity are generally too low, and it predicts that P-velocity for brine saturation is higher than that for oil saturation, in contradiction to the experimental data. The Gassmann predictions are for shear wave velocity to be

σ_{eff} (MPa)	κ_{sat} (Pa)	μ_{sat} (Pa)	V_p (ms^{-1})	V_s (ms^{-1})
10	1.75×10^{10}	9.83×10^{9}	3657	2073
20	1.90×10^{10}	1.34×10^{10}	4014	2420
30	1.94×10^{10}	1.48×10^{10}	4135	2543
40	1.96×10^{10}	1.53×10^{10}	4181	2586

Table 6–4: Gassmann predicted moduli and velocities for the brine saturated ultrasonic plug.

σ_{eff} (MPa)	κ_{sat} (Pa)	μ_{sat} (Pa)	V_p (ms^{-1})	V_s (ms^{-1})
10	1.55×10^{10}	9.83×10^{9}	3584	2101
20	1.73×10^{10}	1.34×10^{10}	3974	2453
30	1.78×10^{10}	1.48×10^{10}	4105	2578
40	1.80×10^{10}	1.53×10^{10}	4152	2621

Table 6–5: Gassmann predicted moduli and velocities for the oil saturated ultrasonic plug.

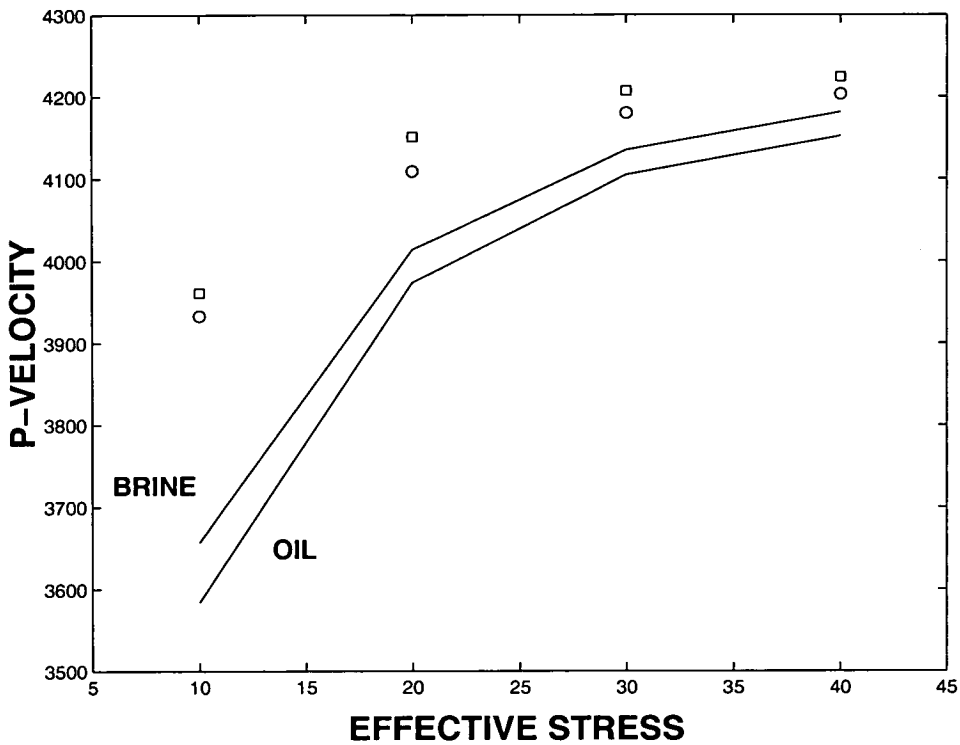

Figure 6–6: Ultrasonic velocity measurements for oil (□) and brine (○) saturations for different values of effective stress (MPa), together with the Gassmann predictions.

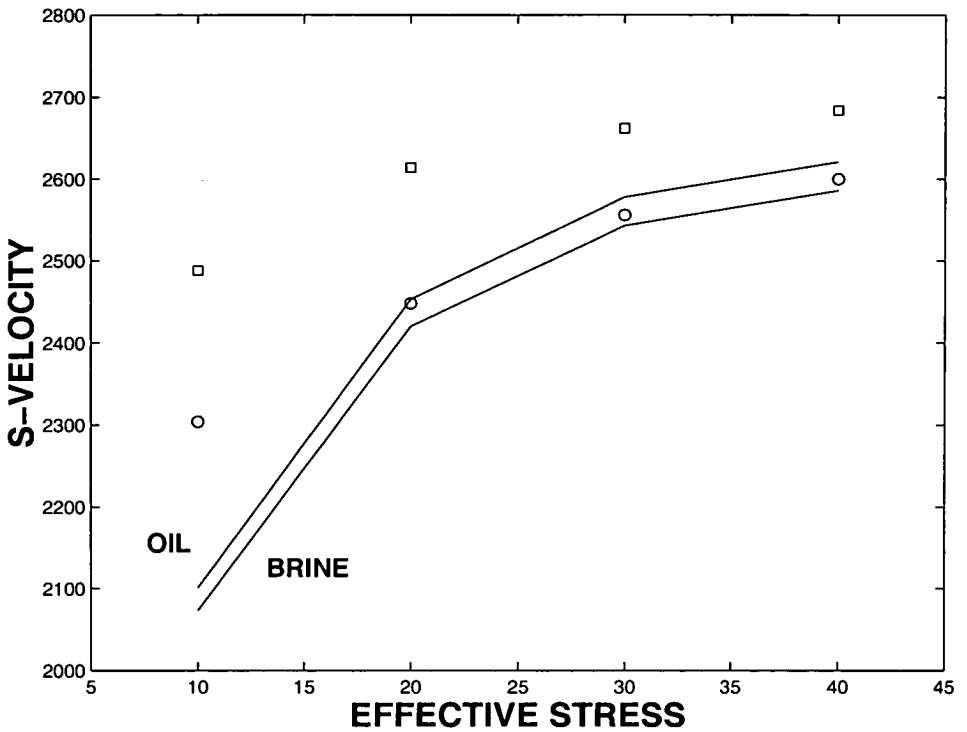

Figure 6–7: Ultrasonic velocity measurements for oil (□) and brine (○) saturations for different values of effective stress (MPa), together with the Gassmann predictions.

rather insensitive to the change of pore fluid, but the data shows that shear wave velocity is more sensitive to the saturating fluid than is P-wave velocity. It should be noted, however, that the predictions are better at high levels of effective stress, suggesting that the cause of the discrepancy involves microcracks, which would be expected to remain open at low effective stress.

The fact that Gassmann's Theorem gives poor results is not surprising. A key assumption of the theorem is that of perfect pressure equalisation in the fluid. This is suited to low frequency waves where the fluid has time to move to in response to pressure gradients, but could be unsuited to ultrasonic frequencies. Mavko and Jizba (1991), by contrast, derived a theory for fluid substitution at high frequencies, and I now implement their approach.

The Mavko and Jizba (1991) theory is a two stage process; one must first calculate the "unrelaxed frame moduli" κ_{uf} and μ_{uf} for each value of effective stress and then substitute these moduli into Gassmann's Theorem in place of the dry moduli to arrive at the saturated moduli. The formulae for the unrelaxed moduli are:

$$\frac{1}{\kappa_{uf}} = \frac{1}{\kappa_{hiP}} + \phi_{soft}\left(\frac{1}{\kappa_f} - \frac{1}{\kappa_m}\right); \tag{6.23}$$

$$\frac{1}{\mu_{uf}} = \frac{1}{\mu_{dry}} + \frac{4}{15}\left(\frac{1}{\kappa_{uf}} - \frac{1}{\kappa_{dry}}\right). \tag{6.24}$$

There are two ambiguities in these equations. The first concerns the dry bulk modulus at high effective stress, κ_{hiP}. This can be interpreted as being the bulk modulus of the rock when effective stress is high enough to close all microcracks. In the current dataset there is a small difference in velocity between 30 and 40 MPa of effective stress, so I feel justified in taking the dry bulk modulus for 40 MPa, 1.56×10^{10} Pa as κ_{hiP}.

The second ambiguity concerns the "soft porosity" ϕ_{soft}. This is the fractional volume of pore space which closes due to the imposition of stress. Mavko and Jizba (1991) suggest that this is usually small enough to ignore, the figures they quote

σ_{eff}	$\mu_{uf}(Pa)$	V_p (brine)	V_s (brine)	V_p (oil)	V_s (oil)
10	1.03×10^{10}	3817	2122	3774	2151
20	1.36×10^{10}	4061	2438	4028	2471
30	1.49×10^{10}	4153	2552	4123	2587
40	1.53×10^{10}	4181	2586	4152	2621

Table 6–6: Mavko-Jizba predicted velocities for the ultrasonic plug under oil and brine saturation.

for sandstones being of the order of 10^{-3}. I performed numerical experiments for various values of ϕ_{soft} in the range 0-10^{-2} and found that the results could not be improved significantly by a judicious choice of ϕ_{soft}, so for this example I will present the modelling for ϕ_{soft}=0.

With this restriction I find that $\kappa_{uf} = 1.56 \times 10^{10}$ Pa, independently of saturation and applied stress. I then insert this value into Gassmann's formula and find that for brine saturation, $\kappa^b_{sat} = 1.96 \times 10^{10}$ Pa while for oil saturation, $\kappa^o_{sat} = 1.80 \times 10^{10}$ Pa. The values for μ_{uf} and the velocities are then those given in Table (6-6).

I now graph this modelling in Figures (6-8) and (6-9).

The Mavko-Jizba theory certainly performs better than the Gassmann theory. A number of problems remain, however. The modelling is still unreliable at low effective stress, and it again fails to predict the sensitivity of shear wave velocity to pore-fluid type. As with Gassmann's Theorem, the Mavko-Jizba theory predicts that P-wave velocity will be higher for brine saturation than it is for oil saturation, in contradiction to the experimental results.

This represents a formidable problem. In total five cores from the same vicinity were tested with oil and brine and all five showed that P-wave velocity was higher for oil saturation, which suggests that this is a persistent effect. It is very unsatisfactory that the two main theories for fluid substitution are incapable of

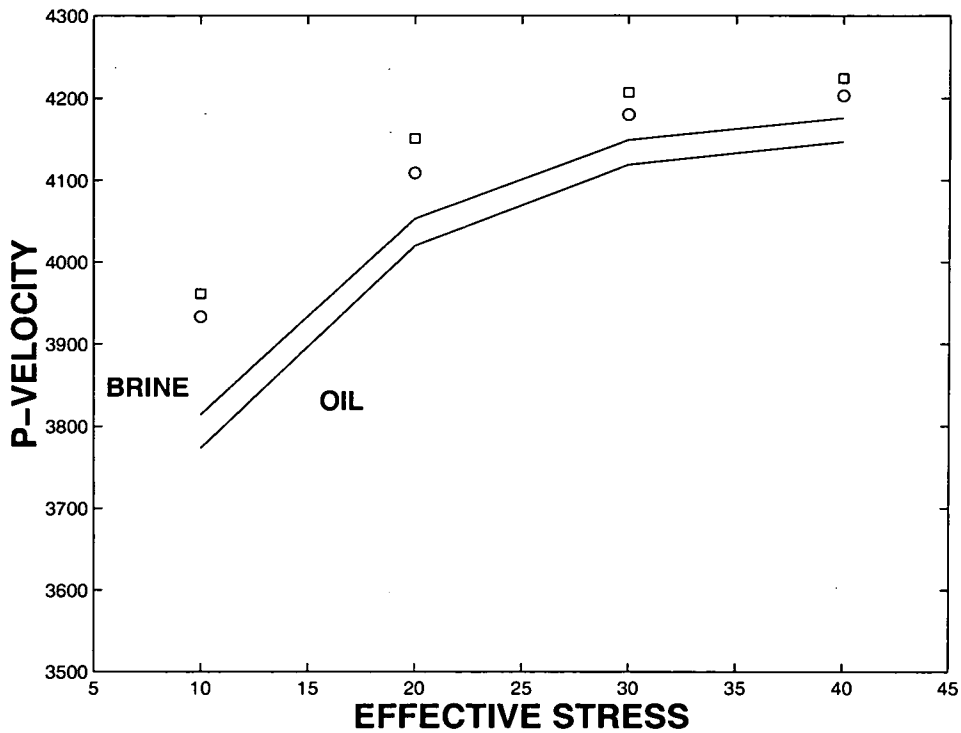

Figure 6–8: Ultrasonic velocity measurements for oil (□) and brine (○) saturations for different values of effective stress (MPa) together with the Mavko-Jizba predictions.

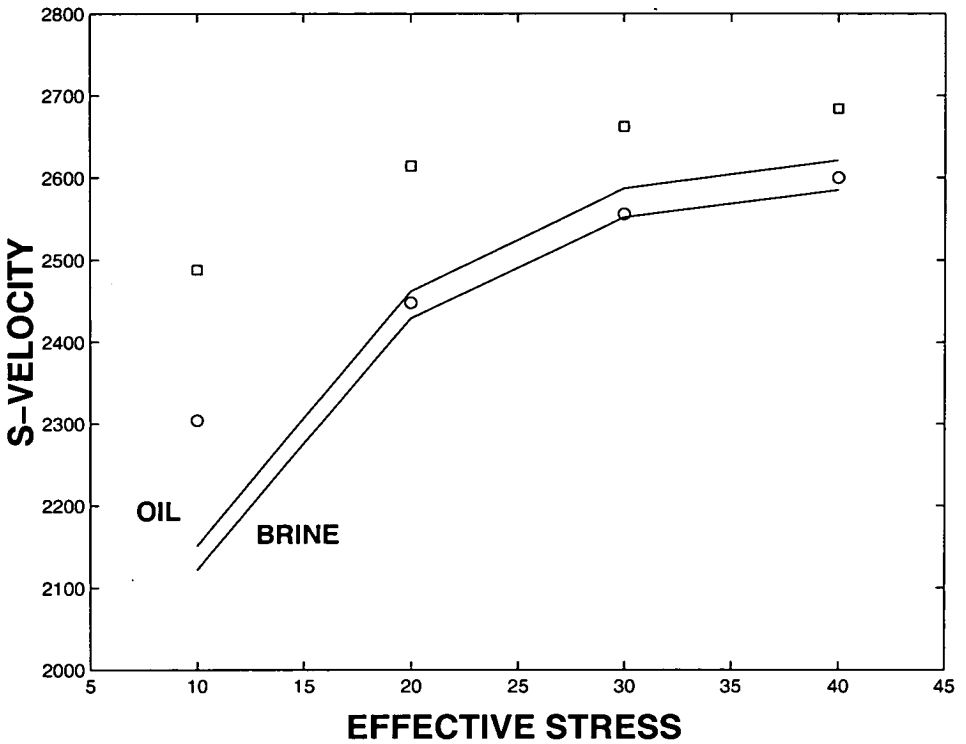

Figure 6–9: Ultrasonic velocity measurements for oil(□) and brine (○) saturations for different values of effective stress (MPa) together with the Mavko-Jizba predictions.

explaining such a basic observation. In the following section I advance a possible explanation for this effect.

6.4 An explanation of the fluid substitution effect

I pointed out earlier that my model is not perfectly suited to the fluid substitution problem since it does not take into account elastic interactions between different pores. Given that the Gassmann and Mavko-Jizba theories have failed, however, it seems appropriate to attempt to use it in this case. I will start my investigations by taking my preliminary calibration for brine saturation and changing the fluid properties to see what effect this has.

A number of parameters from the model are sensitive to the saturating fluid. When the brine was replaced by oil the density of the sample fell from 2288 kgm^{-3} to 2227 kgm^{-3}. We recall also that τ is proportional to fluid viscosity. The viscosity of the oil was 7.5 cP, as opposed to 1 cP for the brine, so I must always have:

$$\tau_{oil} = 7.5\tau_{brine}. \tag{6.25}$$

This results in a value $\tau = 7 \times 10^{-4}$ s for oil saturation.

I must also change the value of γ since this depends on fluid compressibility. The first step once again is to estimate K_p from (6.11):

$$K_p = \frac{4}{3}\frac{\mu}{\kappa_f} \approx \frac{4}{3}\frac{\rho_s}{\rho_f}(\frac{V_s}{V_f})^2. \tag{6.26}$$

A complication immediately arises when we consider that in my previous estimation of γ I took a representative shear wave velocity based on data for brine saturation. It could be argued that I should now take a different value for the representative shear wave velocity. I reject this view. The representative shear

wave velocity comes into the approximation in place of the reference shear wave modulus μ which does not contain any information about the saturation of the sample. In my view it would be incorrect to encode any such information into the γ estimation by changing the representative velocity. Of course there is now ambiguity in the γ estimation since one could equally well take values based on brine saturated, oil saturated or dry conditions, or indeed any average of all or some of these. I believe that ambiguity is to be expected in such approximations, and I suggest that the choice one makes at the outset is not, within reason, important but that being consistent to it is.

I therefore change ρ_f to 810 kgm^{-3} and V_f to 1420 ms^{-1}, keeping all other values constant, and I find:

$$K_p \approx \frac{4(2.28)}{3(.81)}(\frac{2236}{1420})^2 = 9.3. \tag{6.27}$$

γ then follows from:

$$\gamma \approx \frac{3\pi}{8(1-v)}(1+K_p) = 15.2, \tag{6.28}$$

with γ' remaining unchanged at 0.97.

I am now ready to compare the predictions of the model for brine and oil saturations. For 30 MPa of effective stress, the modelling for P and S-wave velocities for the two saturations are given in Figures (6-10) and (6-11).

In the P-wave example, at very low frequency there are competing effects of density and compressibility. The oil is less dense, and this on its own would mean that the velocity for oil saturation would be higher than for brine saturation. Brine is less compressible however, raising the velocity for brine saturation relative to oil saturation. The compressibility effect dominates the density effect and the brine velocity is higher. This is the result obtained earlier with Gassmann's Theorem. At very high frequencies, the fluid cannot move between elements of pore space, and this weakens the effect of fluid compressibility. It is still large enough to

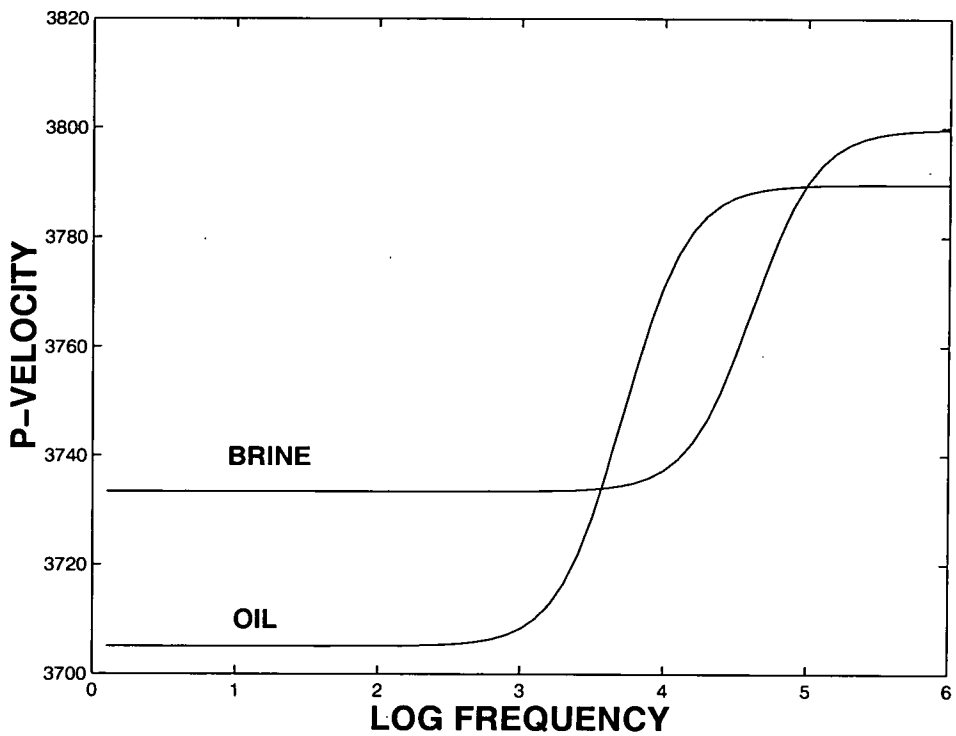

Figure 6–10: Theoretical dispersion curves under 30 MPa effective stress for oil and brine saturation implied by the preliminary calibration.

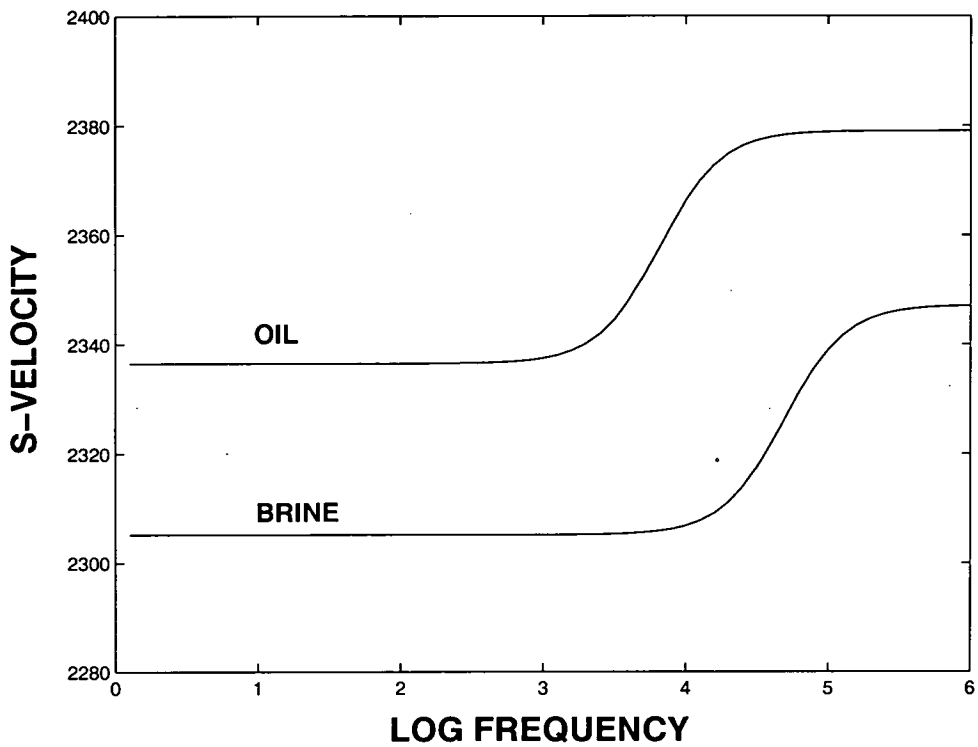

Figure 6–11: Theoretical dispersion curves under 30 MPa effective stress for oil and brine saturation implied by the preliminary calibration.

dominate the density effect, but not by such a large amount. This is the result which we obtained with the Mavko and Jizba theory.

The oil, having a larger viscosity than brine, has a larger τ and therefore begins the transition from the low frequency case to the higher frequency case at a lower frequency. This results in a transition region in which the oil velocity is temporarily higher than the brine velocity.

For S-wave velocity my model does not predict that there is any compressibility effect, since the cracks have very low aspect ratio and the pores are perfectly spherical. If there were pores of intermediate aspect ratio ($\frac{1}{2}$, say) there would be some dependence on fluid compressibility at high frequency (Endres and Knight, 1997) but this would be small compared to the effect for P-wave velocity. The density effect therefore means that at both high and low frequency the S-wave velocity in oil is higher than that in brine. Once again the oil saturated sample begins its transition between the low and high frequency regimes at a lower frequency, meaning that there is a region in which the velocity of the oil saturation is very much higher than the brine saturation.

Now consider frequencies f such that $3.5 < \log_{10} f < 3.9$ or $4.5 < \log_{10} f < 4.9$. At these frequencies P-wave velocities for oil saturation are slightly higher than those for brine saturation, but S-wave velocities are substantially higher for oil saturation. This is exactly the effect which was observed in the ultrasonic tests and which we could not explain with reference to the Gassmann or Mavko-Jizba theories.

I cannot hope to explain the ultrasonic results on the basis of the preliminary calibration. The frequency used for the ultrasonic tests was 700 kHz, so $\log_{10}$f was 5.85 - in which region the preliminary calibration predicts that brine saturation is faster. I therefore will need to move the transition region to higher frequencies, which means reducing the value of τ.

I find that the width of the transition region decreases, and the position of the region moves to lower frequencies, with increasing effective stress. If there is to be a significant band of frequencies over which this effect occurs for all values of

Parameter	Unit	Value (brine)	Value (oil)
λ_m	Pa	3.33×10^9	3.33×10^9
μ	Pa	3.33×10^{10}	3.33×10^{10}
ρ	kgm^{-3}	2288	2227
ϕ_p	number	0.227	0.227
ϵ_0	number	0.3	0.3
c_{cr}	MPa^{-1}	0.035	0.035
τ	s	2×10^{-6}	1.5×10^{-5}
γ	number	9.15	15.20
γ'	number	0.97	0.97
ς	m	2×10^{-4}	2×10^{-4}

Table 6–7: The calibration chosen for the ultrasonic data.

effective stress, a necessity if I am to explain why this effect occurs in five different cores, then the magnitude of dispersion will have to be higher than was the case in the preliminary calibration. A higher magnitude of dispersion is also necessary to explain the resonant bar data, since decreasing τ to produce the fluid substitution effect at ultrasonic frequencies would lead to predictions of no dispersion at the resonant bar frequencies without a corresponding increase in ϵ.

I shall proceed as follows. To begin with I will model the fluid substitution effect at ultrasonic frequencies, basing my interpretation on the fact that τ must be chosen to make sure that I am at the high frequency end of the transition region. I will then compare the resulting dispersion curves with the resonant bar data. Since the resonant bar and the ultrasonic plug are different rock samples, with different dry velocities, I do not expect good agreement, but I hope that the comparison will nevertheless be useful.

My choice for the reference elastic constants for the new model is $\lambda_m = 3.33 \times 10^9$ Pa and $\mu = 3.33 \times 10^{10}$ Pa. I will change ϵ_0 to 0.3, c_{cr} to 3.5×10^{-2} MPa^{-1} and τ to 2×10^{-6} s. All other parameters are the same as before. This calibration is summarised in Table (6-7).

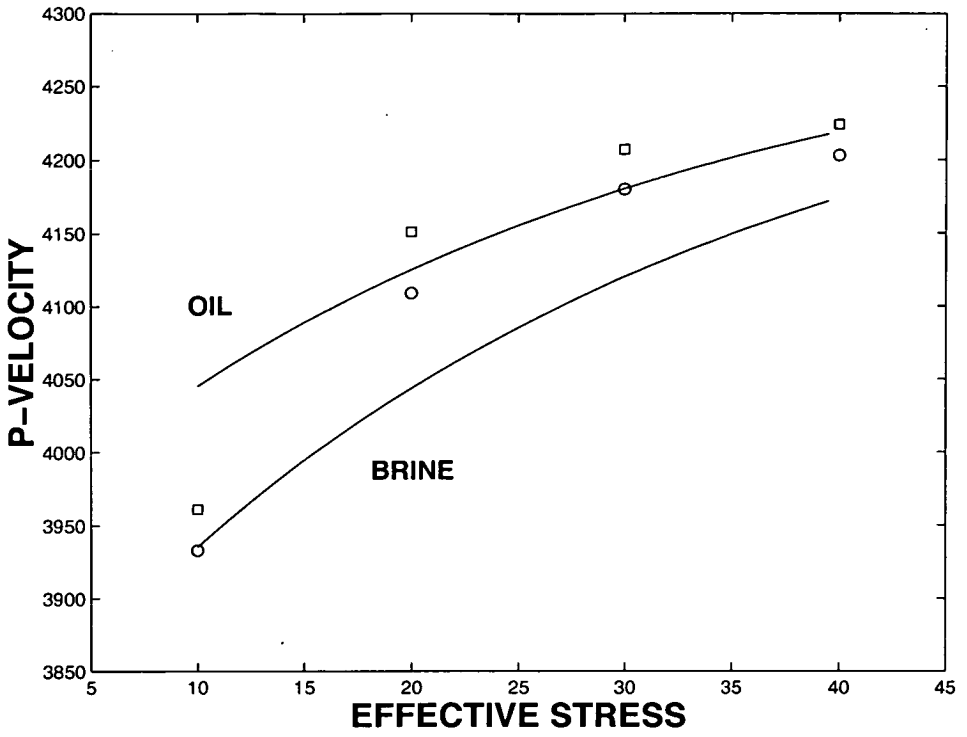

Figure 6–12: Ultrasonic velocity measurements for oil (□) and brine (○) saturations for different values of effective stress (MPa) together with the theoretical curves.

I reproduce the modelling resulting from this calibration in Figures (6-12) and (6-13). I consider it to be a reasonable fit to the data.

In Figures (6-14) and (6-15) I compare the dispersion curves implied by the fit to the ultrasonic data with the resonant bar measurements. To model the shear wave Quality factor I require once again to specify the Q- intercepts. The modelling for the choice $Q^0_{10} = 30$, $Q^0_{20} = 55$, $Q^0_{30} = 75$ and $Q^0_{40} = 90$ is given in Figure (6-16).

Naturally this model is not as good a visual fit to the data as was given by the preliminary calibration. This would be too much to expect given the requirement to simultaneously model data from two different rock samples. We know from experience that different plugs from the same piece of rock often have different velocities and respond differently to the imposition of effective stress. Nevertheless

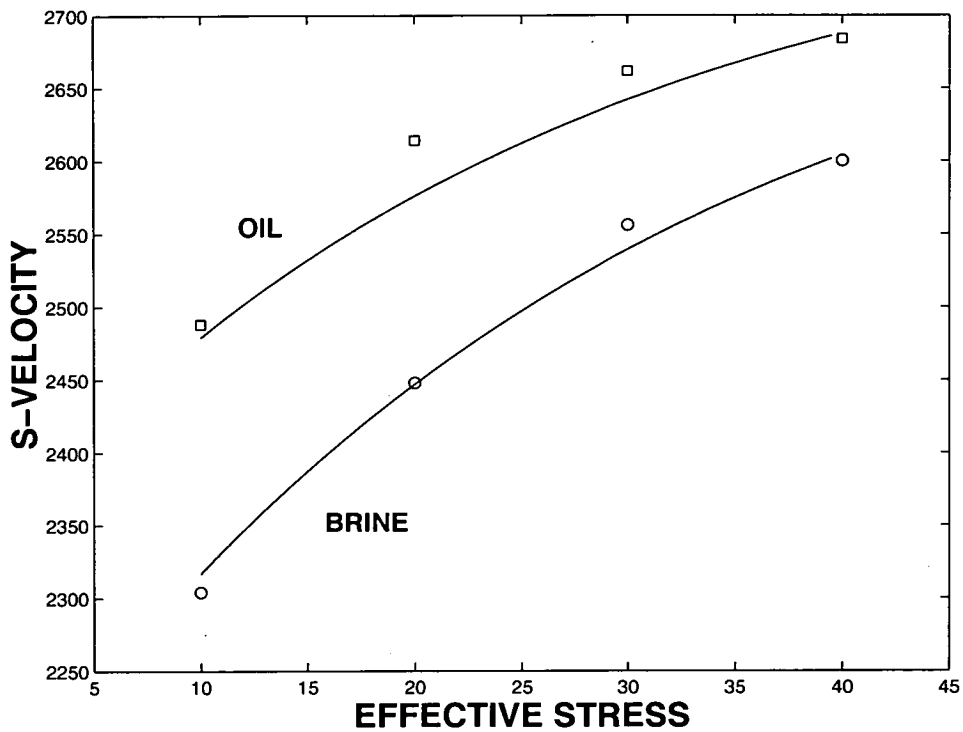

Figure 6–13: Ultrasonic velocity measurements for oil (□) and brine (○) saturations for different values of effective stress (MPa) together with the theoretical curves.

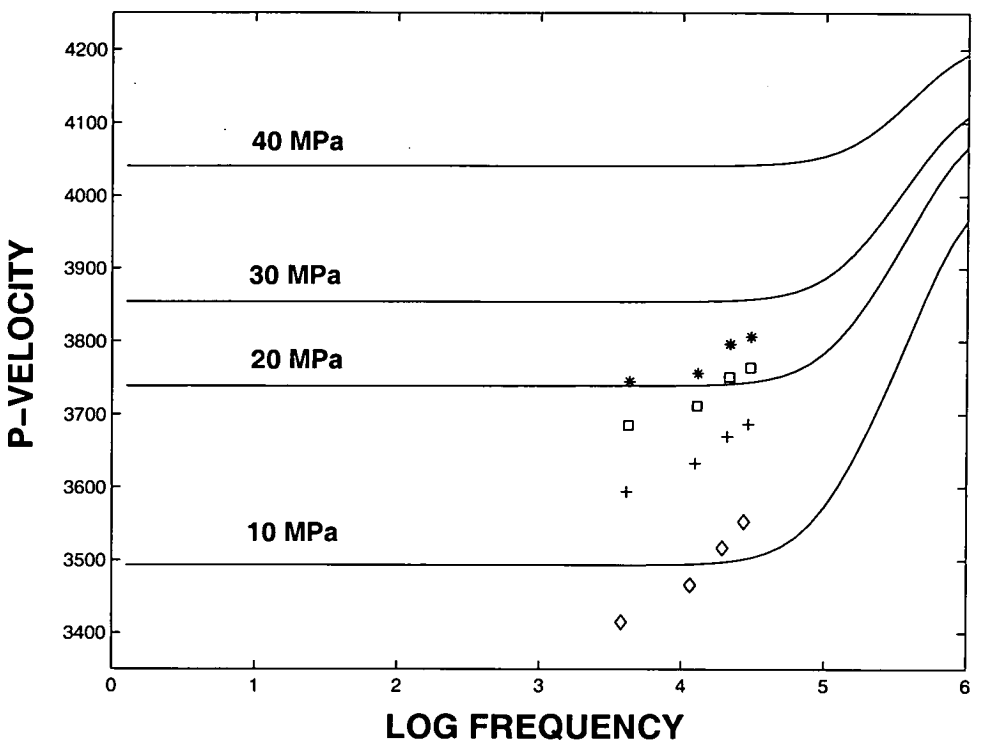

Figure 6–14: Dispersion curves implied by the ultrasonic model together with the resonant bar measurements: $*$ - 40 MPa, $\square$ - 30 MPa, $+$ - 20 MPa, $\diamond$ - 10 MPa.

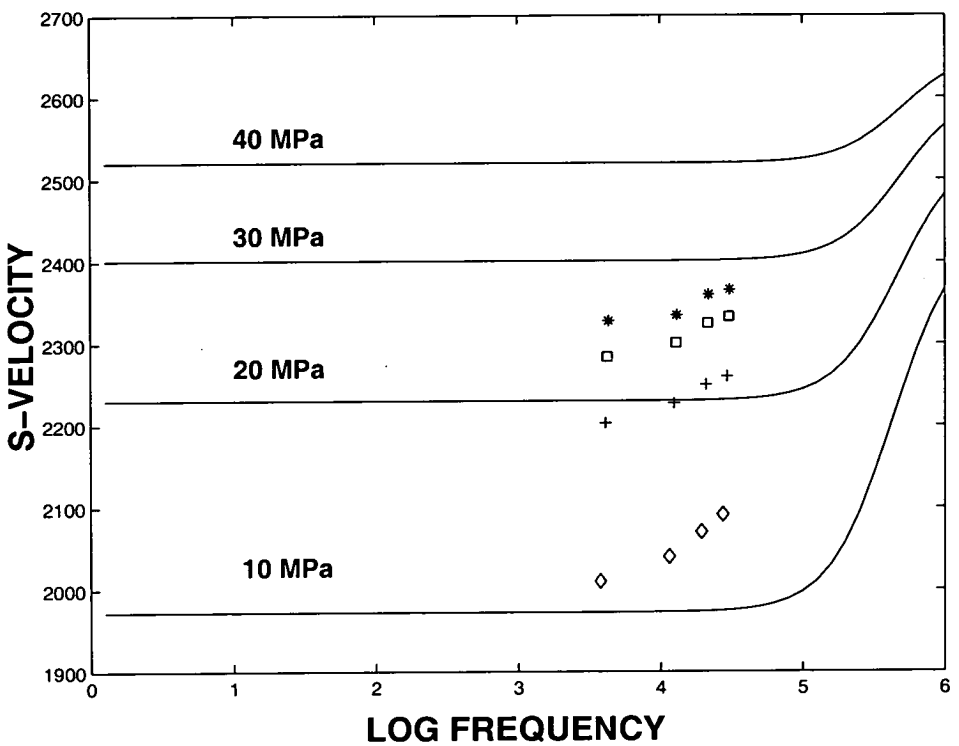

Figure 6–15: Dispersion curves implied by the ultrasonic model together with the resonant bar measurements: $*$ - 40 MPa, $\square$ - 30 MPa, $+$ - 20 MPa, $\diamond$ - 10 MPa.

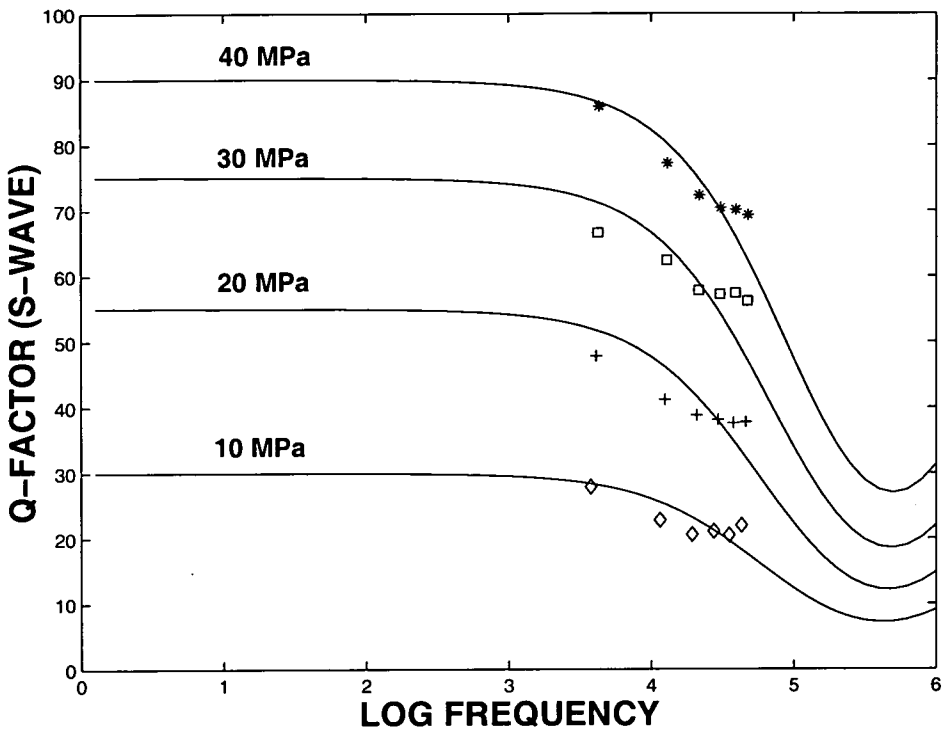

Figure 6–16: Theoretical modelling of Qs for different effective stresses implied by the ultrasonic model, together with resonant bar measurements: $*$ - 40 MPa, $\square$ - 30 MPa, $+$ - 20 MPa, $\diamond$ - 10 MPa.

I consider the latter model to be a more valid representation of the properties of the rocks under consideration.

The two main differences between the preliminary and final calibrations are the positioning of the transition region and the magnitude of dispersion. As mentioned earlier the requirement to model the ultrasonic data immediately implies a higher magnitude of dispersion than was present in the preliminary calibration. The value of τ in the final calibration was rather tightly constrained. The fluid substitution effect observed in the ultrasonic data, oil saturation being slightly faster for P-waves and substantially higher for S-waves occurs at two positions on the dispersion curve, at the beginning of the transition region and at the end of the transition region. If I had just had access to the ultrasonic data I could not have distinguished between these possibilities, but knowing that substantial dispersion is observed in the resonant bar data indicated that I had to choose the latter possibility. The final calibration is also consistent with the observed low values of Qs in ultrasonic experiments, in contrast to the preliminary calibration.

Of course it is quite possible that the different rock samples have entirely different properties and any attempt to constrain a model by tacitly assuming that their properties are similar is doomed to failure. Given the difficulty, if not impossibility, of extracting information from any one observation alone I believe this assumption is necessary if any progress is to be made.

It is helpful to consider the number of free parameters which I have employed to fit the data. I had to choose λ_m and μ as reference elastic moduli, although I could plausibly argue that the choice had limited impact on the variation of velocity with frequency, fluid type and pressure. Two further parameters were chosen to specify the relationship between crack density and effective stress. This was not an entirely free choice; I was required to use values which were at least broadly consistent with previous measurements of crack density (Peacock et al., 1994), although some scope for fitting remained. The τ parameter was the only truly free parameter which I chose to fit the data.

Given that I am, strictly speaking, applying my model to rocks with porosities beyond its range of validity I consider it helpful to compare the results with those

σ_{eff} (MPa)	κ_{dry} (Pa)	μ_{dry} (Pa)
10	8.51×10^9	8.18×10^9
20	1.11×10^{10}	1.05×10^{10}
30	1.22×10^{10}	1.17×10^{10}
40	1.24×10^{10}	1.23×10^{10}

Table 6–8: Dry moduli of the resonant bar sample.

obtained from a model which does not share this restriction. To that end I now attempt to repeat my interpretation of the data within the framework of Dvorkin et al. (1995).

6.5 Application of the Dvorkin et al. (1995) theory.

To apply the Dvorkin et al. (1995) theory to the data I require to specify the dry rock elastic moduli, the limiting value of the dry bulk modulus under high effective stress and the value of the fitting parameter Z. This arrangement has the advantage that the fact that the two rock samples are different, with different dry moduli can be incorporated into the modelling.

There is a complication in the calculation of the resonant bar dry rock moduli since the dry velocities were measured at a range of frequencies with slightly different results. My choice is to use the velocities at the lowest measured frequency for the calculation. This results in the values given in Table (6-8).

Once again I will take the value of the bulk modulus under 40 MPa of effective stress as being the limiting value κ_{hiP}. The values for the ultrasonic plug will be exactly as before.

The Z value is analogous to τ in my model in that it controls the position of

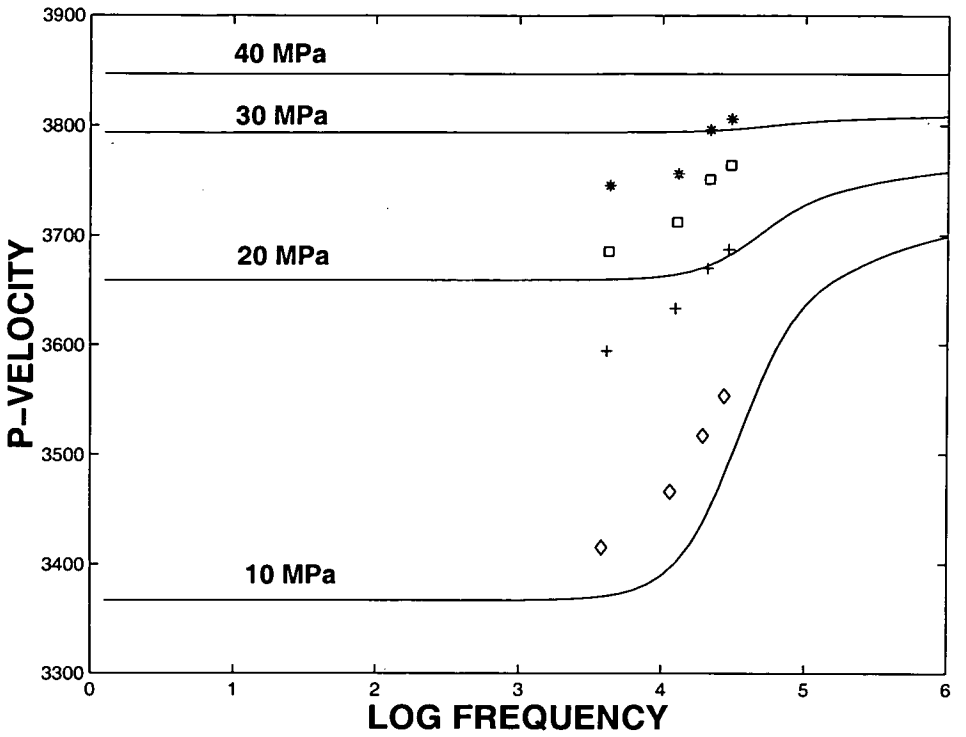

Figure 6–17: Theoretical dispersion curves implied by the Dvorkin et al. model for different values of effective stress, together with resonant bar measurements: $*$ - 40 MPa, $\square$ - 30 MPa, $+$ - 20 MPa, $\diamond$ - 10 MPa.

the transition from low to high frequency regimes. Choosing Z=10^{-2} to optimise the fit to the resonant bar data leads to the modelling in Figures (6-17) and (6-18).

The P-wave modelling gives a reasonable fit, but it is fair to say that the model underestimates the magnitude of S-wave dispersion. If I am to model both the resonant bar and ultrasonic data I will have to increase the magnitude of dispersion and move the transition region to higher frequencies. The problem of moving the transition region can be solved by taking a smaller Z value. Strictly speaking nothing can be done about increasing the amount of dispersion. This is controlled by the difference between the measured dry frame bulk modulus and the limiting bulk modulus κ_{hiP} which I estimated from the trend in the dry moduli.

To allow progress to be made with the model I will now suspend the interpretation of κ_{hiP} as the limiting value of the bulk modulus and allow it to become

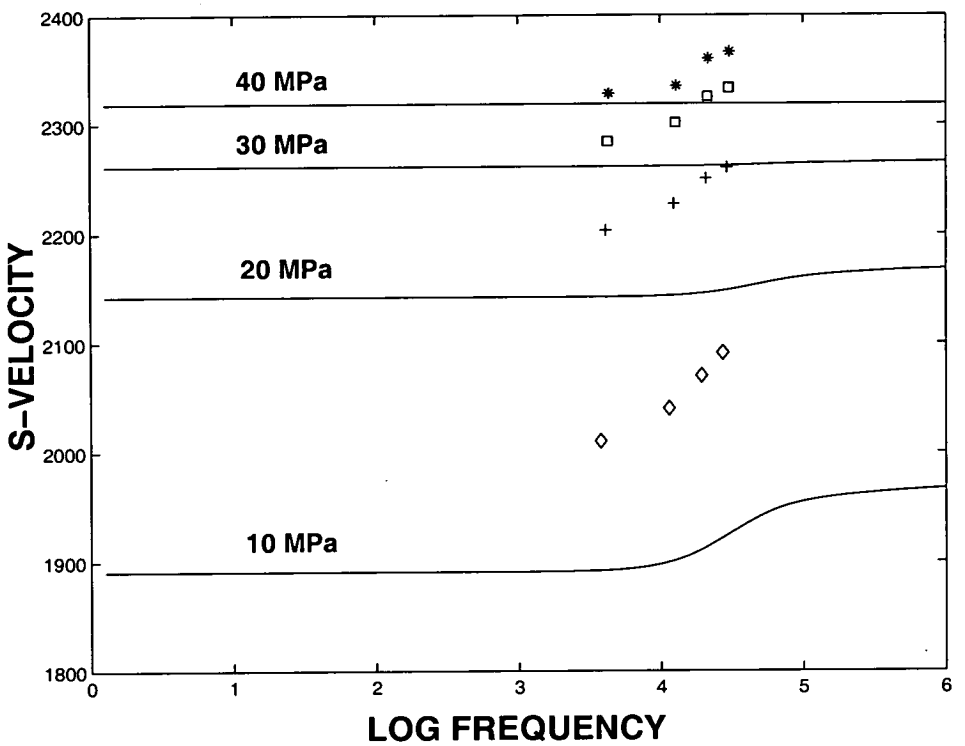

Figure 6–18: Theoretical dispersion curves implied by the Dvorkin et al. model for different values of effective stress, together with resonant bar measurements: $*$ - 40 MPa, $\square$ - 30 MPa, $+$ - 20 MPa, $\diamond$ - 10 MPa.

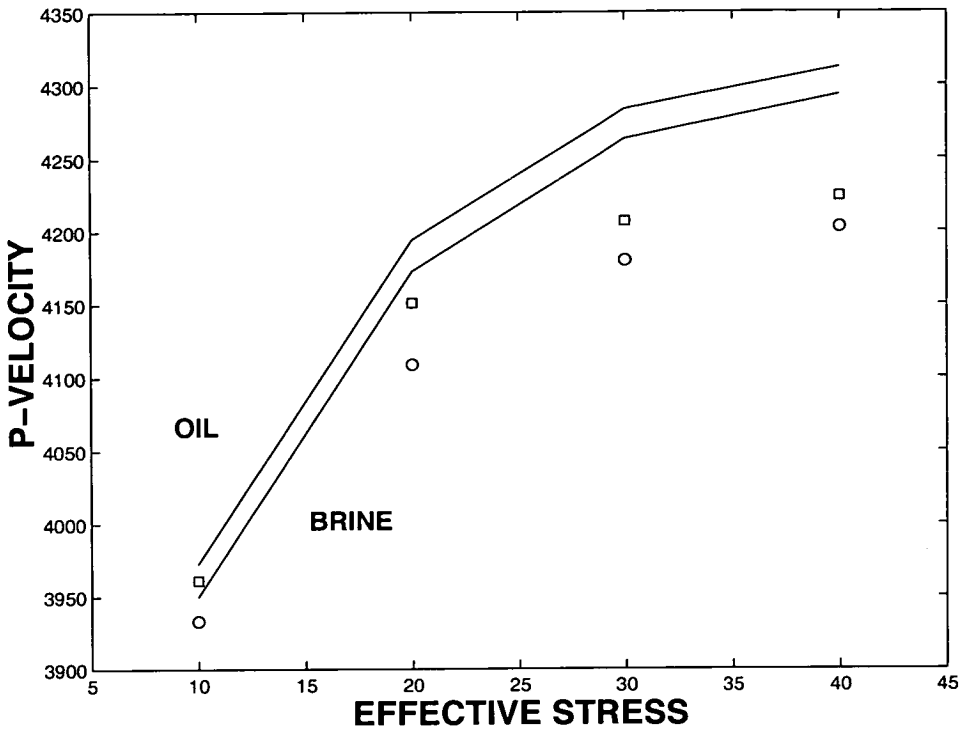

Figure 6–19: Ultrasonic velocity measurements for oil (□) and brine (○) saturation together with the predictions of the Dvorkin et al. model (relaxed interpretation).

an additional fitting parameter. I will change κ_{hiP} to 1.8×10^{10} Pa for both the resonant bar and ultrasonic plug and take $Z = 5 \times 10^{-3}$. With these parameters the modelling of the ultrasonic data is as presented in Figures (6-19) and (6-20).

The P-wave modelling fits the data rather well. The model supports my interpretation of the ultrasonic data in terms of the intermediate region in which P-velocity in oil saturated rock is temporarily higher than that in brine saturated rock.

The situation with the S-wave modelling is less favourable. The model underpredicts the difference in velocity between oil and brine saturation, markedly so at low effective stress. Indeed the predictions of S- velocities at 10 MPa of effective stress are both too low.

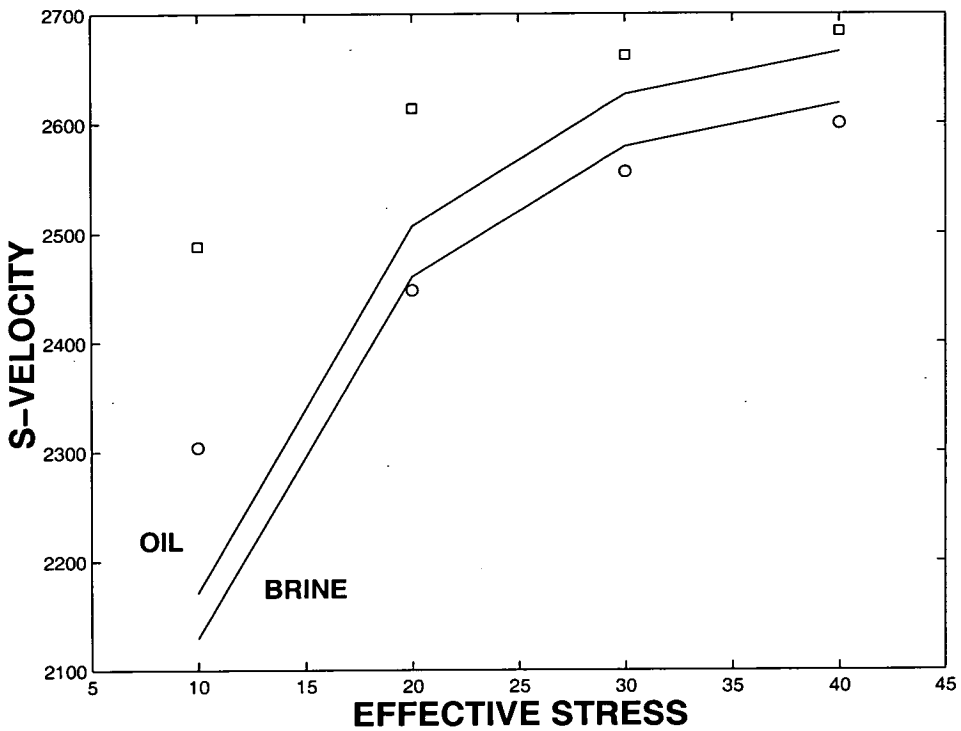

Figure 6–20: Ultrasonic velocity measurements for oil (□) and brine (○) saturation together with the predictions of the Dvorkin et al. model (relaxed interpretation).

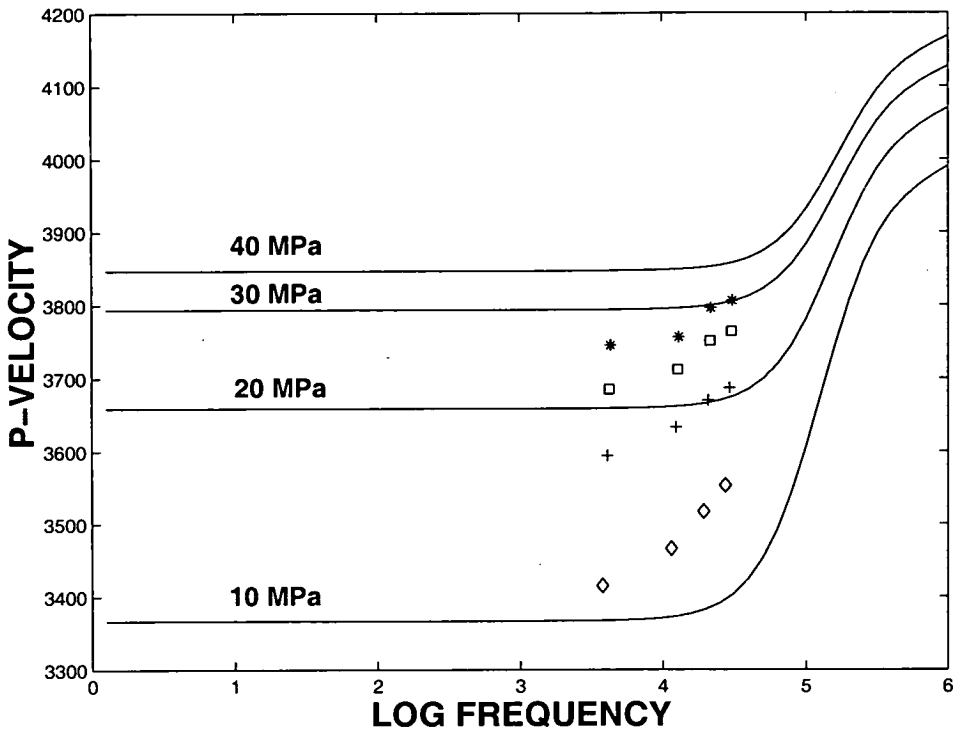

Figure 6–21: Dispersion curves implied by the Dvorkin et al. model (relaxed interpretation) for different values of effective stress together with resonant bar measurements: $*$ - 40 MPa, $\square$ - 30 MPa, $+$ - 20 MPa, $\diamond$ - 10 MPa.

The predictions of the velocities for the resonant bar data are given in Figures (6-21) and (6-22).

This confirms once again that the P-wave modelling is better than the S-wave modelling. It appears that the model of Dvorkin et al. (1995) systematically underestimates the magnitude of S-wave velocity dispersion in the rocks under consideration.

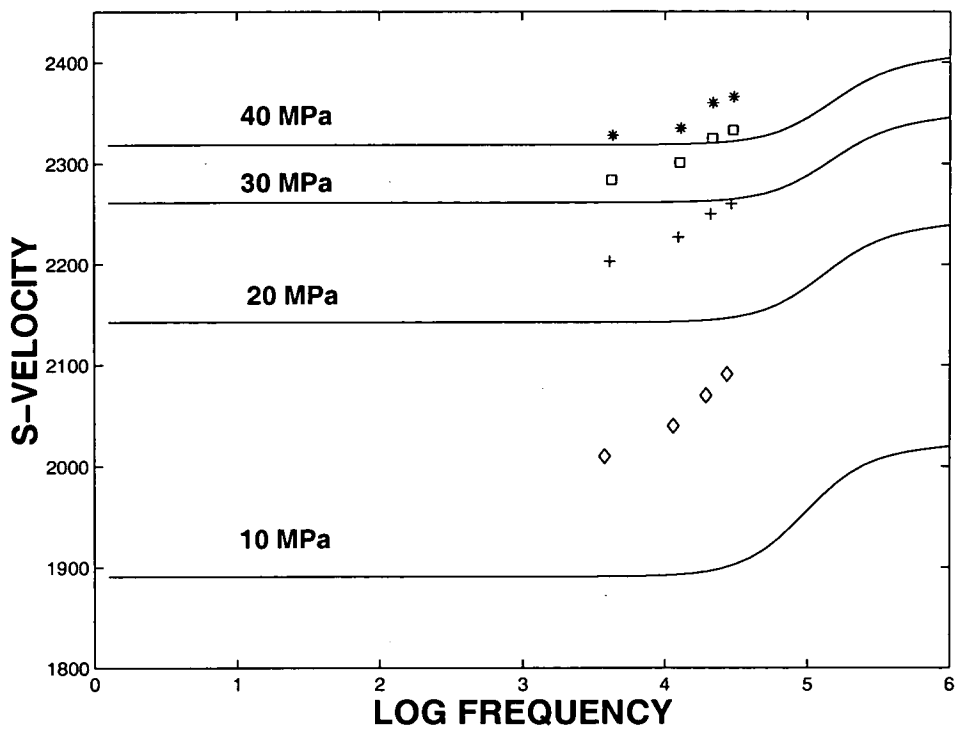

Figure 6–22: Dispersion curves implied by the Dvorkin et al. model (relaxed interpretation) for different values of effective stress together with resonant bar measurements: $*$ - 40 MPa, $\square$ - 30 MPa, $+$ - 20 MPa, $\diamond$ - 10 MPa.

6.6 Possible chemical effects.

The anomalous fluid substitution effects which we observed in the ultrasonic tests have been observed before, (Bacri & Salin, 1982; Wang et al., 1991). It has been suggested (Wang & Nur, 1992) that the cause of these effects is related to chemical interaction between the pore fluid and the rock sample. Brine, being a wetting fluid, was expected to soften the mineral making up the rock, whereas oil was not. This effect was thought to be particularly important in cases where there are large deposits of clay, which swells when brine is added, or shale. A particular indicator of these chemical effects was taken to be Gassmann's equation overestimating shear wave velocity.

It is clear that I cannot rule out effects due to chemical reactions, although the fact that the samples have low clay content, roughly 3 %, and that Gassmann's theorem underestimates shear wave velocity do not suggest that they are overly important. The velocities must be dispersive whatever we assume about chemical effects; we observe dispersion in the resonant bar data and the Gassmann predictions of shear wave velocity for brine saturation can only be lowered if we assume that the brine softens the frame. Both dispersion models, Dvorkin et al.'s and my own, then necessarily predict the structure of two regions in which the P-wave is faster for brine saturation separated by a region in which it is faster for oil saturation. I conclude that chemical effects by themselves cannot explain the data, and that the data have to be explained in terms of the dispersive models with or without chemical effects. Chemical effects are therefore to be considered as a potential source of error within the general framework I describe rather than being the controlling influence.

6.7 Conclusions.

In this chapter I explained how I consider that my model should be used in practice. I made estimates wherever possible in an attempt to reduce the number of adjustable parameters, but was left with having to specify a time constant τ and the relationship between crack density and effective stress, given by two constants ϵ_0 and c_{cr}. The time constant τ has the interpretation of giving the frequency at which the transition from low to high frequency regimes occurs, while the relationship between crack density and effective stress controls the magnitude of dispersion.

By choosing these parameters judiciously I was able to arrive at a preliminary fit to Sothcott et al.'s (2000) resonant bar data. I suggested, however, that a number of alternative fits were possible and that it was important to find a means of distinguishing between them. I rejected least squares fitting and visual comparison of data and predictions as inappropriate techniques.

I proposed a method to constrain the modelling based on an analysis of the fluid substitution effect at ultrasonic frequencies. Both the low frequency Gassmann and high frequency Mavko-Jizba (1991) theories predicted incorrectly that P-wave velocity in brine saturated rock was higher than that in oil saturated rock. I showed that my model, while agreeing with both the low and high frequency limits, predicted the existence of a region in which oil-saturated velocity was higher. This was supported by the modelling of Dvorkin et al. (1995). On the basis of ignoring possible chemical effects I argued that the ultrasonic frequencies used in the experiments had to lie in this region.

This represents an important result in itself. A number of authors have attempted to determine whether ultrasonic experiments are better described by low frequency theories, where the fluid is assumed to be relaxed, or high frequency theories where the fluid is unrelaxed. Murphy (1985) showed that the high frequency effective medium theories performed better than the low frequency Biot-Gassmann theories in the interpretation of ultrasonic tests on granite, but that the reverse

was true for lower frequency resonant bar tests, indicating that the transition occurred at some frequency in between the two. Mavko & Jizba (1991) have pointed out that, for a range of sandstones and granites, saturated S-velocity at low effective stress exceeds dry velocity, indicating that the fluid should be considered to be unrelaxed at ultrasonic frequencies. My analysis is the first direct evidence of a case in which neither the low nor high frequency limit is in itself adequate and where data can only be explained with the assumption that the ultrasonic frequencies are in an intermediate transition region. This interpretation is consistent with the common observation of low Quality factor results for ultrasonic tests. The modelling of the ultrasonic data on its own was extremely satisfactory.

My attempts to find a single model which would simultaneously explain both the ultrasonic and resonant bar data were rather poor. Undoubtedly the fact that the observations were carried out on different rock samples, which had different velocities and stress-sensitivities, was partly to blame for this. It was noticeable that the resonant bar modelling would have benefited from a higher τ value than was implied by the ultrasonic data. This might be indicative of different rock properties, but it might also suggest that the model is under-predicting the width of the transition region. More observations are required to differentiate these possibilities. Despite these objections I think it is fair to say that the ultrasonic tests suggest strongly that τ is smaller and the magnitude of dispersion is higher than was implied by the preliminary calibration, and I claim to have significantly constrained my model.

A strict interpretation of the model Dvorkin et al. (1995) leads to magnitudes of dispersion which are too small to explain the data. A more relaxed interpretation, taking κ_{hiP} as a fitting parameter, allows reasonable agreement, but the values of the S-wave dispersion still appear to be too low.

The strengths of the Dvorkin et al. approach lie in the fact that it models the elastic interactions between the pores and that it allows estimates for the magnitude of dispersion to be made with a minimum of observations. With my model calculating the magnitude of dispersion depends on knowing the crack density, which has to be inferred from a range of observations, but I would argue that the

resulting fit to the data is better. Clearly both models have their place in the analysis of laboratory data.

Chapter 7

Some predictions of the model.

Summary: I examine the relationships which are predicted by the calibration proposed in the previous chapter. P-wave attenuation in the absence of friction can be calculated but there is no way to estimate the frequency independent frictional component. The Biot wave is found to be slow and attenuated, but very sensitive to permeability. Velocities increase with fluid viscosity, but the precise nature of the relationship is complicated and frequency dependent.

7.1 P-wave Quality factor

I decided in the previous chapter not to model Sothcott et al.'s (2000) experimental data for the P-wave quality factor since they contained a great deal of noise and were likely to be unreliable. Nevertheless my calibration of the model leads to predictions for the effect of fluid flow on P-wave attenuation. My modelling for S-wave Quality factor contained a frequency independent frictional component which had to be estimated from the data. In the absence of data I have no means to estimate this component, and so I will reproduce, in Figure (7-1), the results derived only from a consideration of the squirt flow effect, for brine saturation.

In this graph I have plotted the attenuation 1/Q since in the absence of frictional effects Q is almost infinite at low frequencies. It is clear that the peak of attenuation lies in the ultrasonic frequency band. I note the expected result that

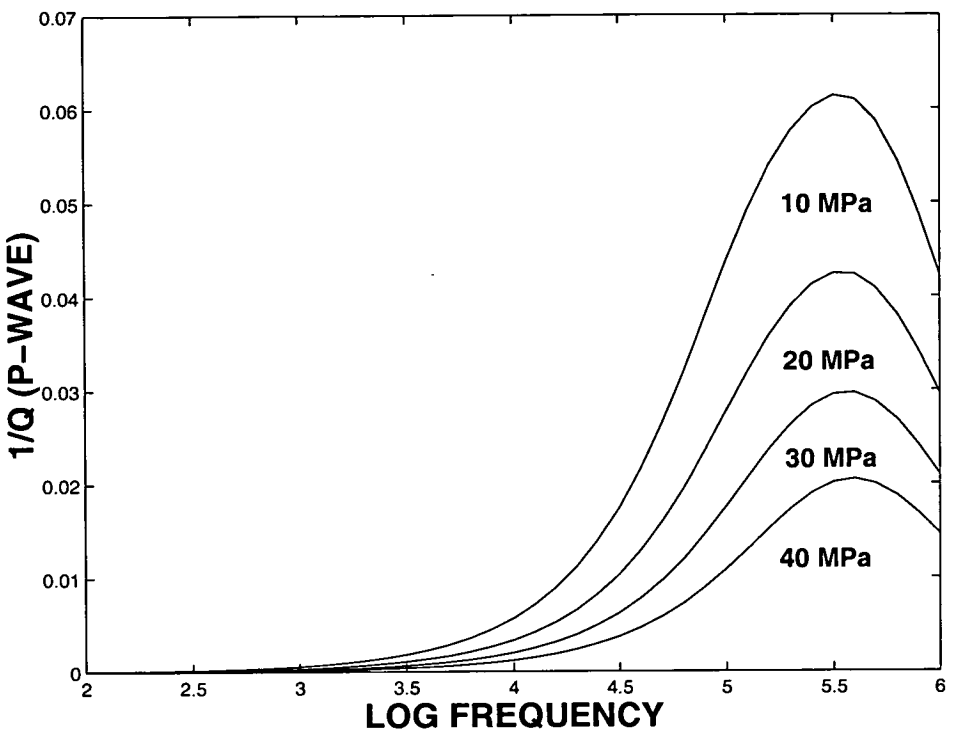

Figure 7–1: P-wave attenuation as a function of frequency for different values of effective stress.

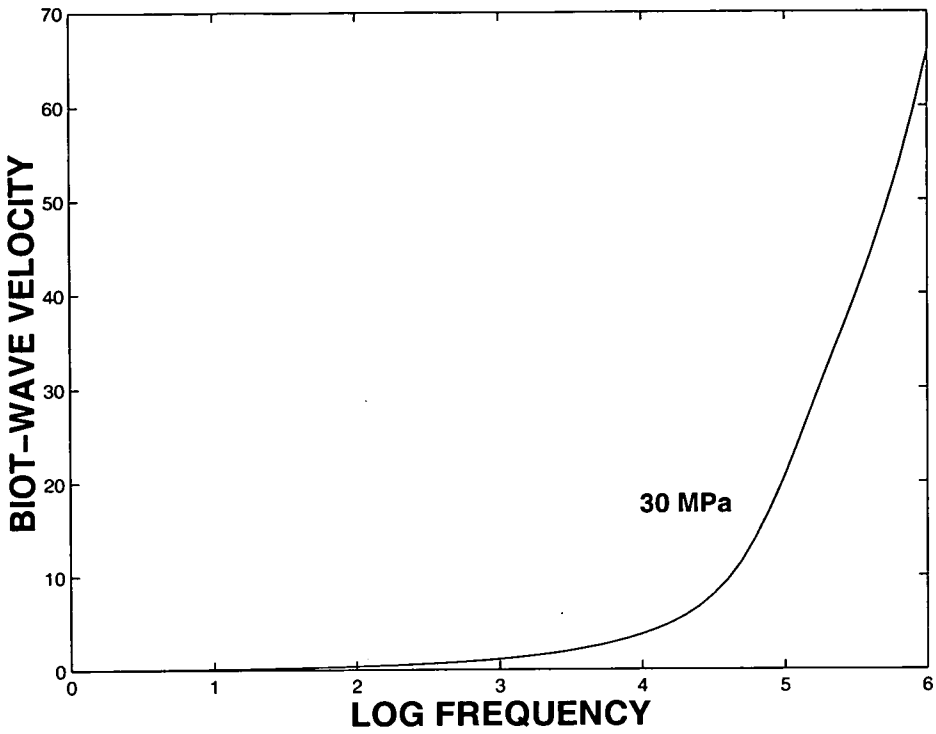

Figure 7–2: Dispersion curve for the Biot wave under 30 MPa effective stress.

increasing effective stress reduces attenuation by closing cracks and limiting the scope for squirt flow to take place.

7.2 Behaviour of the Biot wave.

My model predicts that the Biot wave is slow and highly attenuated. In contrast to the other two waves there is hardly any dependence of velocity on effective stress. I reproduce the dispersion curve for the Biot wave under 30 MPa of effective stress for brine saturation in Figure (7-2).

One can see that at low frequency the velocity is almost zero, but a strong increase takes places above 1 kHz. The resulting velocity of around 70 ms^{-1} at 1 MHz is still extremely low in comparison to the other wave speeds. The formal calculation of the Quality factor gives values close to 1, but the notion of Quality factor is not strictly defined for such an over-damped system.

The Biot wave is sensitive to the permeability of the rock. Permeability enters the model only through the time scale parameter τ, which was a fitted parameter, and so permeability measurements have played no part up until now. Permeability varies significantly between individual plugs, but a representative value of 200 mD is a fair reflection of the permeability of the rocks on which the model was calibrated. I can now calculate the effect of varying the permeability under the assumption that all other rock properties stay the same. The value of τ in the final calibration was 2×10^{-6} s. Since this corresponds to a permeability of 200 mD and since:

$$\tau \sim \frac{1}{k}; \tag{7.1}$$

I can calculate τ for any permeability.

I now plot, in Figure (7-3), the dispersion curves for the velocity of the Biot wave under 30 MPa of effective stress for permeabilities between 2 mD and 2 D.

It is apparent that the Biot wave velocity increases strongly with permeability. It is interesting to relate this result to the only observation to date of the Biot wave in a real rock, Kelder and Smeulders' (1997) measurement of the wave in Nivelsteiner Sandstone. The sample on which they performed their experiment had a permeability of 5 D, and the velocity which they found for the slow wave was of the order of 750 ms^{-1}. My results give at least a qualitative explanation of why such a velocity could be found in an extremely high permeability sandstone but not in a rock of lower permeability.

I find also that the Biot wave velocity is sensitive to the grain size of the rock. An increase in the grain size leads to an increase in velocity. This may explain why clay particles inhibit the propagation of the Biot wave (Klimentos and McCann, 1988). These results are consistent with the discussion in Bourbie et al. (1987).

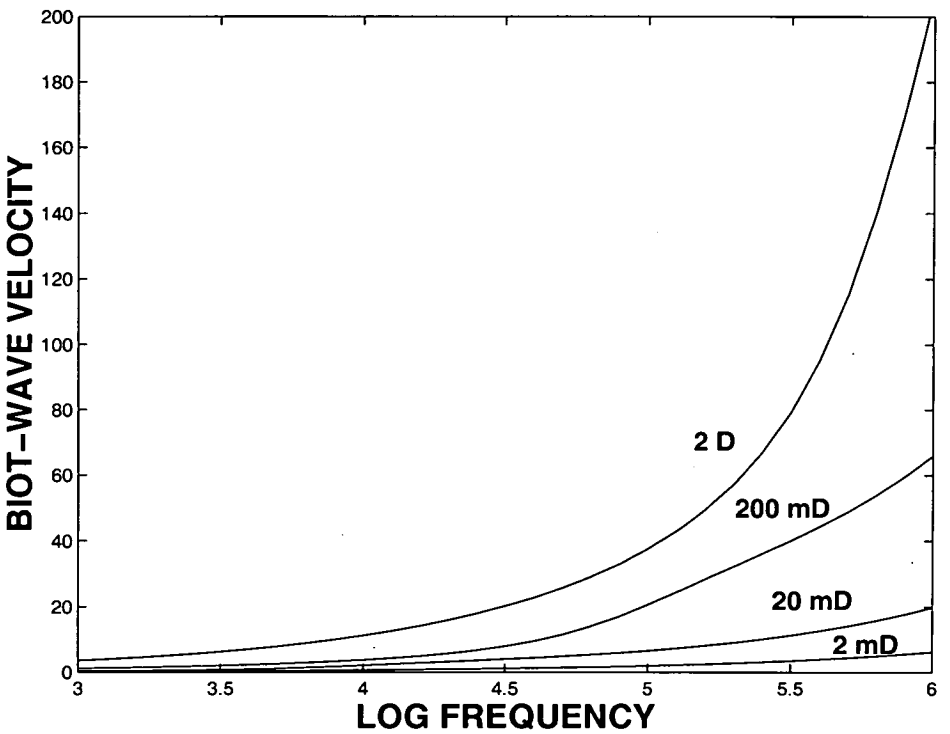

Figure 7–3: Biot wave dispersion curves for various permeabilities.

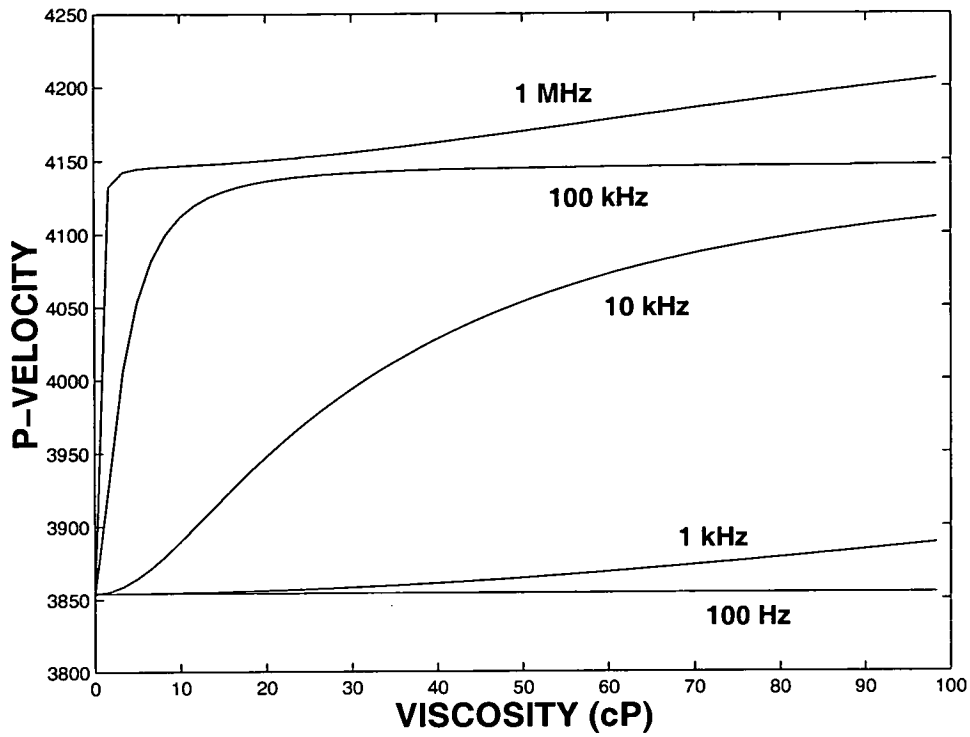

Figure 7–4: P-wave velocity as a function of fluid viscosity for various frequencies.

7.3 The effect of fluid viscosity on velocity

The characteristic relaxation time τ depends linearly on viscosity:

$$\tau \sim \eta; \tag{7.2}$$

and since I know that the τ value of 2×10^{-6} corresponds to a viscosity of 1 cP I may calculate τ for all viscosities. In Figures (7-4) and (7-5) I model P- and S-velocities as a function of fluid viscosity over the 0 cP to 100 cP range for a number of frequencies. It is assumed that the fluid has the bulk modulus and density of brine.

The interpretation of these diagrams is as follows. In the limits of both zero and infinite viscosity, both velocities are independent of frequency. For a frequency of

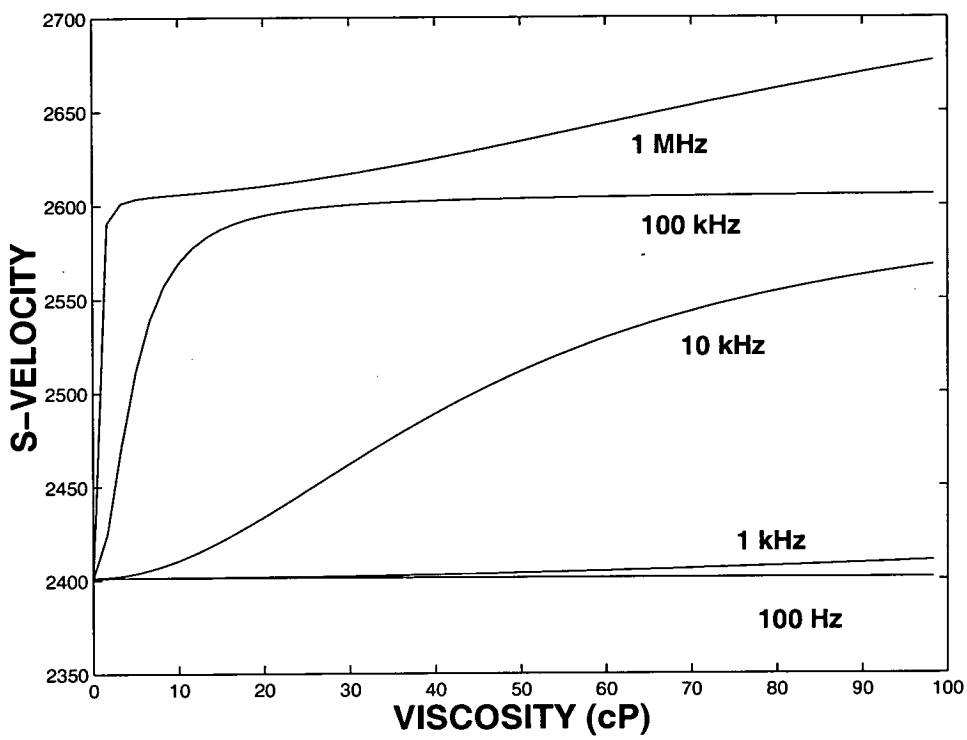

Figure 7–5: S-wave velocity as a function of fluid viscosity for various frequencies.

1 MHz the transition region between the fully communicating, or Gassmann, limit and the isolated inclusions limit occurs over a range of viscosities less than 1 cP. The corresponding transition for a frequency of 10 Hz takes place over viscosities which are higher than 100 cP. For the frequencies of 10 kHz and 100 kHz one can see the transition over the 1 - 100 cP range. Notice that the transition is sharper for the 100 kHz case since for low viscosities it takes a smaller arithmetic change to increase τ by a factor of ten than is the case at higher viscosities. The increase in velocities above around 45 cP for frequencies of 1 MHz is due to the Walsh effect becoming operable for my standard aspect ratio of 10^{-3}.

The complexity of these diagrams highlights the difficulty of interpreting experimental data for velocity as a function of viscosity. Nevertheless, these results indicate that one should not expect dependence on viscosity at seismic frequencies, in other words frequencies less than 100 Hz, even if this dependence is observed in high frequency laboratory experiments.

7.4 Conclusions

In this chapter I have examined the implications of the calibration of the model which I arrived at in the previous chapter. Aside from the complication of not being able to estimate frictional attenuation for P-wave Quality factor these results constitute predictions of the model which could in principle be tested by carrying out appropriate measurements.

The modelling of the Biot wave shows strong dependence on permeability and frequency. This gives at least a qualitative explanation of why Kelder and Smeulders (1997) were able to measure the Biot wave in their sample of Nivelsteiner sandstone despite the fact that the wave has proved elusive in other rocks (Klimentos & McCann, 1988).

The model predicts that velocities increase with increasing fluid viscosity, in contrast to the decrease with viscosity which was predicted by Biot. This was of course one of the reasons the concept of squirt flow was introduced in the first

instance. The precise nature of the relationship between viscosity and velocity is complicated and frequency dependent, but the modelling argues strongly that viscosity dependence is not to be expected at seismic frequencies even when it is seen to exist in laboratory experiments.

Chapter 8

Conclusions and discussion.

There can be little doubt that the Biot-Gassmann theory of poroelasticity is a strong basis on which to begin any study of wave propagation in fluid saturated rocks. Most laboratory investigations of the subject, however, are carried out at high frequency whereas Gassmann's theorem is valid only for extremely low frequency. This focuses attention on Biot's dynamic results.

Biot's prediction of the existence of a slow compressional wave represents an achievement which can hardly be bettered. The lack of any adjustable parameters in the theory means that its predictions are definite. Nevertheless the theory can be criticised on two main grounds.

There is strong evidence that Biot's theory underestimates the magnitude of velocity dispersion and attenuation, and that its behaviour with respect to changing fluid viscosity is incorrect. The introduction of the concept of squirt flow simultaneously addresses both of these concerns. Bourbie et al. (1987) have argued that it is in general unwise to attempt to complicate Biot's theory by including further mechanisms to explain specific observations. The fact that a single mechanism is able to address two fundamental weaknesses of the model provides an effective answer to this argument.

Whilst I have argued that Biot's results depending only on macroscopic parameters is a strength of the approach, for many purposes this can be a weakness. It is a common goal to attempt to interpret seismic velocities in terms of fracture

intensity and orientation. In Biot's work, all information about fracturing is encoded into the dry frame velocities. This means that even if one could invert data perfectly for the input parameters for the Biot theory this would not necessarily yield any information about the fracture networks. Because of this most work in which fracture distributions are important takes place within the framework of Eshelby based effective medium theory.

The approach of Dvorkin and Nur (1993) and Dvorkin et al. (1995) is nevertheless to incorporate squirt flow into the original Biot formulation. The resulting models are not entirely consistent with poroelastic theory. Dvorkin and Nur's (1993) BISQ model violates Gassmann's theorem at zero frequency and is only strictly valid for partial saturation. No Biot flow or slow wave is present in the Dvorkin et al. (1995) formulation.

Attempts have been made to incorporate various forms of squirt flow into the Eshelby formulation (O'Connell and Budiansky, 1977; Johnston et al., 1979; Thomsen, 1995; Hudson et al., 1996), without attempting to achieve consistency with dynamic poroelasticity. A remarkable degree of inconsistency exists between the predictions of these models.

Endres and Knight (1997) gave a comprehensive analysis of the magnitude of dispersion induced by the local flow effect as a function of microstructural geometry on the basis of Eshelby's theory. The most simple case which they analyse, that of a pore space consisting of a collection of randomly oriented cracks and spherical pores, shows behaviour which is more complicated than that of any of the squirt flow models. I consider that the logic of Endres and Knight is mathematically rigorous and intuitively clear, and that the validity of their results is unarguable. Nevertheless the limitation of their approach is that they only consider the zero frequency, Gassmann, limit and the high frequency, isolated inclusions, limit without analysing what occurs in between. This also means that they cannot make any statements about attenuation.

In the derivation of my model I have attempted to preserve the comprehensive logic of Endres and Knight while reproducing the main results of dynamic poroelasticity. I have shown that the model is consistent with Gassmann's theorem at

zero frequency and with the existence of a slow compressional wave. Both of these features require some discussion.

Gassmann's theorem gives a relationship between the dry and saturated elastic moduli and allows one set of values to be calculated from the other. In my model the theoretical relationship between the predicted dry moduli and the predicted saturated moduli is identical to Gassmann's theorem. This suggests that my description of the fluid dynamics is adequate. An important distinction between my model and Gassmann-Biot theory, however, is that the dry moduli are not an input parameter into my model. They may be associated with combinations of the reference elastic moduli, crack density and porosity but it is not in general possible to meaningfully invert these parameters from the dry moduli since my model assumes only dilute concentrations of cracks and pores.

It might be argued that since the Biot wave is never observed in practice it is irrelevant whether or not my model predicts the existence of this wave. I disagree with this statement. Thomsen (1985) and Bourbie et al. (1987) have argued that the confirmation of the existence of the slow P-wave suggests the validity of the remainder of Biot's predictions. The derivation of an independent poroelastic theory which also predicts the existence of the Biot wave undermines this argument considerably. I note also that the Biot wave forms the basis of Shapiro et al.'s (1997) method for estimating permeability from micro-seismicity following fluid injection. The calculation of attenuation due to the generation of the Biot wave at interfaces in finely layered materials (Gurevich & Lopatnikov, 1995) and as a result of scattering by inclusions embedded in poroelastic media (Gurevich et al., 1998) depends on a clear understanding of the behaviour of the Biot wave. Reflection and transmission coefficient could depend significantly on the behaviour of the Biot wave under certain circumstances (Bourbie et al., 1987). The implications of my results for these areas could form the basis of future work.

A further important distinction between my model and earlier work is the dependence on fracture distributions only through the crack density parameter rather than through the aspect ratio distribution. The freedom from having to specify entire distribution functions for the aspect ratio is vital if the model is

ever to be properly constrained and tested. My formulation of the fluid dynamics suggested a characteristic time scale parameter, τ, which was independent of the shape of the cracks. For identically sized cracks this allowed me to analyse crack distributions with a range of aspect ratios without complicating the mathematical form of the model. It is not at all clear how to extend the analysis to rock with cracks of different sizes, although a plausible technique indicated that it would make no difference. It is important to note however that the application of the model in its current form, with a single τ, incorporates an assumption which has been justified by an appeal to Occam's Razor rather than rigorously proven. Similar considerations apply to the application of Dvorkin et al.'s (1995) model in which there is a single characteristic squirt flow length rather than a distribution of these lengths. The dependence on crack density makes the model useful for studying crack distributions. Changes due to the application of effective stress can be related directly to crack closing rather than indirectly through modifications of the dry rock velocities.

The most serious weakness of the formulation is its inability to model the elastic interactions amongst the elements of pore space. An application of Eshelby's interaction energy formulation under the dilute concentration assumption is inadequate for predicting velocity from mineralogy, crack density and porosity. I assume that this problem may be separated from the problem of studying the variation of a given velocity with frequency, effective stress and fluid type. In this way the reference elastic moduli, λ_m and μ, should be considered to be fitting parameters rather than mineral elastic moduli. This will presumably introduce errors into the calculations since λ_m and μ themselves appear in the corrections to reference moduli for the presence of cracks and pores. Nevertheless I consider that this is to be preferred in the first instance to the use of any of the techniques for extending effective medium theory to high concentrations of cracks and pores. These techniques would introduce considerable additional mathematical complications without giving any guarantee of improving the results.

With this understanding, and with the methods I give for estimating γ and ι, the only free parameters are the crack density and τ. This freedom was sufficient

to introduce ambiguity into my modelling of the resonant bar data. Two main possibilities presented themselves. The first was that the characteristic frequency, $1/\tau$, was directly in the region in which measurements were taken and that crack density, and therefore the magnitude of dispersion, was low. A second possibility was that the characteristic frequency lay outside the region where measurements were taken, with the magnitude of dispersion being correspondingly higher. The first possibility gave the better visual, and indeed least squares, fit, but there is a strong tendency for models with low magnitudes of dispersion to give the best fit to limited data and I rejected this argument.

This demonstrated the need for an additional constraint on the modelling. I argued that such a constraint came from the fluid substitution effect at ultrasonic frequencies. My argument relied on their being no, or identical, chemical effects on the frame moduli when the rock was saturated with brine and oil. The danger to my argument was the possibility that when the rock was saturated with brine, reactions would take place between the brine and clay or shale deposits, leading to a loss of shear rigidity, but that such effects would not take place when the rock was saturated with oil. In this way the difference in behaviour between the two fluids would not be due to dispersion.

I have no direct evidence to suggest that such chemical effects took place, and the fact that the rocks were of low clay content mitigates against the possibility. It is striking also that the Gassmann predictions for brine saturation appear to work extremely well for brine saturation and for effective stresses of 20 MPa and above. If strong chemical weakening were a factor then Gassmann's predictions would be expected to give an overestimate of this shear velocity, rather than a small underestimate consistent with modest dispersion. Nevertheless if I assume that there is chemical weakening, I am forced to accept that Gassmann's theorem will then predict that velocities at zero frequency are much lower than those at high frequency, even at high effective stress. This implies the existence of strong dispersion. Both my model and that of Dvorkin et al. (1995) will then predict the fluid substitution effect which I describe anyway. I conclude that dispersion must play an important role in the analysis of the ultrasonic fluid substitution data.

My analysis is then the simplest possible given the lack of evidence in support of chemical weakening. Very low frequency tests (Spencer, 1981) could determine whether and to what extent this analysis should be modified for chemical effects.

The need to interpret the ultrasonic data in terms of dispersion rules out the first possibility for modelling the resonant bar data. When I find the best fit to the ultrasonic data and compare its predictions with the resonant bar measurements I find a fairly poor agreement. The variation in properties between different rock samples imposes constraints upon the extent to which this situation can be rectified. It is tempting to construct a range of calibrations which fit neither the resonant bar nor ultrasonic data extremely well but which give rough fits to both. I have not found any such calibration which is truly compelling, so the need for simplicity demands that I take my fit to the ultrasonic data as the final calibration. There is some evidence in the comparison of this calibration with the resonant bar data that the transition from low frequency to high frequency conditions is less abrupt than is implied by my single τ model. The resolution of this issue would require resonant bar experiments to be carried out on a wide range of different samples to remove the possibility that the mismatch is due to different rock properties.

I found that the Dvorkin et al. (1995) model had a tendency to underestimate dispersion. This was particularly pronounced for S-wave dispersion. I noted earlier that shear dispersion in Dvorkin et al.'s model was simply proportional to bulk dispersion, whereas a simple fluid flow mechanism, flow between cracks of different orientation, could produce shear dispersion without any associated bulk dispersion. This provides an explanation for the underprediction of S-wave dispersion. The final fit to the data which I achieved with my model is superior to that of Dvorkin et al., but it must be noted that my model has more adjustable parameters than are present in the Dvorkin et al. model.

I think that the two models complement each other rather well. Although my approach is more flexible when one is required to fit a range of different observations, the lack of adjustable parameters in the Dvorkin et al. approach allows estimates to be made when there are a minimum of observations. The greatest

weakness of my model, the inability to model the elastic interactions, is perfectly accounted for in Dvorkin et al.'s model where the dry frame moduli are inputs into the calculation. The parameterisations are also different, whereas Dvorkin et al. relate behaviour to macroscopic parameters I relate it to the microstructural crack density.

Although the modelling of the shear wave quality factor provided the best visual fit to any dataset which I achieved in the thesis there must be some reservations about the results. Squirt flow alone cannot be entirely responsible for attenuation since otherwise infinite Q would be observed in dry rocks. Some frictional component must be introduced into the modelling. The strong stress-sensitivity and weak frequency dependence observed in dry rock measurements of Q suggest the method I applied in my modelling, namely to add in a different frequency independent frictional component for each value of effective stress. I have no theoretical criteria for deciding what this value should be, I simply have to choose it to fit the data. Unfortunately this assumption, while still being the simplest reasonable assumption available, provides sufficient latitude to achieve good fits to the data even when, as with the final calibration, the other components to the modelling give a poor fit. This makes constraining and testing the Q modelling very difficult, and I certainly have not achieved this in this thesis. Nevertheless, in the absence of other information, my predicted Q curves provide a reasonable qualitative picture of what I expect the true relationship to be.

I examined the implications of the calibration of my model at which I arrived. The prediction of the model is that the Biot wave velocity would be very small in the rocks under consideration. The velocity is very sensitive to the permeability of the rock, and my results are in broad agreement with the observations of the Biot wave in highly permeable rocks.

The relationship between velocity and fluid viscosity is highly complex and frequency dependent. My results indicate that it should not be assumed that dependence on viscosity which is observed in the laboratory will also be observed in field observations. This indicates the importance of understanding the effect of frequency dispersion when interpreting laboratory measurements.

Chapter 9

References

Bacri, J-C. and Salin, D., 1986. Sound velocity of a sandstone saturated with oil and brine at different concentrations. *Geophys. Res. Lett.*, **13**, 326-328.

Berryman, J.G., 1980. Confirmation of Biot's theory. *Appl. Phys. Lett.*, **37**, 382-384.

Biot, M.A., 1956a. Theory of propagation of elastic waves in a fluid-saturated porous solid. I. Low frequency range. *J. Acoust. Soc. Am.*, **28**, 168-178.

Biot, M.A., 1956b. Theory of propagation of elastic waves in a fluid-saturated porous solid. II. Higher frequency range. *J. Acoust. Soc. Am.*, **28**, 179-191

Biot, M.A., 1962. Mechanics of deformation and acoustic propagation in porous media. *J. Appl. Phys.*, **33**, 1482-1498.

Bourbie, T., Coussy, O. and Zinszner, B. 1987. Acoustics of porous media. Gulf Publishing Company.

Brown, R. and Korringa, J., 1975. On the dependence of the elastic properties of a porous rock on the compressibility of the pore fluid. *Geophysics*, **40**, 608-616.

Budiansky, B. and O'Connell, R.J., 1976. Elastic moduli of a cracked solid. *Int. J. Solids Structures*, **12**, 81-97.

Budiansky, B. and O'Connell, R.J., 1980. Bulk dissipation in heterogeneous media. *Solid Earth Geophys. and Geotech.*, **42**, 1-10.

Cadoret, T., 1993. Effet de la Saturation Eau/Gaz sur les Proprietes Acoustiques des Roches. PhD dissertation, University of Paris, VII.

Christensen, R.M., 1980. Mechanics of composite materials. John Wiley & Sons.

De Vries, S., 1989. Propagation of transient acoustic waves in porous media. PhD thesis. Delft University.

Dvorkin, J., Mavko, G., and Nur, A., 1995. Squirt flow in fully saturated rocks, *Geophysics,* **60,** 97-107.

Dvorkin, J., and Nur, A., 1993. Dynamic poroelasticity: A unified model with the squirt and Biot mechanisms. *Geophysics,* **58,** 524-533.

Endres, A.L. and Knight, R.J., 1997. Incorporating pore geometry and fluid pressure communication into modeling the elastic behaviour of porous rocks. *Geophysics*, **62**, 106-117.

Eshelby, J.D., 1957. The determination of the elastic field of an ellipsoidal inclusion, and related problems, *Proc. R. Soc. Lond.,* **A, 241,** 376-396.

Gassmann, F., 1951. Uber die Elastizitat poroser Medien. *Vier. der Natur. Gesellschaft in Zurich,* **96,** 1-23.

Geertsma, J. and Smit, D.C., 1961. Some aspects of elastic wave propagation in fluid-saturated porous solids. *Geophysics*, **26**, 169-181.

Gordon, R.B., 1974. Mechanical relaxation spectrum of crystalline rock containing water. *J. Geoph. Res.*, **79**, 2129-2131.

Gurevich, B. and Lopatnikov, S.L., 1995. Velocity and attenuation of elastic waves in finely layered porous rocks. *Geophys. J. Int.*, **121**, 933-947.

Gurevich, B., Sadovnichaja, A.P., Lopatnikov, S.L. and Shapiro, S.A., 1998. Scattering of a compressional wave in a poroelastic medium by an ellipsoidal inclusion. *Geophys. J. Int.*, **133**, 91-103.

Han, D., 1987. Effects of porosity and clay content on wave velocities in sandstones and unconsolidated sediments, *PhD Thesis, Stanford Univ., Calif.*

Hashin, Z. and Shtrikman, S., 1963. A variational approach to the elastic behaviour of multiphase materials. *J. Mech. Phys. Solids*, **11**, 127-140.

Hill, R., 1965. A self-consistent mechanics of composite materials. *J. Mech. Phys. Solids,* **11**, 213-222.

Hornby, B.E., Schwartz, L.M., and Hudson, J.A., 1994. Anisotropic effective-medium modeling of the elastic properties of shales. *Geophysics*, **59**, 1570-1583.

Hudson, J.A., 1980. Overall properties of a cracked solid. *Math. Proc. Cambridge Phil. Soc.,* **88**, 371-384.

Hudson, J.A., 1981. Wave speeds and attenuation of elastic waves in material containing cracks. *Geophys. J. Royal Astr. Soc.,* **64**, 133-150.

Hudson, J.A., 1991. Overall properties of heterogeneous materials. *Geophys. J. Int.*, **107**, 505-511.

Hudson, J.A., Liu, E. and Crampin, S., 1996. The mechanical properties of materials with interconnected cracks and pores. *Geophys. J. Int.*, **124**, 105-112.

Hudson, J.A., Pointer, T. and Liu, E., 1999. Effective medium theories for fluid saturated materials with aligned cracks. *Submitted to Geophys. Prosp.*

Johnston, D.H., Toksoz, M.N. and Timur, A., 1979. Attenuation of seismic waves in dry and saturated rocks: II. Mechanisms. *Geophysics*, **44**, 691-711.

Jones, T. and Nur, A., 1983. Velocity and attenuation in sandstone at elevated termperatures and pressures. *Geophys. Res. Lett.*, **10**, 140-143.

Jones, T., 1986. Pore fluids and frequency-dependent wave propagation in rocks. *Geophysics*, **51**, 1939-1953.

Kelder, O. and Smeulders, D.M.J., 1997. Observation of the Biot slow wave in water-saturated Nivelsteiner sandstone. *Geophysics*, **62**, 1794-1796.

King, M. S., Chaudhry, N. A. and Ahmed, S., 1994. Experimental ultrasonic velocities and permeability of sandstones with aligned cracks. *56th EAGE Meeting, Vienna, Expanded Abstracts*, 3888-3889.

Klimentos, T. and McCann, C., 1988. Why is the Biot slow compressional wave not observed in real rocks? *Geophysics*, **53**, 1605-1609.

Korringa, J., Brown, R.J.S., Thompson, D.D. and Runge, R.J., 1979. Self-Consistent Imbedding and the Ellipsoidal Model for Porous Rocks. *J. Geoph. Res.*, **84**, 5591-5598.

Kuster, G.T. and Toksoz, M.N., 1974. Velocity and attenuation of seismic waves in two-phase media. *Geophysics*, **39**, 587-618.

Love, A.E.H., 1927. Theory of elasticity. Cambridge University Press.

Mair, K., Main, I.G., and Elphick, S., 2000. Sequential growth of deformation bands in the laboratory. *J. Struct. Geol.*, **22**, 25-42.

Mavko, G. and Jizba, D., 1991. Estimating grain-scale fluid effects on velocity dispersion in rocks. *Geophysics*, **56**, 1940-1949.

Mavko, G., Mukerji, T. and Dvorkin, J., 1998. The Rock Physics Handbook. Cambridge University Press.

Mavko, G. and Nur, A., 1975. Melt squirt in the asthenosphere. *J. Geophys. Res.*, **80,** 1444-1448.

Mochizuki, S., 1982. Attenuation in partially saturated rocks. *J. Geoph. Res.*, **87**, 8598-8604.

Murphy, W.F., 1985. Sonic and ultrasonic velocities: Theory versus experiment. *Geophys. Res. Lett.* **12**, 85-88.

Murphy, W.F., Schwartz, L.M. and Hornby, B., 1991. Interpretation physics of Vp and Vs in sedimentary rocks. *Transactions SPWLA 32nd Ann. Logging Symp.*, 1-24.

Murphy, W.F., Winkler, K.W. and Kleinberg, R.L., 1984. Contact microphysics and viscous relaxation in sandstones. In "Physics and Chemistry of porous media, D.L. Johnson and P.N. Sen, eds. American Institute of Physics, New York, 176-190.

Norris, A.N., 1985. A differential scheme for the effective moduli of composites. *Mechanics of Materials*, **4**, 1-16.

Nur, A., 1971. Effects of stress on velocity anisotropy in rocks with cracks, *J. Geophys. Res.*, **8** 2022-2034

Nur, A., 1980. Seismic velocities in low porosity rocks. In "Source mechanisms and earthquake prediction, Hommage au Prof. J. Coulom, Ed. CNRS, Paris."

Nur, A. and Simmons, G. 1969. The effect of viscosity of a fluid phase on velocity in low porosity rocks. *Earth and Planet. Sci. Lett.*, **7**, 99-108.

O'Connell, R.J. and Budiansky, B., 1977. Viscoelastic properties of fluid-saturated cracked solids, *J. Geophys. Res.*, **82,** 5719-5735.

Peacock, S., McCann, C., Sothcott, J. and Astin, T.R., 1994. Seismic velocities in fractured rocks; an experimental verification of Hudson's theory. *Geophys. Prosp.*, **42**, 27-80.

Plona, T., 1980. Observation of a second bulk compressional wave in a porous medium at ultrasonic frequencies, *Appl. Phys. Lett.*, **36,** 259-261

Pointer, T., Liu, E. and Hudson, J.A., 2000. Seismic wave propagation in cracked porous media. *Geophys. J. Int.*, **142**, 199-231.

Pride, S.R., Gangi, A.F. and Morgan, F.D., 1992. Deriving the equations of motion for porous isotropic media. *J. Acoust. Soc. Am.*, **6**, 3278-3290.

Reuss, A., 1929. Berechnung der fliessgrense von mischkristallen auf grund der plastzitatbedingung fur einkristalle. *Zeitschrift fur Angewandte Mathematik aus Mechanik*, **9**, 49-58.

Sams, M.S., Neep, J.P., Worthington, M.H. and King, M.S., 1997. The measurement of velocity dispersion and frequency-dependent intrinsic attenuation in sedimentary rocks. *Geophysics,* **62**, 1456-1464.

Savage, J., 1966. Thermoelastic attenuation of seismic waves by cracks. *J. Geophys. Res.*, **71**, 3929-3938.

Shapiro, S.A., Huenges, E. and Borm, G., 1997. Estimating the crust permeability from fluid-injection-induced seismic emission at the KTB site. *Geophys. J. Int.*, **131**, F5-F18.

Sothcott, J., McCann, C. and O'Hara, S.G., 2000. The influence of two different pore fluids on the acoustic properties of reservoir sandstones at sonic and ultrasonic frequencies. *Expanded Abstracts, 70th SEG Meeting, Calgary*, 1883-1886.

Spencer, J. W., 1981. Stress relaxation at low frequencies in fluid saturated rocks: attenuation and modulus dispersion. *J. Geophys. Res.*, **86**, 1803-1812.

Thimus, J. F., Abousleiman, Y., Cheng, A. H. D., Coussy, O. and Detournay, E., 1998. Poromechanics: A tribute to Maurice A. Biot. *Proceedings of the Biot conference on poromechanics, Louvain-La-Neuve, Belgium, September 1998.*

Thomsen, L., 1985. Biot-consistent elastic moduli of porous rocks: Low frequency limit. *Geophysics*, **50**, 2797-2807.

Thomsen, L., 1995. Elastic anisotropy due to aligned cracks in porous rock. *Geophys. Prosp.*, **43**, 805-829.

Tutuncu, A.N. and Sharma, M.M., 1992. The influence of grain contact stiffness and frame moduli in sedimentary rocks. *Geophysics*, **57**, 1571-1582.

Voigt, W., 1928. Lehrbuch der Kirstallphysik: Teubner, Leipzig.

Walsh, J.B., 1966. Seismic wave attenuation in rock due to friction. *J. Geophys. Res.*, **71**, 2591-2599.

Walsh, J.B., 1969. New analysis of attenuation of partially melted rock. *J. Geoph. Res.*, **14**, 4333-4337.

Wang, Z., Hirsche, W.K. and Sedgwick, G., 1991. Seismic monitoring of water flood? A petrophysical study. *Geophysics*, **56**, 1614-1623.

Wang, Z., and Nur, A., 1990. Dispersion analysis of acoustic velocities in rocks, *J. Acoust. Soc. Am.*, **87**, 2384-2395.

Wang, Z., and Nur, A., 1992. Elastic wave velocities in porous media: a theoretical recipe. In "Seismic and Acoustic Velocities in Reservoir Rocks, Vol. 2. Theoretical and Model Studies". SEG.

Watt, P., Davies, G. F. and O'Connell, R., 1976. The elastic properties of composite materials, *Rev. Geophys. Space Phys.*, **14,** 541-563.

White, J.E., 1983. Underground Sound: Application of Seismic Waves. Elsevier, New York.

Winkler, K.W., 1985. Dispersion analysis of velocities and attenuation in Berea sandstone, *J. Geophys. Res.*, **90,** 6793-6800

Winkler, K.W., 1986. Estimates of velocity dispersion between seismic and ultrasonic frequencies. *Geophysics*, **51**, 183-189.

Wu, T.T., 1966. The effect of inclusion shape on the elastic moduli of a two phase material. *Int. J. Solids Structures,* **2**, 1-8.

Zatsepin, S. V. and Crampin, S., 1997. Modelling the compliance of crustal rock. I, Response of shear wave splitting to differential stress, *Geophys. J. Int.,* **129** 477-494.

Appendix A

In this appendix I reproduce Jeremy Sothcott's experimental data. He carried out tests on a resonant bar and an ultrasonic plug taken from Clashach sandstone. The rock had a porosity of 22.7 % and a dry density of 2044 kgm^{-3}.

The resonant bar was tested dry and brine saturated. The ultrasonic plug was tested dry, brine saturated and crude oil saturated. The brine had a density of 1097 kgm^{-3}, a bulk modulus of 2.9 GPa and an acoustic velocity of 1630 ms^{-1}. The oil had a density of 810 kgm^{-3}, a bulk modulus of 1.68 GPa and an acoustic velocity of 1420 ms^{-1}. The density of the saturated rock was 2288 kgm^{-3} with brine and 2227 kgm^{-3} with oil.

According to Jeremy Sothcott, calibration tests show that the ultrasonic measurements are correct to 0.3% for velocity and 0.1 dB/cm for attenuation. The resonant bar data are correct to 0.3% for S-velocity, to 1% for P-velocity and to 0.3% for Qs. The pressure measurements are correct to 0.5 MPa for both the resonant bar and ultrasonic apparatus.

The following measurements of Velocity against frequency were taken on the dry resonant bar under 10 MPa effective stress:

Frequency (Hz)	Vp	Frequency (Hz)	Vs	Frequency (Hz)	Qs
3779	3081	3779	2000	3779	370
11396	3100	11396	2012	11396	370
19062	3112	19062	2020	19062	345
26770	3117	26770	2023	26770	344
-	-	49393	2026	34348	339
-	-	-	-	41770	340

For the dry resonant bar under 20 MPa effective stress:

Frequency (Hz)	Vp	Frequency (Hz)	Vs	Frequency (Hz)	Qs
4227	3509	4227	2270	4227	481
12723	3522	12723	2279	12723	480
21324	3546	21324	2294	21324	452
29910	3552	29910	2298	29910	454
-	-	-	-	38365	454
-	-	-	-	46645	438

For the dry resonant bar under 30 MPa effective stress:

Frequency (Hz)	Vp	Frequency (Hz)	Vs	Frequency (Hz)	Qs
4435	3690	4435	2395	4435	565
13336	3701	13336	2401	13336	570
22381	3727	22381	2419	22381	545
31387	3736	31387	2425	31387	543
-	-	-	-	40243	543
-	-	-	-	46645	470

For the dry resonant bar under 40 MPa effective stress:

Frequency (Hz)	Vp	Frequency (Hz)	Vs	Frequency (Hz)	Qs
4530	3750	4530	2451	4530	632
13611	3757	13611	2456	13611	658
22862	3789	22862	2477	22862	587
32054	3796	32054	2481	32054	603
-	-	-	-	41095	614
-	-	-	-	49892	552

For the brine saturated resonant bar under 10 MPa effective stress:

Frequency (Hz)	Vp	Frequency (Hz)	Vs	Frequency (Hz)	Qs
3791	3415	3791	2010	3791	27.9
11523	3466	11523	2040	11523	22.8
19452	3517	19452	2070	19452	20.6
27470	3553	27470	2091	27470	21.1
-	-	-	-	35231	20.5
-	-	-	-	43032	

For the brine saturated resonant bar under 20 MPa effective stress:

Frequency (Hz)	Vp	Frequency (Hz)	Vs	Frequency (Hz)	Qs
4112	3594	4112	2203	4112	47.8
12457	3633	12457	2227	12457	41.2
20957	3670	20957	2250	20957	38.8
29451	3687	29451	2260	29451	38.1
-	-	-	-	37800	37.6
-	-	-	-	46074	37.8

For the brine saturated resonant bar under 30 MPa effective stress:

Frequency (Hz)	Vp	Frequency (Hz)	Vs	Frequency (Hz)	Qs
4248	3685	4248	2284	4248	66.6
12828	3712	12828	2301	12828	62.4
21583	3751	21583	2325	21583	57.8
30316	3764	30316	2333	30316	57.2
-	-	-	-	38921	57.4
-	-	-	-	47347	56.2

For the brine saturated resonant bar under 40 MPa effective stress:

Frequency (Hz)	Vp	Frequency (Hz)	Vs	Frequency (Hz)	Qs
4323	3745	4323	2328	4323	85.9
13000	3756	13000	2335	13000	77.2
21880	3796	21880	2360	21880	72.3
30705	3806	30705	2366	30705	70.4
-	-	-	-	39387	70.1
-	-	-	-	47880	69.3

The measurements for the P-wave velocity of the ultrasonic plug were (700 kHz):

σ_{eff} (MPa)	dry	brine	oil
10	3537	3933	3961
20	3999	4109	4151
30	4146	4180	4207
40	4201	4203	4224

The measurements for the S-wave velocity of the ultrasonic plug were (700 kHz):

σ_{eff} (MPa)	dry	brine	oil
10	2193	2304	2488
20	2558	2448	2614
30	2692	2556	2662
40	2734	2600	2684

Appendix B

From equation (3.3):

$$16\pi\mu(1-v)G_{ij} = \frac{3-4v}{r_0}\delta_{ij} + \frac{l_i l_j}{r_0}; \tag{B.1}$$

but:

$$\partial_k l_i = \frac{l_i l_k}{r_0} - \frac{\delta_{ik}}{r_0}; \tag{B.2}$$

and:

$$\partial_k \frac{1}{r_0} = \frac{l_k}{r_0}; \tag{B.3}$$

so:

$$\begin{aligned} \partial_k \frac{l_i l_j}{r_0} &= l_i l_j \partial_k r_0^{-1} + 2 l_i r_0^{-1} \partial_k l_j \\ &= r_0^{-2}(3 l_i l_j l_k - l_i \delta_{jk} - l_j \delta_{ik}); \end{aligned} \tag{B.4}$$

and therefore:

$$16\pi\mu(1-v)G_{ij,k} = r_0^{-2}[(3-4v)l_k\delta_{ij} - l_i\delta_{jk} - l_j\delta_{ik} + 3 l_i l_j l_k]. \tag{B.5}$$

From equation (3.4):

$$u_i^c(x) = \sigma_{jk}^T \int_V G_{ij,k} dV; \tag{B.6}$$

and since σ is symmetric we have:

$$l_k \delta_{ij} \sigma_{jk} = l_j \delta_{ik} \sigma_{jk}; \tag{B.7}$$

so that:

$$u_i^c(x) = \frac{\sigma_{jk}}{16\pi\mu(1-v)} \int_V r_0^{-2}[(1-2v)(l_k\delta_{ij} + l_j\delta_{ik}) - l_i\delta_{jk} + 3l_i l_j l_k] dV. \tag{B.8}$$

For convenience we write this as:

$$u_i^c(x) = \frac{\sigma_{jk}}{16\pi\mu(1-v)} \int_V r_0^{-2} f_{ijk} dV. \tag{B.9}$$

If we now note that:

$$\frac{\sigma_{jk}^T}{2\mu} = \epsilon_{jk}^T + \frac{v}{1-2v} \epsilon_{ll}^T \delta_{jk} \tag{B.10}$$

then:

$$\begin{aligned} u_i^c(x) &= \frac{\epsilon_{jk}^T + \frac{v}{1-2v}\epsilon_{ll}^T\delta_{jk}}{8\pi(1-v)} \int_V r_0^{-2} f_{ijk} dV \\ &= \frac{\epsilon_{jk}^T}{8\pi(1-v)} \int_V r_0^{-2}(f_{ijk} + 2v l_i \delta_{jk}) dV \\ &= \frac{\epsilon_{jk}^T}{8\pi(1-v)} \int_V r_0^{-2} g_{ijk} dV. \end{aligned} \tag{B.11}$$

This is the required equation.

Appendix C

We fix some position x inside the ellipsoid.

The equation of the surface of the ellipsoid is:

$$\frac{z_1^2}{a_1^2} + \frac{z_2^2}{a_2^2} + \frac{z_3^2}{a_3^2} = 1; \tag{C.1}$$

so for a particular ψ and θ:

$$\frac{(x_1 + r_0 l_1)^2}{a_1^2} + \frac{(x_2 + r_0 l_2)^2}{a_2^2} + \frac{(x_3 + r_0 l_3)^2}{a_3^2} = 1; \tag{C.2}$$

where l is given by equation (3.6) and so r_0 is the solution of:

$$g r_0^2 + 2 f r_0 - e = 0; \tag{C.3}$$

where:

$$f = \frac{x_1 l_1}{a_1^2} + \frac{x_2 l_2}{a_2^2} + \frac{x_3 l_3}{a_3^2}; \tag{C.4}$$

$$g = \frac{l_1^2}{a_1^2} + \frac{l_2^2}{a_2^2} + \frac{l_3^2}{a_3^2}; \tag{C.5}$$

$$e = 1 - \frac{x_1^2}{a_1^2} - \frac{x_2^2}{a_2^2} - \frac{x_3^2}{a_3^2}. \tag{C.6}$$

We find that r_0 is given by:

$$r_0 = -\frac{f}{g} \pm [\frac{f^2}{g^2} + \frac{e}{g}]^{\frac{1}{2}}. \tag{C.7}$$

Geometrically there must indeed be to values of r_0 since the line through x parallel to l cuts the surface of the ellipsoid at 2 points. We choose to select the positive root, which since $e > 0$ for x inside the ellipsoid is given by:

$$r_0(\psi, \theta) = -\frac{f}{g} + [\frac{f^2}{g^2} + \frac{e}{g}]^{\frac{1}{2}}. \tag{C.8}$$

Equation(3.11) then becomes:

$$u_i^c(x) = \frac{\epsilon_{jk}^T}{8\pi(1-v)} \int_0^{2\pi} \int_0^{\pi} \{-\frac{f}{g} + [\frac{f^2}{g^2} + \frac{e}{g}]^{\frac{1}{2}}\} g_{ijk} \sin\psi d\psi d\theta. \tag{C.9}$$

Now if we define:

$$h(\theta, \psi) = g_{ijk} \sin\psi; \tag{C.10}$$

then h will have the symmetry:

$$h(\theta, \psi) = -h(\theta + \pi, \pi - \psi); \tag{C.11}$$

for $\theta \in [0, \pi]$ and $\psi \in [0, \frac{\pi}{2}]$, whilst if:

$$H(\theta, \psi) = [\frac{f^2}{g^2} + \frac{e}{g}]^{\frac{1}{2}}; \tag{C.12}$$

then H has the symmetry:

$$H(\theta, \psi) = H(\theta + \pi, \pi - \psi). \tag{C.13}$$

The expression for u_i^c can therefore be simplified to:

$$u_i^c(x) = \frac{\epsilon_{jk}^T}{8\pi(1-v)} \int_0^{2\pi} \int_0^{\pi} -\frac{f}{g} g_{ijk} \sin\psi d\psi d\theta; \tag{C.14}$$

which with the conventions (3.12), (3.13) gives (3.14).

Appendix D

The stated result is equivalent to the following theorem

Theorem Let $i+j+k=4$, $i,j,k \in N$ with one of i, j or k odd. Then

$$\int_0^{2\pi}\int_0^{\pi} \frac{l_1^i l_2^j l_3^k}{g} \sin\psi d\psi d\theta = 0 \tag{D.1}$$

Proof If k is odd, $l_1^i l_2^j l_3^k(\psi+\frac{\pi}{2}) = -l_1^i l_2^j l_3^k(\psi)$ for $\psi \in [0, \frac{\pi}{2}]$ whilst $g(\psi) = g(\psi+\frac{\pi}{2})$. Hence the integral $= 0$

If k is even we have 3 possibilities; $l_1^3 l_2$, $l_1 l_2^3$, $l_1 l_2 l_3^2$.

a) $\frac{l_1^3 l_2}{g}\sin\psi = \frac{\sin^5\psi\cos^3\theta\sin\theta}{g}$. But $\sin^5\psi\cos^3\theta\sin\theta = \sin^5\cos^3(\theta+\pi)\sin(\theta+\pi)$, $\theta \in [0,\pi]$ and $\sin^5\psi\cos^3(\theta+\frac{\pi}{2})\sin(\theta+\frac{\pi}{2}) = -\sin^5\psi\cos^3\theta\sin\theta$, $\theta \in [0,\frac{\pi}{2}]$ whilst $g(\theta) = g(\theta+\pi)$, $\theta \in [0,\pi]$ and $g(\theta) = g(\theta+\frac{\pi}{2})$ for $\theta \in [0,\pi]$ Hence integral =0.

b) $\frac{l_1 l_2 l_3^2}{g}\sin\psi = \frac{\sin^3\psi\sin\theta\cos\theta\cos\psi}{g}$ In this case, for $\psi \in [0,\frac{\pi}{2}]$, $\sin^3\psi\sin\theta\cos\theta\cos\psi = -\sin^3(\pi-\psi)\sin\theta\cos\theta\cos(\pi-\psi)$ but $g(\psi) = g(\pi-\psi)$. Hence integral=0

c) $\frac{l_1 l_3^3}{g}\sin\psi = \frac{\sin^3\psi\sin\theta\cos\theta\cos\psi}{g}$, but here we have $\cos(\theta+\pi)\sin(\theta+\pi) = \cos\theta\sin^3\theta$ for $\theta \in [0,\pi]$ and $\cos(\theta+\frac{\pi}{2})\sin^3(\theta+\frac{\pi}{2}) = -\cos\theta\sin^3\theta$ for $\theta \in [0,\frac{\pi}{2}]$ and therefore the integral=0 since $g(\theta) = g(\theta+\pi)$ for $\theta \in [0,\pi]$ and $g(\theta) = g(\theta+\frac{\pi}{2})$ for $\theta \in [0,\pi]$.

Appendix E

Consider first I_3:

$$I_3 = \frac{1}{a_3^2}\int_0^{2\pi}\int_0^{\pi} \frac{\cos^2\psi\sin\psi}{\frac{\sin^2\psi\cos^2\theta}{a_1^2}+\frac{\sin^2\psi\sin^2\theta}{a_2^2}+\frac{\cos^2\psi}{a_3^2}}d\psi d\theta \tag{E.1}$$

$$= \frac{8}{a_3^2}\int_0^{\frac{\pi}{2}}\int_0^{\frac{\pi}{2}} \frac{\cos^2\psi\sin\psi\sec^2\theta}{(\frac{\sin^2\psi}{a_1^2}+\frac{\cos^2\psi}{a_3^2})+(\frac{\sin^2\psi}{a_2^2}+\frac{\cos^2\psi}{a_3^2})\tan^2\theta}d\psi d\theta \tag{E.2}$$

$$= \frac{8}{a_3^2}\int_0^{\frac{\pi}{2}}\int_0^{\infty} \frac{\sin\psi\cos^2\psi}{(\frac{\sin^2\psi}{a_1^2}+\frac{\cos^2\psi}{a_3^2})+(\frac{\sin^2\psi}{a_2^2}+\frac{\cos^2\psi}{a_3^2})t^2}dtd\psi \tag{E.3}$$

$$= \frac{4\pi}{a_3^2}\int_0^{\frac{\pi}{2}} \frac{\sin\psi\cos^2\psi}{(\frac{\sin^2\psi}{a_1^2}+\frac{\cos^2\psi}{a_3^2})^{\frac{1}{2}}(\frac{\sin^2\psi}{a_2^2}+\frac{\cos^2\psi}{a_3^2})^{\frac{1}{2}}}d\psi. \tag{E.4}$$

If we now write $u = a_3^2\tan^2\psi$ then:

$$I_3 = \frac{2\pi}{a_3^2}\int_0^{\infty} \frac{du}{(1+\frac{u}{a_3^2})^{\frac{3}{2}}(1+\frac{u}{a_1^2})^{\frac{1}{2}}(1+\frac{u}{a_2^2})^{\frac{1}{2}}} \tag{E.5}$$

$$= 2\pi a_1a_2a_3\int_0^{\infty}\frac{du}{(a_3^2+u)\Delta}; \tag{E.6}$$

where:

$$\Delta = (a_1^2+u)^{\frac{1}{2}}(a_2^2+u)^{\frac{1}{2}}(a_3^2+u)^{\frac{1}{2}}. \tag{E.7}$$

By a similar argument:

$$\int_0^{2\pi}\int_0^{\pi}\frac{\cos^4\psi\sin\psi}{\frac{\sin^2\psi\cos^2\theta}{a_1^2}+\frac{\sin^2\psi\sin^2\theta}{a_2^2}+\frac{\cos^2\psi}{a_3^2}}d\psi d\theta = 2\pi\int_0^{\infty}\frac{du}{(1+\frac{u}{a_3^2})^2\Delta} \tag{E.8}$$

$$= 2\pi a_1a_2a_3^5\int_0^{\infty}\frac{du}{(a_3^2+u)^2\Delta} \tag{E.9}$$

We now introduce the notation:

$$\alpha_i = \frac{1}{a_1^2}; \tag{E.10}$$

$$u = \frac{1}{v}; \tag{E.11}$$

then by equation E.5

$$\frac{1}{a_3^2}\int_0^{2\pi}\int_0^{\pi}\frac{l_3^2}{l_i^2\alpha_9}\sin\psi d\psi d\theta = 2\pi\int_0^{\infty}\frac{v^{\frac{1}{2}}dv}{(v+\alpha_1)^{\frac{1}{2}}(v+\alpha_2)^{\frac{1}{2}}(v+\alpha_3)^{\frac{3}{2}}}. \tag{E.12}$$

Take $j \neq 3$, then differentiating with respect to α_j we find:

$$\int\frac{l_3^2l_j^2}{(l_i^2\alpha_i)^2}d\Omega = \pi\int_0^{\infty}\frac{v^{\frac{1}{2}}dv}{(v+\alpha_j)(v+\alpha_1)^{\frac{1}{2}}(v+\alpha_2)^{\frac{1}{2}}(v+\alpha_3)^{\frac{3}{2}}}. \tag{E.13}$$

Now integrating with respect to α_3 and noting that both sides $\to 0$ as $\alpha_3 \to \infty$ we find:

$$\int\frac{l_j^2}{(l_i^2\alpha_i)}d\Omega = 2\pi\int_0^{\infty}\frac{v^{\frac{1}{2}}dv}{(v+\alpha_j)(v+\alpha_1)^{\frac{1}{2}}(v+\alpha_2)^{\frac{1}{2}}(v+\alpha_3)^{\frac{1}{2}}} \tag{E.14}$$

$$= 2\pi a_1a_2a_3a_j^2\int_0^{\infty}\frac{du}{(a_j^2+u)\Delta}. \tag{E.15}$$

This establishes the formula:

$$I_n = 2\pi a_1a_2a_3\int_0^{\infty}\frac{du}{(a_n^2+u)\Delta}, \qquad n=1,2,3. \tag{E.16}$$

Now from equation E.8 we find:

$$\int \frac{l_3^4}{l_i^2 \alpha_i} d\Omega = 2\pi \int_0^\infty \frac{v^{\frac{3}{2}} dv}{(\alpha_1 + v)^{\frac{1}{2}} (\alpha_2 + v)^{\frac{1}{2}} (\alpha_3 + v)^{\frac{5}{2}}}. \tag{E.17}$$

For $j \neq 3$ we now differentiate with respect to α_j to obtain:

$$\int \frac{l_3^4 l_j^2}{(l_i^2 \alpha_i)^2} d\Omega = \pi \int_0^\infty \frac{v^{\frac{3}{2}} dv}{(\alpha_j + v)^{\frac{1}{2}} (\alpha_1 + v)^{\frac{1}{2}} (\alpha_2 + v)^{\frac{1}{2}} (\alpha_3 + v)^{\frac{5}{2}}}; \tag{E.18}$$

and integrating with respect to α_3:

$$\int \frac{l_3^2 l_j^2}{l_i^2 \alpha_i} d\Omega = \frac{2}{3}\pi \int_0^\infty \frac{v^{\frac{3}{2}} dv}{(\alpha_j + v)^{\frac{1}{2}} (\alpha_1 + v)^{\frac{1}{2}} (\alpha_2 + v)^{\frac{1}{2}} (\alpha_3 + v)^{\frac{3}{2}}} \tag{E.19}$$

$$= \frac{2}{3}\pi a_1 a_2 a_3 a_j^2 \int_0^\infty \frac{du}{(a_3^2 + u)(a_j^2 + u)\Delta}. \tag{E.20}$$

Similarly, equation E.17 may be differentiated with respect to α_1 and α_2 and then integrated twice with respect to α_3 to yield:

$$\int \frac{l_1^2 l_2^2}{l_i^2 \alpha_i} d\Omega = \frac{2}{3}\pi a_1^3 a_2^3 a_3 \int_0^\infty \frac{du}{(a_1^2 + u)(a_2^2 + u)\Delta}; \tag{E.21}$$

so that we now have:

$$I_{ij} = \frac{2}{3}\pi a_1 a_2 a_3 \int_0^\infty \frac{du}{(a_i^2 + u)(a_j^2 + u)\Delta}, \qquad i \neq j. \tag{E.22}$$

If equation E.17 is differentiated twice with respect to α_j for $j \neq 3$ and integrated twice with respect to α_3 we find:

$$\int \frac{l_j^2}{l_i^2 \alpha_i} d\Omega = 2\pi \int_0^\infty \frac{v^{\frac{3}{2}} dv}{(\alpha_j + v)^2 (\alpha_1 + v)^{\frac{1}{2}} (\alpha_2 + v)^{\frac{1}{2}} (\alpha_3 + v)^{\frac{1}{2}}} \tag{E.23}$$

$$= 2\pi a_1 a_2 a_3 a_j^4 \int_0^\infty \frac{du}{(a_j^2 + u)^2 \Delta}. \tag{E.24}$$

This establishes the formula:

$$I_{ij} = 2\pi a_1 a_2 a_3 \int_0^\infty \frac{du}{(a_i^2 + u)(a_j^2 + u)\Delta}, \qquad i = j. \tag{E.25}$$

Appendix F

Since from equations (3.26), (3.27):

$$I_{ij} = \int \frac{l_i^2 l_j^2}{a_i^2 a_j^2 g} d\Omega; \tag{F.1}$$

$$I_i = \int \frac{l_i^2}{a_i^2 g} d\Omega; \tag{F.2}$$

we have:

$$\begin{aligned} I_{i1} + I_{i2} + I_{i3} &= \int \frac{l_i^2}{a_i^2 g} \left(\frac{l_1^2}{a_1^2} + \frac{l_2^2}{a_2^2} + \frac{l_3^2}{a_3^2}\right) d\Omega & \text{(F.3)} \\ &= \int \frac{l_i^2}{a_i^2} d\Omega & \text{(F.4)} \\ &= \frac{4\pi}{3a_i^2}; & \text{(F.5)} \end{aligned}$$

and similarly:

$$\begin{aligned} a_1^2 I_{i1} + a_2^2 I_{i2} + a_3^2 I_{i3} &= \int \frac{l_i^2 (l_1^2 + l_2^2 + l_3^2)}{g a_1^2} d\Omega & \text{(F.6)} \\ &= \int \frac{l_i^2}{a_i^2 g} d\Omega & \text{(F.7)} \\ &= I_i; & \text{(F.8)} \end{aligned}$$

as required.